Université Fédérale
Toulouse Midi-Pyrénées

THÈSE

Institute of Science and Technology
Nara NAIST

En vue de l'obtention du

DOCTORAT DE L'UNIVERSITÉ DE TOULOUSE

Délivré par :

Université Toulouse III Paul Sabatier (UT3 Paul Sabatier)

Cotutelle internationale avec Nara Institute of Science and Technology (NAIST)

Présentée et soutenue par :
Alexis DUPRE - DEMORSY
le 27 Mars 2023

Titre :

Polymérisation radicalaire contrôlée par transfert de chaîne réversible par addition-fragmentation de N-vinylamides non cycliques

Reversible addition-fragmentation chain-transfer polymerization of acyclic N-vinylamides

---

École doctorale et discipline ou spécialité :

ED SDM : Chimie macromoléculaire et supramoléculaire - CO044

Unité de recherche :

IMRCP - Laboratoire des Intéractions Moléculaires et Réactivité Chimique et Photochimique

Directeurs de thèse :

Mathias DESTARAC, Hiroharu AJIRO

Jury :

Mme. Jutta RIEGER	Sorbonne Université Paris	Rapporteure
M. Franck D'AGOSTO	Univ. Claude Bernard Lyon	Rapporteur
M. Shigeru YAMAGO	Univ. de Kyoto	Examinateur
M. Gwénaël RAPENNE	UT3 Paul Sabatier Toulouse et NAIST	Examinateur
M. Takashi MATSUO	NAIST Nara	Examinateur
M. Mathias DESTARAC	UT3 Paul Sabatier Toulouse	Directeur de thèse
M. Hiroharu AJIRO	NAIST Nara	Co-directeur de thèse
M. Tsuyoshi ANDO	NAIST Nara	Co-encadrant de thèse
M. Olivier COUTELIER	UT3 Paul Sabatier Toulouse	Invité

ACKNOWLEDGEMENTS

This PhD thesis was performed at the Interactions Moleculaires et Reactivites Chimiques et Photochimiques (IMRCP) laboratory at Paul Sabatier III University, Toulouse, France, as well as at the Nanomaterials and Polymer Chemistry laboratory at division of Materials Science, graduate school of Science and Technology, Nara Institute of Science and Technology (NAIST), Nara, Japan, and financed by the Ministere de l'Education Nationale de l'Enseignement Superieur et de la Recherche.

I would like to start by thanking my thesis directors, Mr. Mathias DESTARAC and Mr. Hiroharu AJIRO, for letting me participate in this project, welcoming me in their laboratories and supporting me all those years. I would also like to thank my supervisors, Mr. Olivier COUTELIER and Mr. Tsuyoshi ANDO for their precious help and advices. I have learned a lot from all of them, and will always be grateful to them for this knowledge.

I would like to thank Mr. Christophe MINGOTAUD, IMRCP director, for welcoming me in the laboratory

I would like to express my sincere thanks to all the members of the jury, Mrs. Jutta RIEGER, Mr. Franck D'AGOSTO, Mr. Shigeru YAMAGO, Mr. Takashi MATSUO for evaluating my work, with a special thanks to Mr. Gwenael RAPENNE for his precious help with all the administrative matters for this double-degree program.

I would like to express my thanks to the people I had the chance to work with and helped me get important data: Mrs. Caroline TOPPAN for NMR, Mrs. Valerie BOURDON for mass spectrometry at the Institut de Chimie de Toulouse, Mr. Stephane BALAYSSAC for DOSY-NMR at IMRCP, and Mrs. Marie HENNETIER, Mrs. Audrey RIC and all the people from their laboratory at the Engineering school in Purpan for welcoming me and teaching me about the AF4 technique.

I would like to express my gratitude to all the members of both laboratories, especially the P3R team on the French side and the sub-B members on the Japanese side. It was a great pleasure to come and see you every day in the lab, in the office or at the coffee machine, and have fruitful -or not- discussions about random subjects.

I would like to thank the managers, Mrs. Celine BARAFFE, Mrs. Sandrine FERRERE, and Mrs. Naoko KASHIHARA, for helping me with all the administrative matters for both universities.

I would like to express my warm gratitude to all the friends I made during this project. The Upsi'Team: Marjorie, Camille, Sara, Sasha, Orelia, Judith, Solene, Vincent, Maksym, Izabela. To the Crew-Tachi: Tojo, Ren, Shuga, Nag. Also, to the NAIST international volleyball club, Maria, Aissam, Sergio, Kostja, Magin and the many others.

I would like to express my deepest thanks to my family, my parents Isabelle and Benoît, and my sister Debora, who were always here for me and supporting me for all these years.

Finally, I would like to thank you, for reading this manuscript.

TABLE OF CONTENTS

LIST OF ABBREVIATIONS AND STRUCTURES

AF4: Asymmetrical flow field flow fractionation

AIBN: Azobisisobutyronitrile

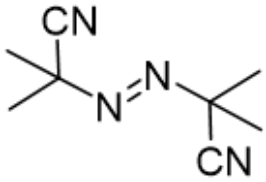

ATRP: Atom-transfer radical polymerization

CMRP: Cobalt-mediated radical polymerization

CRP: Controlled radical polymerization

CTA: Chain transfer agent

D_h: Hydrodynamic diameter

DHBC: Double-hydrophilic block copolymer

DLS: Dynamic light scattering

DMA/PDMA: *N*,*N*-dimethylacrylamide/ poly(*N*,*N*-dimethylacrylamide)

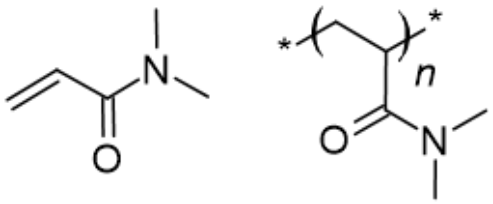

DMF: Dimethylformamide

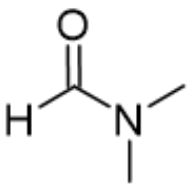

DMSO: Dimethylsulfoxide

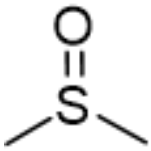

DOSY-NMR: Diffusion-ordered spectroscopy-nuclear magnetic resonance

ESI-TOF-MS: Electrospray ionization-time of flight mass spectrometry

LAM: Less activated monomer

LCST: Lower critical solution temperature

LED: Light-emitting diode

MALDI-TOF-MS: Matrix-assisted laser desorption/ionization-time of flight mass spectrometry

MAM: More activated monomer

MMA/PMMA: Methyl methacrylate/poly(methymethacrylate)

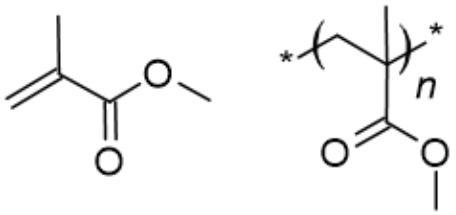

NIPAAm/PNIPAAm: *N*-isopropylacrylamide/poly(*N*-isopropylacrylamide)

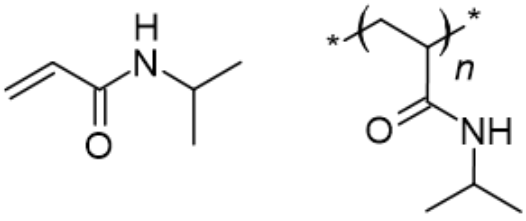

NMR: Nuclear magnetic resonance

NMVA/PNMVA: *N*-methyl-*N*-vinylacetamide/poly(*N*-methyl-*N*-vinylacetamide)

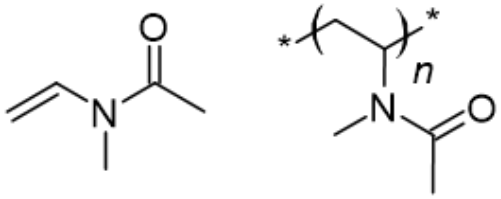

NVA/PNVA: *N*-vinylacetamide/poly(*N*-vinylacetamide)

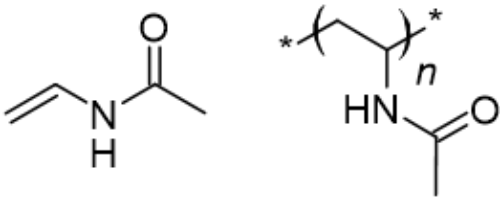

NVF/PNVF: *N*-vinylformamide/poly(*N*-vinylformamide)

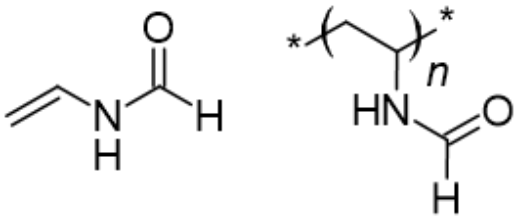

NVIBA/PNVIBA: *N*-vinylisobutyramide/poly(*N*-vinylisobutyramide)

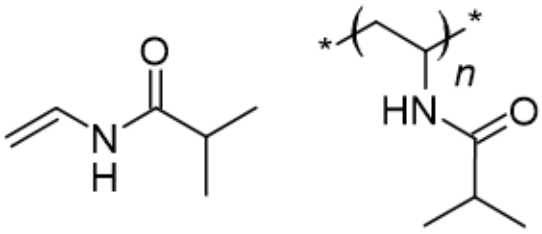

NVP/PVP: *N*-vinylpyrrolidone/poly(*N*-vinylpyrrolidone)

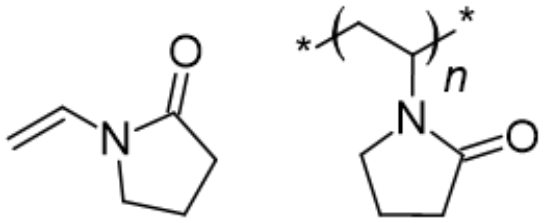

OMRP: Organometallic-mediated radical polymerization

PEG/PEO: poly(ethylene glycol)/poly(ethylene oxide)

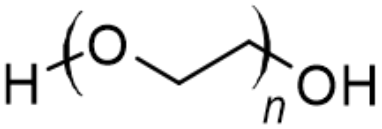

PET-RAFT: Photoinduced electron-transfer reversible addition-fragmentation chain-transfer

PVAm: polyvinylamine

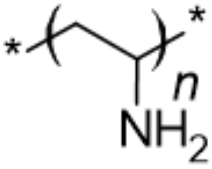

RAFT/MADIX: Reversible addition-fragmentation chain-transfer/macromolecular design by interchange of xanthates

RDRP: Reversible-deactivation radical polymerization

SEC: Size-exclusion chromatography

T_{cp}: Cloud point temperature

TERP: Tellurium-mediated controlled living polymerization

V-70: 2,2'-Azobis(4-methoxy-2,4-dimethylvaleronitrile)

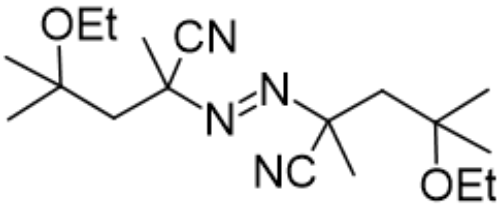

VCL/PVCL: *N*-vinylcaprolactam/poly(*N*-vinylcaprolactam)

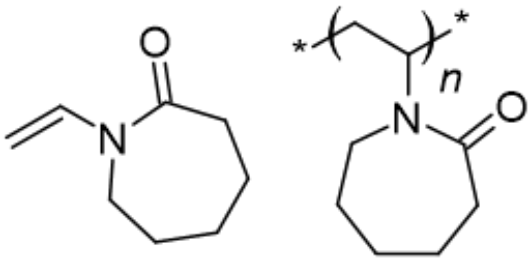

VPI/PVPI: *N*-vinylpiperidine/poly(*N*-vinylpiperidine)

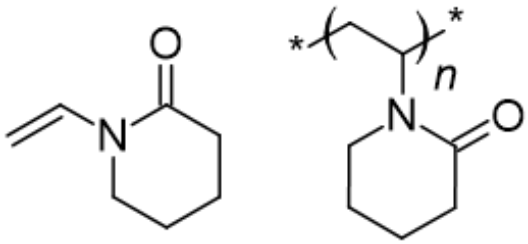

GENERAL INTRODUCTION

Polymers are an essential part of our everyday lives. From plastic cups made of polystyrene to batteries electrolytes made of poly(vinylidene fluoride), a large variety of very useful synthetic polymers are obtained from radical polymerization. In order to control the macromolecular characteristics of polymers, such as molecular weight, dispersity or architecture, polymerization techniques were developed. Following the work of Szwarc in 1956 on anionic polymerization,[1] defined as "living polymerization", the 1980s saw the emergence of "controlled radical polymerization" (CRP) techniques. However, as chain termination and irreversible chain transfer are present in radical polymerization, these cannot be labelled as "living". The term "reversible-deactivation radical polymerization" (RDRP) as it was recommended by IUPAC,[2] is now used to describe them.

Using RDRP techniques, almost all classes of vinyl monomers have been polymerized and copolymerized in a controlled fashion. A few remain however, among which are *N*-vinylamides, more specifically acyclic *N*-vinylamides. In those monomers family, whereas the cyclic derivatives now have their successful controlled polymerization well-known, there is a very contrastive lack of studies on the acyclic ones.

After a general presentation of poly(*N*-vinylamide)s in part 1.1 and some of the commonly used RDRP techniques applied to *N*-vinylamides in part 1.2, advances on their application to this monomers family will be detailed in part 1.3.

1 Poly(N-vinylamide)s

1.1 Properties and applications

Poly(*N*-vinylamide)s are water-soluble and biocompatible polymers.[3] As such, they find applications in fields like medicine, as drug delivery agents.[4–7] Some of those polymers also show thermoresponsive properties with lower critical solution temperature (LCST) behavior, such as poly(*N*-vinylcaprolactam) (PVCL),[8,9] which can be tuned when copolymerized with other monomer.[10,11] Their water-solubility also makes them useful in fields like water treatment, where they can be used for the removal of toxins[12,13] and detect the presence of metals.[14] For petroleum industrials, the property of poly(*N*-vinylamide)s to show kinetic hydrate inhibition behavior at low dosage[15–19] makes them very interesting for preventing the obstruction and clogging of the extraction pipelines. Poly(*N*-vinylamide)s also find applications in more distant fields, like energy and batteries[20–22] or textile[23,24] industries. In addition, some of the polymers obtained from acyclic monomers containing secondary amide like poly(*N*-vinylformamide) (PNVF) or poly(N-vinylacetamide) (PNVA), are precursors to polyvinylamine (PVAm) which cannot be obtained through the direct polymerization of vinylamine.[25–29] Thus, in addition to all the applications for polyvinylamine, they also provide tools for generating cationic interfaces[30] and form complexes with metals[31] or with oppositely charged polyelectrolytes.[32]

1.2 Polymerization techniques

Different techniques are used to polymerize acyclic *N*-vinylamides since a few decades. The first and major one is free radical polymerization.[33,34] It has mainly been done in aqueous media using azo-initiator,[35–39] and Gu and coworkers highlighted a limit of the system in the case of NVF polymerization.[40] They observed that if the monomer concentration is above a certain value (40% in their case), a gel effect and auto-acceleration was observed during the reaction due to crosslinking taking place via the amide group and H-bonds formation.[41] Ajiro and Akashi investigated the effect of the presence of bulky constituents on the tacticity of obtained polymers. They found that polymerization conditions influenced their stereoregularity, and that monomers with bulky substituents polymerized at lower temperatures give more regulated polymer structures.[42,43]

Through emulsion copolymerization of styrene with NVF[44,45] or styrene with NVA,[46,47] those *N*-vinylamides have been used to create porous particles which can later be used to contain materials for further applications. In the latter's case, Yamamoto and coworkers observed that the use of NVA in the soap-free emulsion copolymerization with styrene, increased the yield and the stability of dispersion of the polymeric particles through hydrogen bonding between the particle surface and surrounding water molecules.[46]

Aside from radical polymerization, Madl and coworkers investigated the cationic polymerization of *N*-vinylamides, with a focus on NVF.[48–50] They reported that via the regeneration of active species is permitted through the formation of *N*-formylimine intermediate and its interaction with monomer unit in the polymer chain. However, as the formation of this intermediate requires some amount of

monomer to be done, low conversions are achieved and only oligomers are produced this way.

Polymers and copolymers containing cyclic *N*-vinylamides of well-defined molar masses and narrow dispersities, on the other hand, can already be obtained through several controlled radical polymerization techniques which will be developed later.

2 Reversible-deactivation radical polymerization

In 1982, Otsu introduced the concept of "iniferter" which describes a single compound acting as *ini*tiator, trans*fer* agent and *ter*minator.[51,52] They also proposed a model for living radical polymerization in a homogeneous system, with the polymerizations of styrene and methyl methacrylate monomers using tetraethylthiuram disulfide and dibenzoyl disulfide iniferters.

Reversible-deactivation radical polymerization techniques play on a dynamic exchange between active or propagating radical chains, and inactive or dormant chains throughout the polymerization (scheme 1), governed by a controlling agent. With a sufficient difference between activation and deactivation constant rates, respectively k_a and k_d, the chances of irreversible termination reactions are lowered, thus enabling the polymerization to proceed with control by having polymers chains mainly under their dormant state.

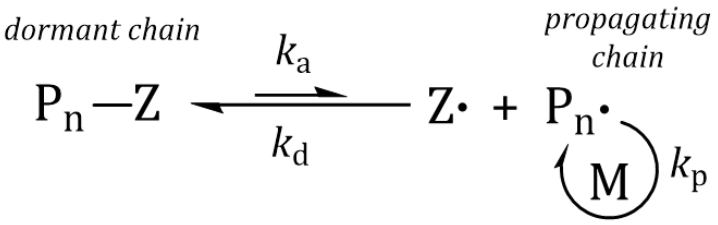

Scheme 1. General mechanism of reversible-deactivation radical polymerization.

In ideal conditions, controlled polymerization should give a linear evolution of ln(1/(1-conversion)) with time, a linear increase of molecular weight (M_n) with monomer conversion, values of polydispersity close to 1, specific capping of polymer chains depending on the controlling agent used, as well as the possibility to re-start polymerization when additional monomer is used.

2.1 Reversible addition-fragmentation chain-transfer polymerization (RAFT)

Reversible addition-fragmentation chain-transfer (RAFT) polymerization was first reported in 1998[53] and patented almost at the same time by two different groups, one at CSIRO referring it as RAFT,[54] and the other one at Rhodia company as macromolecular design by interchange of xanthates (MADIX).[55] It has since then been one of the highlights of radical polymerization.[56]

2.1.1 Mechanism

Like other RDRP techniques, RAFT is based on a dynamic exchange between active and dormant chains, although here the process undergoes degenerative transfer to achieve the exchange. Three components are required, the monomer, an initiator to generate radicals and a chain transfer agent (CTA). As described in scheme 2, first, radicals are generated from the initiator. Those radicals will begin to

polymerize the monomer to produce some polymer chains (initiation step). Those chains will then react with the CTA to reach the pre-equilibrium step, and release the CTA's leaving group R as a new radical. Following this, new polymer chains will be formed from those radicals (re-initiation step). Finally, active polymer chains (radicals) and dormant polymer chains (capped with CTA) will reach the main equilibrium step and process with the dynamic exchange until the polymerization is stopped.

- *Initiation*

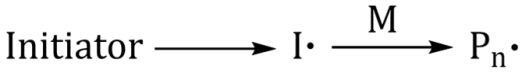

- *Pre-equilibrium (reversible chain transfer)*

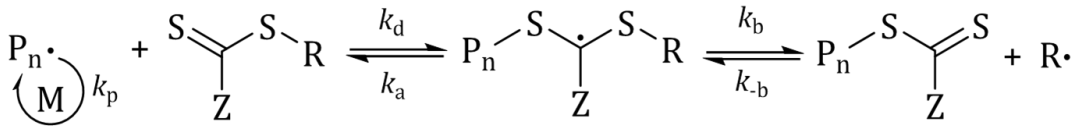

- *Re-initiation*

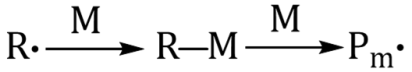

- *Main equilibrium (chain equilibration)*

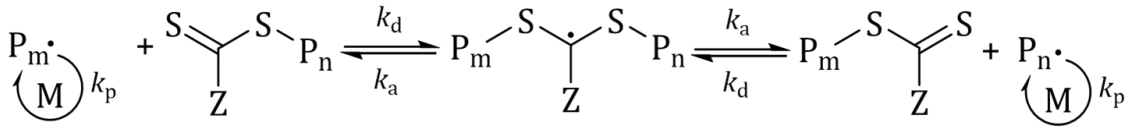

Scheme 2. General mechanism of reversible addition-fragmentation chain-transfer polymerization.

With sufficiently high rates of addition/fragmentation (k_a and k_d) compared to propagation rate (k_p), all polymer chains add a small amount of monomer units when they are active and all chains grow at the same speed. Also, a key point of the degenerative transfer process is that, ideally, the number of radicals remains constant throughout the process. As it is directly linked to the number of radicals generated from the beginning of the reaction by the initiator, it can thus be tuned by applying specific polymerization conditions such as the initiator initial concentration or temperature if it follows thermal decomposition like azo-initiators.

2.1.2 Chain transfer agent

As a core component of RAFT polymerization, the design of CTA is crucial for the reaction to proceed in the desired way and each monomer might require a different one. From the general formula RSC(Z)=S, two elements can obviously be played with, the R and Z groups.[57]

On one hand, the R group should be a good leaving group and the R· radical must be able to quickly re-initiate polymerization so there is no significant retardation occurring. For this, Chong and coworkers report that the leaving group ability is heavily influenced by steric factors, radical stability and polarity.[58]

On the other hand, The Z group has the major influence on the reactivity of the C=S double bond and on the chain-transfer constant of the CTA. Chiefary and coworkers reported that chain-transfer rate decreases in the order dithiobenzoates > trithiocarbonates > xanthates > dithiocarbamates.[59] It is important to note that for the last 2, xanthates and dithiocarbamates where an oxygen or a nitrogen are involved, their lone pair of electrons is conjugated with the C=S double bond, thus

lowering its reactivity. Using electron-withdrawing groups on the Z substituent can greatly improve the reactivity by delocalizing those lone pairs, thus making the C=S double bond more available towards radical addition.

Research has been conducted on the design of CTAs,[60–63] and also on the design outside of the 4 previously mentioned families, organometallic ones with tungsten, chromium or molybdenum complexes of phosphinocarbodithioates,[64,65] other phosphorus groups,[66,67] tin complexes,[68] or with the use of selenium instead of sulfur.[69–71]

2.1.3 Modes of initiation

In order to generate radicals for the reaction, the initiator is also an important factor for RAFT polymerization. Indeed, it will have a heavy impact on the rate of the reaction, but also on its control as it can be linked to the proportion of generated dead chains.

Several modes of initiation were developed, with the most commonly found being thermal initiation through the use of azo-initiator.[72] In this case, elevated temperature causes the initiator to decompose and form radicals. A second popular initiation method is through light, with photo-initiation. Two major ways to conduct RAFT polymerization are usually used with this method, by direct photo-dissociation of the CTA thanks to its iniferter properties,[52] or by photoinduced electron-transfer reversible addition-fragmentation chain-transfer (PET-RAFT) polymerization (scheme 3).

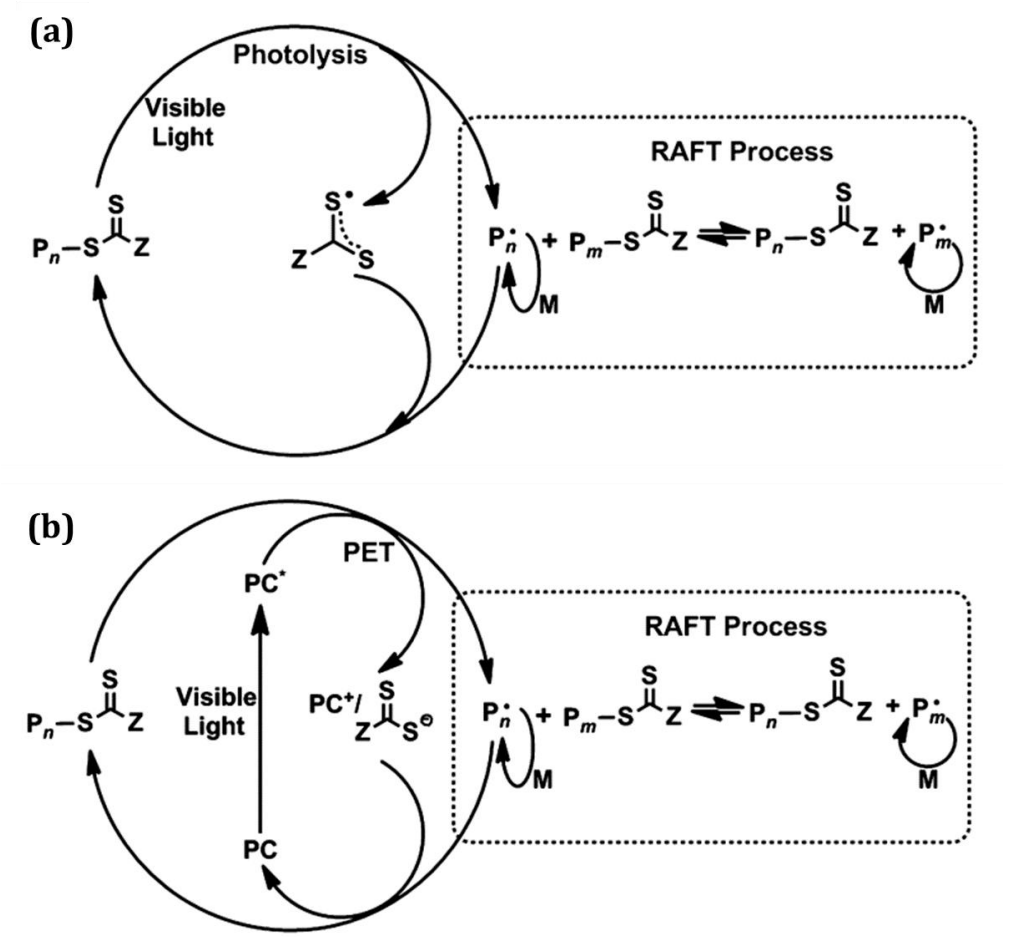

Scheme 3. General mechanism for RAFT polymerization initiated via **(a)** photo-dissociation of the CTA or **(b)** photoinduced electron transfer (PET-RAFT). PC: Photo-redox catalyst. Reprinted with permission from ref [73]. Copyright 2015 American Chemical Society.

In a typical photo-dissociation RAFT polymerization, light will induce a homolytic cleaving of the propagating chain from the CTA to generate the growing radical which undergoes RAFT process (scheme 3a). Generally, UV light can be used, as it was reported by Quinn and coworkers for the successful photo-RAFT polymerization of styrene using light of λ=365nm,[74] giving polystyrenes of M_n up to 27kg mol^{-1} with $Đ$ maintained below 1.3. More recent studies made use of UV-visible light-emitting diodes (LEDs) to conduct photo-RAFT polymerization. As Allegrezza and coworkers reported in their work on methyl methacrylate (MMA),[75] the light

wavelength can be optimized and is strongly dependent of the nature of the CTA. For example, whereas green light of λ=550nm can be used for dithiobenzoates, the same wouldn't be applicable to xanthates for which a wavelength around 400nm (purple light) is better suited.

PET-RAFT involves an additional component, typically a photo-redox catalyst, which, after excitation by light, reduces the CTA to generate the propagating radical (scheme 3b). Catalysts of different natures can be used, including metal complexes (*fac*-[Ir(ppy)$_3$],[76,77] [Ru(bpy)$_3$]Cl$_2$,[78,79] ZnTPP[80,81]) and organic compounds (eosin Y,[82] tertiary amines,[83] 10-phenylphenothiazine[84]). This method has mainly been applied to acrylates, acrylamides, styrene and vinyl ester.[76–84]

A third major mode of initiation is via redox reaction, mainly using peroxides or persulfates. Through this way, the reaction can be carried at room temperature and in different media such as water, in which the RAFT polymerization of acrylamide and NIPAAm,[85] *N*-vinylpyrrolidone,[86] and the synthesis of multiblock copolymers[87] have notably been achieved.

Other initiation paths have been successfully reported, using ultrasonic irradiation,[88] or enzymes.[89]

2.1.4 Controllable monomers

Ultimately, it is the monomer that will decide on the reaction conditions and the choice and design of the CTA. Whereas RDRP techniques can be applied to a wide array of monomers, there are still limits. With the well-known nitroxide-mediated polymerization (NMP), the family of methacrylates has long been a challenge due to side-reaction competition, which prevents the reaction to reach high conversion and

causes a low chain-end fidelity[90]. Although recently, this difficulty has been circumvented through the use of comonomers in the reaction,[91,92] it also means the homopolymerization of this monomers family has yet to be achieved using NMP. As for atom-transfer radical polymerization (ATRP), some non-conjugated monomers such as vinyl esters pose a challenge due to the difficult reactivation of the dormant chains, causing a large disparity in reaction speed comparing to other monomers. Gillies and coworkers calculated that, to reach 90% monomer conversion, only 2h would be needed for methyl acrylate whereas 30 years would be needed for vinyl acetate and 340000 years for ethylene.[93]

RAFT polymerization has the advantage to also be applicable to a wide range of monomers, even including ethylene,[94] only excepting those which would undergo side-reaction with the thiocarbonylthio group of the RAFT agent.[56] Vinyl monomers are usually categorized in two families: more activated monomers (MAMs) where the double bond is conjugated, and less activated monomers (LAMs) where the double bond has a heteroatom or a saturated carbon in the alpha position. As was stated before for the choice of CTA, there is a difference in reactivity depending on the nature of the RAFT agent. As such, different CTAs will be more suitable for the polymerization of certain monomers. As Keddie and coworkers reported,[95] when handling a MAM monomer such as methacrylate or acrylamide, dithiobenzoates or trithiocarbonates would be favored. When handling LAM monomers such as vinyl acetate or *N*-vinylamides, xanthates or dithiocarbamates would be recommended.

2.2 Cobalt-mediated radical polymerization (CMRP)

Cobalt-mediated radical polymerization (CMRP) has first been used to control the polymerization of acrylates in 1994.[96] A decade later, the report on the controlled polymerization of vinyl acetate[97] opened the way for CMRP to other kinds of monomers, such as acrylic acid,[98] acrylonitrile,[99] vinyl chloride[100] or other vinyl monomers including *N*-vinylamides.[101]

CMRP relies on the dynamic exchange between the propagating radical chains, active species, and their deactivated state by complexing with cobalt(II) to produce cobalt(III) complexes, the dormant species (scheme 4). At first, either an organocobalt(III) species undergoes Co-C homolytic cleavage to produce a free radical R· and a cobalt(II) complex species, or the radical is generated from an external initiator. The radical species will then initiate polymerization by adding monomer units. In the ideal case where side transfer reaction (k_{tr} pathway in scheme 4) doesn't occur, only the deactivation of growing polymer chains by forming Co-C bond with the cobalt(II) complex to produce dormant, organocobalt(III) species mainly happens (k_c pathway). The subsequent cleaving of this low strength bond (k_d pathway) will in turn regenerate the active, radical polymer chains species, which will then continue to propagate (k_p).

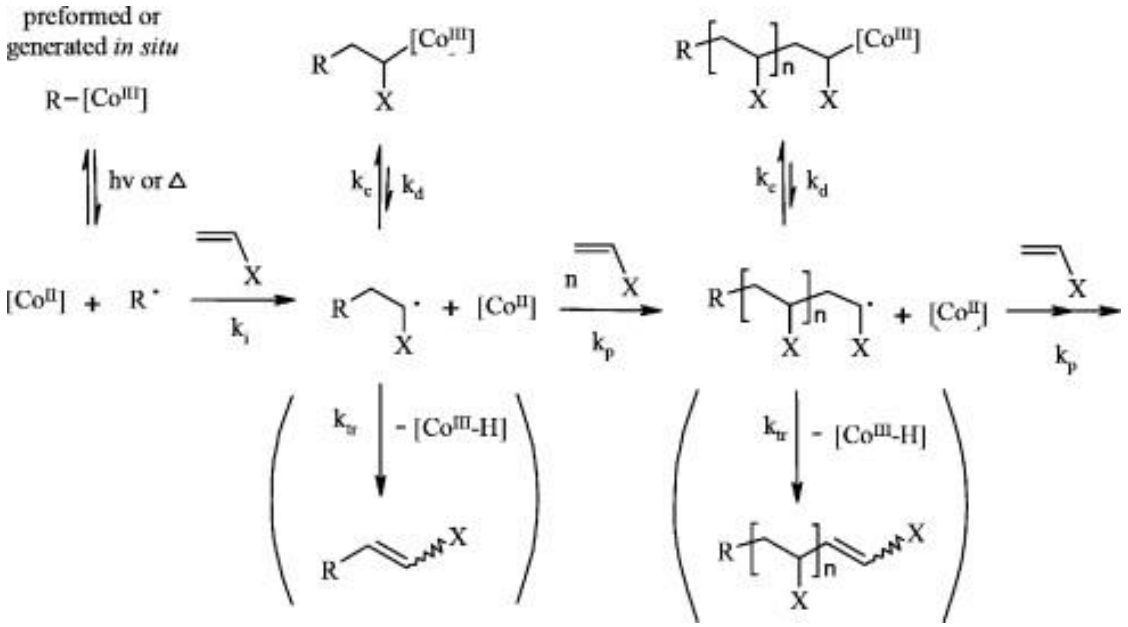

Scheme 4. General mechanism of CMRP. Reprinted with permission from ref [102] Copyright 2009 Elsevier Ltd.

From the CMRP mechanism, it clearly appears that the strength of the Co-C bond between polymer chains and cobalt complexes is a crucial factor to ensure the desired polymerization process. If the bond's strength is too low, the generation of a high concentration of radical species might lead to cross coupling reactions between the growing chains. On the other hand, if the bond's strength is too high, polymerization might not proceed as all polymer chains would stay in their dormant state. Thus, particular attention should be given to the choice of the cobalt complex for a given monomer. Depending on the nature of the cobalt complex/monomer association, and by choosing the appropriate initiator, polymerization can be conducted by thermal or photo-initiation ways, at it has been illustrated in the case of N-vinylacetamide where both ways were applied.[28]

2.3 Organotellurium-mediated living radical polymerization (TERP)

Organotellurium-mediated living radical polymerization (TERP) was developed by Yamago and coworkers after observing that organotellurium compounds undergo reversible Te-C homolytic cleavage through thermolysis or photolysis to produce carbon-centered radicals,[103] and after the observation from Takagi and coworkers that introducing diphenyl ditelluride during the polymerization of styrene had a significant effect on the obtained molar masses.[104] At first, the controlled polymerization of styrene was achieved[105] with acrylate monomers following shortly after,[106] and the technique has been applied to various monomers including acrylonitrile,[107] acrylamides,[107–109] vinyl acetate[110] or *N*-vinylamides.[108,109,111]

Like RDRP techniques, TERP mechanism relies on the dynamic exchange between active, propagating species and dormant species (scheme 5).

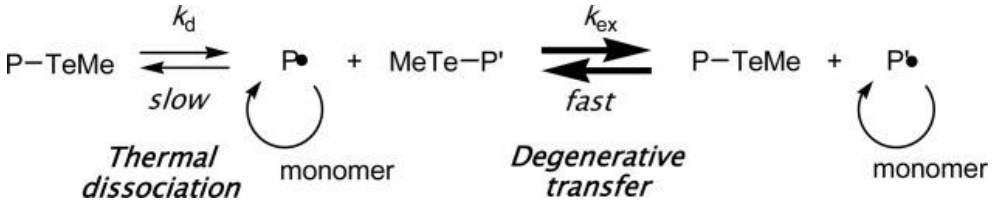

Scheme 5. General mechanism of TERP. Reprinted with permission from ref [107] Copyright 2005 Wiley Periodicals, Inc.

Yamago and coworkers identified two occurring mechanism during kinetic studies of TERP. Thermal dissociation (scheme 5) corresponds to the unimolecular

homolytic cleavage of the Te-C bond upon heating. However, this process only happens at elevated temperatures and very slowly.[107] Thus, in presence of a thermal initiator such as AIBN, working at milder thermal conditions, polymerization only follows the degenerative transfer process (scheme 5). Similarly to the RAFT polymerization process in the main equilibrium step, propagating polymer chains will react with organotellurium species to form the dormant species with the simultaneous regeneration of another active, growing polymer chain. However, as reported by the authors,[107] RAFT and TERP processes differ by their energy profile (scheme 6). Whereas in RAFT polymerization, the generated intermediate radical is relatively stable, in TERP the authors state that the produced intermediate radical is of high energy level. This, way, the re-generation of propagating species should occur in a concerted fashion, and with reduced chances of side-reactions happening.

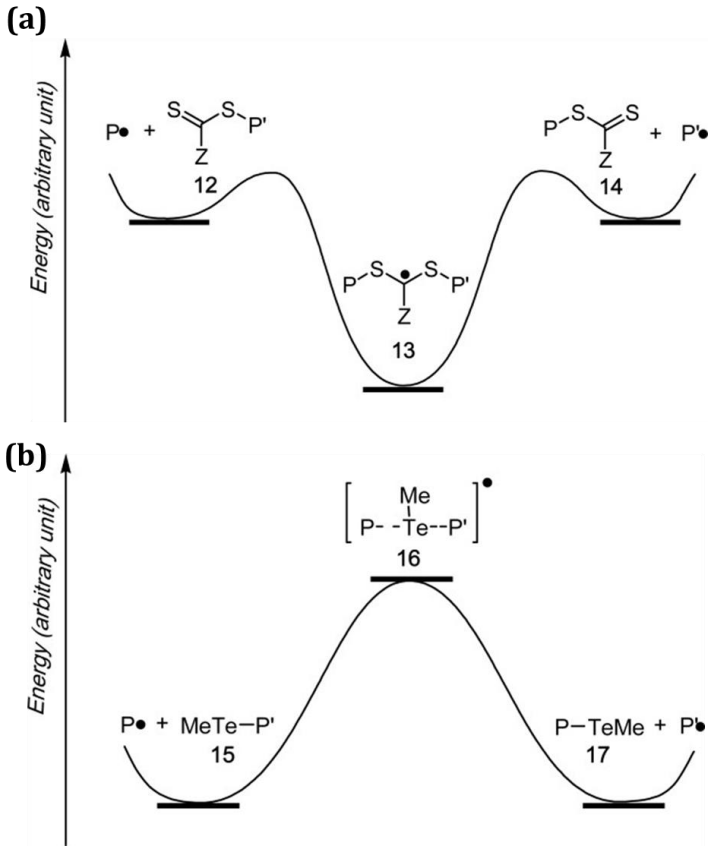

Scheme 6. Hypothetical energy diagram of the degenerative transfer of **(a)** RAFT and **(b)** TERP process. Reprinted with permission from ref [107]. Copyright 2005 Wiley Periodicals, Inc.

Those three RDRP techniques, RAFT, CMRP and TERP, comprise the mainly used polymerization techniques when it comes to the controlled polymerization of *N*-vinylamides, specifically acyclic ones. However, as was stated before, there is a huge contrast in the number of studies concerning cyclic *N*-vinylamides compared to the acyclic derivatives.

3 Controlled polymerization of N-vinylamides

N-vinylamides, as less activated monomers (LAMs), have their vinyl group linked to the nitrogen atom of the amide group of their side-chain. Depending on the nature of their amide group, *N*-vinylamides are classified as cyclic or acyclic.

3.1 Cyclic N-vinylamides

Among cyclic *N*-vinylamides, *N*-vinyllactams and more specifically the very popular *N*-vinylpyrrolidone (VP) and *N*-vinylcaprolactam (VCL) have been at the center of extensive research.[112,113] Aside from these two, the six-membered ring, *N*-vinylpiperidone (VPI) controlled polymerization has only been achieved via RAFT polymerization.[114–116] In their studies, Peng and coworkers performed the RAFT copolymerization of either VP, VPI or VCL with methacrylic acid *N*-hydroxysuccunimide ester[114] or pyridyl disulfide ethyl methacrylate[116] in anisole, using AIBN as the thermal initiator and methyl 2-(ethoxycarbonothioylthio)propanoate (CTA1, Scheme 7), a xanthate as the chain transfer agent, in order to obtain copolymers of designed architectures with molecular weights of less than 10kg mol^{-1} and dispersities maintained under 1.4.

For VP, Moad and coworkers reported its RAFT polymerization using S-cyanomethyl O-ethylxanthate (CTA2, Scheme 7) at 60°C (AIBN initiation) in methanol to obtain polymers of M_n = 17 kg mol^{-1} and $Đ$ = 1.35.[117] As Roka and coworkers reported recently,[113] a plethora of RAFT agents have been used for the controlled polymerization of VP, including xanthates or dithiocarbamates[118] (Scheme 7). Some reports were made using trithiocarbonates[119] with less satisfying

results such as an important induction time, or even inhibition of the polymerization when using a dithiobenzoate.[120] The latter results were expected, as trithiocarbonates and dithiobenzoates are more suited for more activated monomers (MAMs).[59] Those examples mainly use azo-initiator to start the reaction, but other conditions have been reported, such as the RAFT polymerization of VP in water by Guinaudeau and coworkers, using a xanthated CTA and redox reaction to initiate polymerization.[86,121] This way, well-defined PVPs of M_n up to around 10 kg mol^{-1} and $Đ$ maintained below 1.30 were obtained. Recently, the RAFT copolymerization of VP with MAM monomers such as acrylates or styrene has also been achieved by Wang and coworkers, using photo-initiation of a xanthate CTA.[122]

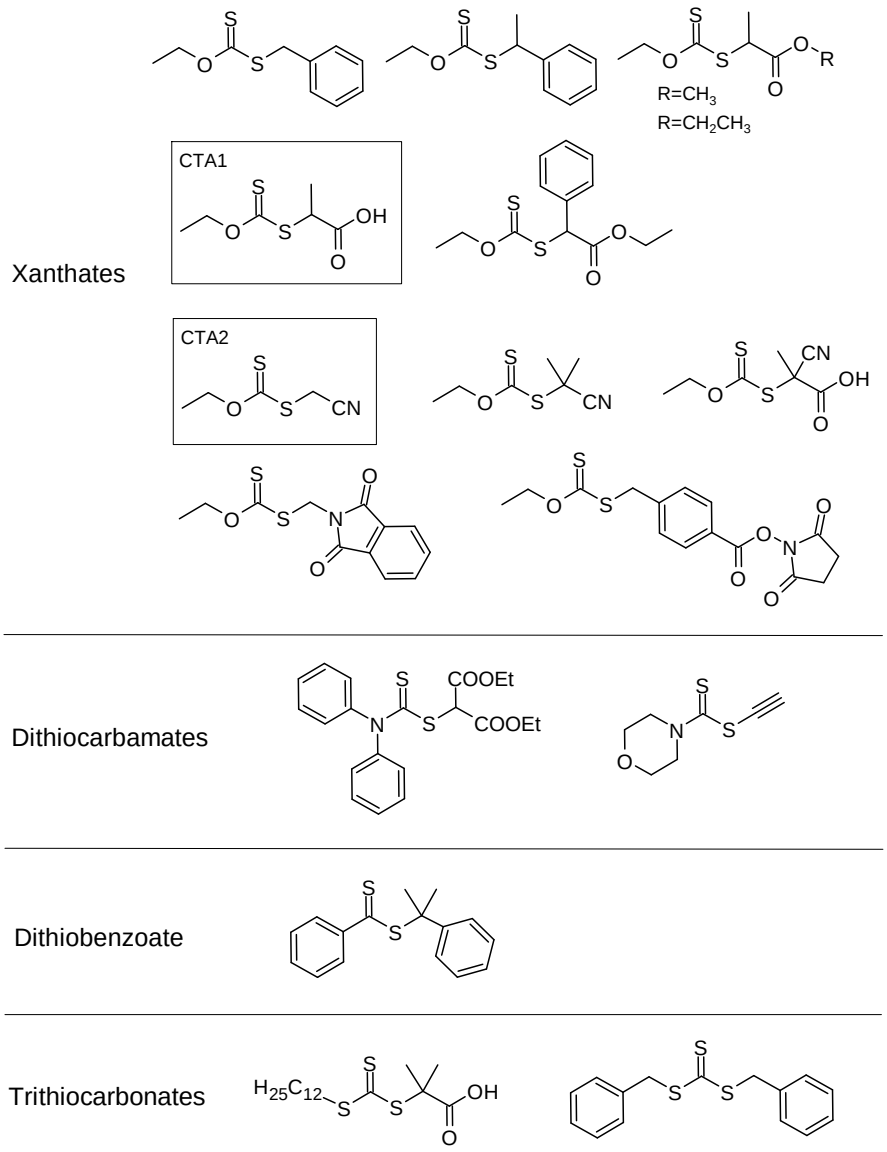

Scheme 7. Various CTAs used for the RAFT polymerization of N-vinylpyrrolidone. Adapted with permission from ref [113]. Copyright 2013 Elsevier Ltd.

VCL, the seven-membered ring *N*-vinyllactam precursor of a thermoresponsive polymer,[10] has also been controlled by RAFT polymerization. Using xanthates, Gois and coworkers obtained PVCL of M_n up to 30 kg mol^{-1} while maintaining $Đ$ below 1.6.[123] Zhao and coworkers synthesized PVCL of M_n up to 40 kg mol^{-1} with low $Đ$ of 1.2 and below, as well as copolymers of VCL with VP.[10] Beija and coworkers, using

CTA1 (scheme 7), achieved excellent control for PVCL of M_n as high as 150 kg mol^{-1} while maintaining $Đ$ below 1.2.[8] Using xanthate and dithiocarbamate CTAs, Wan and coworkers obtained in bulk polymerization, PVCL of M_n around 10 kg mol^{-1} with $Đ$ below 1.5.[124] Shao and coworkers, using a trithiocarbonate CTA, managed to obtain PVCL of M_n up to 20 kg mol^{-1} while maintaining $Đ$ below 1.4.[125] Polymers of very high molecular weights above 1000 kg mol^{-1} and dispersities below 1.4 have also been reported using xanthate CTAs.[126] Amphiphilic thermoresponsive materials containing VCL and vinyl acetate have also been synthesized in a controlled manner using RAFT polymerization, of M_n up to 50 kg mol^{-1} with low $Đ$ of 1.25 and below.[127] Concerning the RAFT polymerization of cyclic *N*-vinylamides, xanthates and dithiocarbamates are the most widely used CTAs.

Although RAFT polymerization is the most commonly used here, other RDRP techniques have also achieved the controlled polymerization of this kind of monomers.

With cobalt-mediated radical polymerization, Hurtgen and coworkers obtained block copolymers of vinyl acetate and VCL of M_n up to 50 kg mol^{-1} with narrow $Đ$ of below 1.1 using the well-known *bis*(acetylacetonato)cobalt(II) ($Co(acac)_2$) complex.[128] The same complex was used by Kermagoret and coworkers[129] to obtain random VCL-based copolymers of tunable LCST with acyclic *N*-vinylamides, vinyl acetate or vinyl pivalate as comonomers. Very narrow dispersities were obtained in the former case, with values below 1.2 for M_n up to 40 kg mol^{-1}. Using photo-initiation, Miao and coworkers conducted the polymerization of VP and VCL, and despite a significant discrepancy between theoretical and experimental molecular weight values, polymers of relatively narrow dispersities

(below 1.3) were obtained.[130]

With tellurium-mediated living radical polymerization, Yusa and coworkers proceeded to the block copolymerization of VP with *N*-isopropylacrylamide, and obtained copolymers of M_n up to 40 kg mol^{-1} with narrow $Đ$ of below 1.2.[109] Using originally synthesized TERP agents, Fan and coworkers applied TERP to several MAM and LAM monomers including VCL, to obtain polymers of M_n of 10 kg mol^{-1} with very narrow $Đ$ of 1.1.[131] Finally, using photo-initiation, Yamago and coworkers conducted the bulk, photoinduced TERP of VP to obtain a polymer of controlled molecular weight (M_n = 9.2 kg mol^{-1} for a $M_{n,th}$ = 10.3 kg mol^{-1}) with a narrow $Đ$ of 1.12.[132]

Other RDRP techniques have managed to control the polymerization of cyclic *N*-vinylamides such as atom-transfer radical polymerization (ATRP). For example, Singh and coworkers reported a thorough study on the successful control of VCL polymerization via ATRP,[133] and Mishra and coworkers reported the successful synthesis of well-defined PVP, with a further success on the cyclization of the polymer.[134] However it has not yet been successfully reported in the controlled polymerization of acyclic *N*-vinylamides.

3.2 Acyclic N-vinylamides

In the case of cyclic *N*-vinylamides, RAFT polymerization is the most used RDRP technique. On the other hand, for acyclic *N*-vinylamides, the opposite can be observed, and in a general fashion as only few studies were reported on the subject. The first report of controlled polymerization of acyclic *N*-vinylamides has been made by Shi and coworkers in 2003 using RAFT block copolymerization of poly(ethylene

glycol) with *N*-vinylformamide (NVF) using a PEG-macro-RAFT agent at 100°C in DMSO.[135] However, the authors stopped polymerizations at relatively low NVF conversions (below 45%), and obtained copolymers of lower molecular weights than expected ($M_{n,SEC}$ = 4.8 kg mol^{-1} for a $M_{n,th}$ = 9.8 kg mol^{-1}) and of high dispersity ($Đ$ = 2.3). Also using RAFT block copolymerization, Lou et al. studied the preparation and assembly of poly(vinyl acetate)-*b*-poly(*N*-vinylacetamide) in water,[136] with only IR and ^{1}H spectroscopy to prove the incorporation of NVA into the copolymer and DLS of the copolymer in water to show the formation of objects, but without any convincing proof of the controlled character of NVA polymerization. Peng and coworkers also used RAFT polymerization to synthesize a series of statistical copolymers pairing NVF with VCL, VPI or VP.[137] Though the obtained copolymers showed relatively low dispersity with compositions close to the expected ones, the authors mainly focused on low molar mass copolymers (M_n of 10 kg mol^{-1}) with a maximum fraction of NVF of 50%. Finally, Kawatani and coworkers performed the random copolymerization of NVF with NVF derivatives monomers bearing alkenyl groups at their amide's Nitrogen side.[138] Using two different CTAs, one xanthate and one dithiocarbamate, they synthesized copolymers of M_n of 1 to 6 kg mol^{-1}. However, the authors reported relatively high dispersity values, going from 1.5 to 3.3 and for relatively long reaction time (7 days).

As such, all RAFT polymerization studies on acyclic *N*-vinylamides only report copolymerization, either statistical or block via the use of macro-RAFT agents. On the other hand, CMRP and TERP have been more successful for the task.

Drean and coworkers report the controlled polymerization of NVA and NMVA through thermal and photo-initiated CMRP,[139,140] with the aim to obtain

polyvinylamine of predetermined molecular weights. First, using $Co(acac)_2$ complex in methanol and a photo-initiator, the photo-initiated CMRP of NVA was conducted at 20°C. Despite the low monomer conversions (below 40%), polymers of narrow dispersities were obtained, with $Đ$ maintained below 1.2 for M_n up to 60 kg mol^{-1}. For M_n higher than 120 kg mol^{-1}, dispersity went up but was still maintained below 1.6. Then, the thermally initiated CMRP of NMVA was conducted using $Co(acac)_2$ complex, in bulk at 40°C. Here, higher monomer conversions were obtained with values up to 70%. Polymers of M_n up to 30 kg mol^{-1} in close agreement with theoretical values and of narrow dispersities ($Đ$ below 1.2) were obtained (Figure 1).

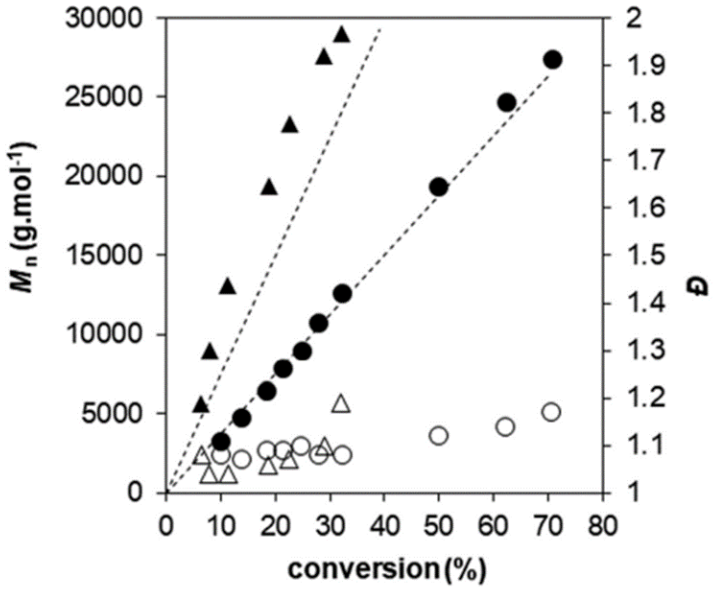

Figure 1. Evolution of M_n (full symbols) and $Đ$ (hollow symbols) on the monomer conversion for the OMRP of NMVA initiated in bulk at 40 °C. [NMVA]/[$Co(acac)_2$-$(CH(OAc)CH_2)_{<4}$-R_0]=380 (•) and 760 (▲). The dotted lines represent the theoretical dependence of M_n vs conversion. Reprinted with permission from ref [140]. Copyright 2018 American Chemical Society.

The authors also conducted the random copolymerization of NMVA with NVA, as well as the successful hydrolysis of the monomer units into vinylamine to finally obtain controlled polyvinylamines.

The most recent report has been made by Fan and Yamago, using TERP to achieve the controlled polymerization of NMVA, NVA and NVF for the first time, at 60°C in bulk (Scheme 8).[141]

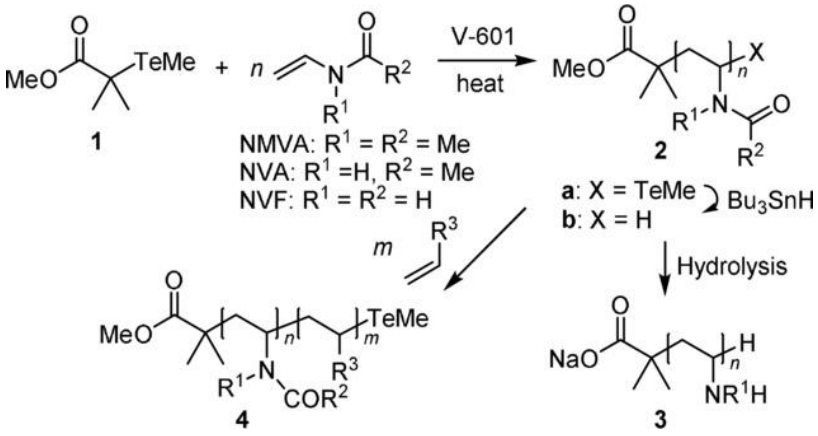

Scheme 8. General scheme of the TERP of NMVA, NVA and NVF. Reprinted with permission from ref [141]. Copyright 2019 Wiley-VCH Verlag GmbH & Co. KGaA, Weinheim

Throughout all polymerizations, excellent control was obtained for molecular weights up to 10 kg mol^{-1}, with values extremely close to expected ones and dispersities maintained below 1.1. When aiming for M_n above 10 kg mol^{-1}, up to 30~40 kg mol^{-1}, a slight difference between theoretical and expected values appears, supposedly due to the analysis conditions as stated by the authors, with dispersities still maintained below 1.3. The authors also conducted the successful hydrolysis of monomer units into vinylamine. This work also marks the first report of the controlled polymerization of NVF.

4 Thesis outline

From the literature, there is obviously a huge difference between the controlled polymerization of cyclic and acyclic *N*-vinylamides. Moreover, the RAFT polymerization technique, which is widely used for the cyclic derivatives, falls behind organometallic-mediated radical polymerization techniques in the case of acyclic *N*-vinylamides. This project thus has the objective of developing satisfying conditions for successful RAFT polymerization of *N*-vinylamides, with comprehensive studies on several examples.

In Chapter 1, the controlled RAFT polymerization of NMVA is demonstrated. This first step will focus on establishing experimental conditions and understanding the limitations of the system.

In Chapter 2, the controlled RAFT polymerization of NVF is demonstrated. As this polymer is a precursor of polyvinylamine, this part aims to provide an easy way to access polyvinylamines of predetermined molecular weights.

In Chapter 3, the controlled RAFT polymerization of NVIBA is demonstrated. With the interesting thermoresponsive properties of PNVIBA, and the ability of RAFT polymerization to produce copolymers of defined architectures, this final part aims to delve in the domain of new materials with tunable thermoresponsivity.

REFERENCES

(1) Szwarc, M. 'Living' Polymers. *Nature* **1956**, *178* (4543), 1168–1169.

(2) Jenkins, A. D.; Jones, R. G.; Moad, G. Terminology for reversible-deactivation radical polymerization previously called "controlled" radical or "living" radical polymerization (IUPAC Recommendations 2010). *Pure Appl. Chem.* **2009**, *82* (2), 483–491.

(3) Kirsh, Y. E. *Water Soluble Poly-N-Vinylamides: Synthesis and Physicochemical Properties.*; Wiley, 1998.

(4) Ajiro, H.; Akashi, M. Interpenetrating Polymer Network Using Amphiphilic Poly(N-Vinylacetamide) and Poly(2-Hydroxyethyl Methacrylate) to Deactivate Phosphate Ester Compounds. *Chem. Lett.* **2013**, *42* (12), 1540–1541.

(5) Eeckman, F.; Moës, A. J.; Amighi, K. Synthesis and Characterization of Thermosensitive Copolymers for Oral Controlled Drug Delivery. *Eur. Polym. J.* **2004**, *40* (4), 873–881.

(6) Panarin, E. F. N-Vinylamides and Related Polymers as Delivery Agents of Biologically Active Compounds. *Russ. Chem. Bull.* **2015**, *64* (1), 15–23.

(7) Santuryan, Y. G.; Malakhova, I. I.; Gorshkov, N. I.; Krasikov, V. D.; Panarin, E. F. Water-Soluble Poly(n-Vinylamides)as a Basis for the Synthesis of Polymeric Carriers of Biologically Active Compounds. *Int. J. Polym. Anal. Charact.* **2019**, *24* (2), 105–113.

(8) Beija, M.; Marty, J.-D.; Destarac, M. Thermoresponsive Poly(N-Vinyl Caprolactam)-Coated Gold Nanoparticles: Sharp Reversible Response and Easy Tunability. *Chem. Commun.* **2011**, *47* (10), 2826–2828.

(9) Liu, J.; Debuigne, A.; Detrembleur, C.; Jérôme, C. Poly(N-Vinylcaprolactam): A Thermoresponsive Macromolecule with Promising Future in Biomedical Field. *Adv. Healthc. Mater.* **2014**, *3* (12), 1941–1968.

(10) Zhao, X.; Coutelier, O.; Nguyen, H. H.; Delmas, C.; Destarac, M.; Marty, J.-D. Effect of Copolymer Composition of RAFT/MADIX-Derived N-Vinylcaprolactam/N-Vinylpyrrolidone Statistical Copolymers on Their Thermoresponsive Behavior and Hydrogel Properties. *Polym. Chem.* **2015**, *6* (29), 5233–5243.

(11) Kermagoret, A.; Mathieu, K.; Thomassin, J.-M.; Fustin, C.-A.; Duchêne, R.; Jérôme, C.; Detrembleur, C.; Debuigne, A. Double Thermoresponsive Di- and Triblock Copolymers Based on N-Vinylcaprolactam and N-Vinylpyrrolidone: Synthesis and Comparative Study of Solution Behaviour. *Polym. Chem.* **2014**, *5* (22), 6534–6544.

(12) Bialczyk, J.; Kochanowski, A.; Czaja-Prokop, U.; Chrapusta, E. Removal of Microcystin-LR from Water by Polymers Based on N-Vinylformamide Structure. *Water Supply* **2013**, *14* (2), 230–237.

(13) Kuznetsov, V. A.; Lavlinskaya, M. S.; Ostankova, I. V.; Shatalov, G. V.; Shikhaliev, K. S.; Ryzhkova, E. A. Synthesis of N-Vinylformamide and 1-Vinyl-(1-Methacryloyl)-3,5-Dimethylpyrazole Copolymers and Their Extraction Ability in Relation to Histidine in Water-Salt Media. *Polym. Bull.* **2018**, *75* (3), 1237–1251.

(14) Chen, M.-Q.; Chen, Y.; Kaneko, T.; Liu, X.-Y.; Cheng, Y.; Akashi, M. Pb2+-Specific Adsorption/Desorption onto Core-Corona Type Polymeric Nanospheres Bearing Special Anionic Azo-Chromophore. *Polym. J.* **2003**, *35* (8), 688–690.

(15) Ajiro, H.; Takemoto, Y.; Akashi, M.; Chua, P. C.; Kelland, M. A. Study of the Kinetic Hydrate Inhibitor Performance of a Series of Poly(N-Alkyl-N-Vinylacetamide)s. *Energy Fuels* **2010**, *24* (12), 6400–6410.

(16) Kawatani, R.; Kawata, Y.; Yusa, S.; Kelland, M. A.; Ajiro, H. Synthesis of Thermosensitive Poly(N-Vinylamide) Derivatives Bearing Oligo Ethylene Glycol Chain for Kinetic Hydrate Inhibitor. *Macromolecules* **2018**, *51* (19), 7845–7852.

(17) Kelland, M. A.; Abrahamsen, E.; Ajiro, H.; Akashi, M. Kinetic Hydrate Inhibition with N-Alkyl-N-Vinylformamide Polymers: Comparison of Polymers to n-Propyl and Isopropyl Groups. *Energy Fuels* **2015**, *29* (8), 4941–4946.

(18) Reyes, F. T.; Kelland, M. A. First Investigation of the Kinetic Hydrate Inhibitor Performance of Polymers of Alkylated N-Vinyl Pyrrolidones. *Energy Fuels* **2013**, *27* (7), 3730–3735.

(19) Zhang, Q.; Kawatani, R.; Ajiro, H.; Kelland, M. A. Optimizing the Kinetic Hydrate Inhibition Performance of N-Alkyl-N-Vinylamide Copolymers. *Energy Fuels* **2018**, *32* (4), 4925–4931.

(20) Lis, M.; Chudzik, K.; Bakierska, M.; Świętosławski, M.; Gajewska, M.; Rutkowska, M.; Molenda, M. Aqueous Binder for Nanostructured Carbon Anode Materials for Li-Ion Batteries. *J. Electrochem. Soc.* **2019**, *166* (3), A5354.

(21) Molenda, M. Carbon electrode composites for li-ion batteries prepared from polymer precursors. *Funct. Mater. Lett.* **2011**, *04* (02), 129–134.

(22) Świder, J.; Molenda, M.; Kulka, A.; Molenda, J. Enhancement of Electrochemical Performance of LiFePO4 Nanoparticles by Direct Nanocoating with Conductive Carbon Layers. *Funct. Mater. Lett.* **2016**, *09* (04), 1641007.

(23) Lee, S.-R.; Miyazaki, K.; Hisada, K.; Hori, T. Application of Silk Sericin to

Finishing of Synthetic Fabrics. *Seni Gakkaishi* **2004**, *60*, 9–15.

(24) Wang, F.; Tanaka, H. Aminated Poly-N-Vinylformamide as a Modern Retention Aid of Alkaline Paper Sizing with Acid Rosin Sizes. *J. Appl. Polym. Sci.* **2000**, *78* (10), 1805–1810.

(25) Dréan, M.; Guégan, P.; Jérôme, C.; Rieger, J.; Debuigne, A. Far beyond Primary Poly(Vinylamine)s through Free Radical Copolymerization and Amide Hydrolysis. *Polym. Chem.* **2015**, *7* (1), 69–78.

(26) Gu, L.; Zhu, S.; Hrymak, A. N. Acidic and Basic Hydrolysis of Poly(N-Vinylformamide). *J. Appl. Polym. Sci.* **2002**, *86* (13), 3412–3419.

(27) Pinschmidt Jr, R. K. Polyvinylamine at Last. *J. Polym. Sci. Part Polym. Chem.* **2010**, *48* (11), 2257–2283.

(28) Stiernet, P.; Dréan, M.; Jérôme, C.; Midoux, P.; Guégan, P.; Rieger, J.; Debuigne, A. Tailor-Made Poly(Vinylamine)s via Thermal or Photochemical Organometallic Mediated Radical Polymerization. In *Reversible Deactivation Radical Polymerization: Mechanisms and Synthetic Methodologies*; ACS Symposium Series; American Chemical Society, **2018**, *1284*, 349–363.

(29) Witek, E.; Pazdro, M.; Bortel, E. Mechanism for Base Hydrolysis of Poly(N-vinylformamide). *J. Macromol. Sci. Part A* **2007**, *44* (5), 503–507.

(30) Pelton, R. Polyvinylamine: A Tool for Engineering Interfaces. *Langmuir* **2014**, *30* (51), 15373–15382.

(31) Kobayashi, S.; Suh, K. D.; Shirokura, Y. Chelating Ability of Poly(Vinylamine): Effects of Polyamine Structure on Chelation. *Macromolecules* **1989**, *22* (5), 2363–2366.

(32) Ajiro, H.; Takemoto, Y.; Asoh, T.; Akashi, M. Novel Polyion Complex with Interpenetrating Polymer Network of Poly(Acrylic Acid) and Partially Protected Poly(Vinylamine) Using N-Vinylacetamide and N-Vinylformamide. *Polymer* **2009**, *50* (15), 3503–3507.

(33) Anand, P. S.; Stahl, H. G.; Heitz, W.; Weber, G.; Bottenbruch, L. Block Copolymers by Radical Polymerization. 3. Block Copolymers of Styrene, Methyl Acrylate, N-Methyl-N-Vinylacetamide, 1-Vinyl-2-Pyrrolidone. *Makromol. Chem.* **1982**, *183*, 1685–1700.

(34) Akashi, M.; Yashima, E.; Yamashita, T.; Miyauchi, N.; Sugita, S.; Marumo, Kuniomi. A Novel Synthetic Procedure of Vinylacetamide and Its Free Radical Polymerization. *J. Polym. Sci. Part Polym. Chem.* **1990**, *28*, 3487–3497.

(35) Chen, Q.; Liu, X.; Xu, K.; Song, C.; Zhang, W.; Wang, P. Phase Behavior and Self-Assembly of Poly[N-Vinylformamide-Co-(Acrylic Acid)] Copolymers under

Highly Acidic Conditions. *J. Appl. Polym. Sci.* **2008**, *109*, 2802–2807.

(36) Cizravi, J. C. Free Radical Kinetics of N-Methyl N-Vinyl Acetamide Polymerization at Low Conversions in Aqueous Media. *J. Appl. Polym. Sci.* **2000**, *79*, 337–341.

(37) Gavrilova, I. I.; Panarin, E. F.; Nesterova, N. A. Homopolymerization of N-Vinylamides in the Presence of Water-Soluble Initiators and Preparation of Polyelectrolytes from the Polymerization Products. *Russ. J. Appl. Chem.* **2012**, *85*, 413–416.

(38) Kathmann, E. E.; White, L. A.; McCormick, C. L. Water-Soluble Copolymers. 67. Polyelectrolytes of N-Vinylformamide with Sodium 3-Acrylamido-3-Methylbutanoate, Sodium 2-Acrylamido-2-Methylpropanesulfonate, and Sodium Acrylate: Synthesis and Characterization. *Macromolecules* **1996**, *29*, 5268–5272.

(39) Santanakrishnan, S.; Stach, M.; Lacik, I.; Hutchinson, R. A. Aqueous-Phase Copolymerization of N-Vinylpyrrolidone and N-Vinylformamide. *Macromol. Chem. Phys.* **2012**, *213*, 1330–1338.

(40) Gu, L.; Zhu, S.; Hrymak, A. N.; Pelton, R. H. Kinetics and Modeling of Free Radical Polymerization of N-Vinylformamide. *Polymer* **2001**, *42*, 3077–3086.

(41) Gu, L.; Zhu, S.; Hrymak, A. N.; Pelton, R. H. The Nature of Crosslinking in N-Vinylformamide Free-Radical Polymerization. *Macromol. Rapid Commun.* **2001**, *22*, 212–214.

(42) Ajiro, H.; Akashi, M. Radical Polymerization of Novel N-Substituted-N-Vinylacetamides and Regulated Polymer Structures by Bulky Substituents and Menthol Coordination. *Macromol. Wash. DC U. S.* **2009**, *42*, 489–493.

(43) Ajiro, H.; Akashi, M. Radical Polymerization of Novel N-Substituted-N-Vinylformamide Derivatives with Bulky Chiral Substituents. *J. Polym. Sci. Part Polym. Chem.* **2012**, *50*, 134–141.

(44) Yakimansky, A. V.; Menshikova, A. Yu.; Shevchenko, N. N.; Shabsels, B. M.; Bazhenova, A. G.; Sel'kin, A. V.; Sazonov, S. K.; Vedernikov, A. I.; Gromov, S. P.; Sazhnikov, V. A.; Alfimov, M. V. From Polymeric Nanoparticles to Dye-Containing Photonic Crystals: Synthesis, Self-Assembling, Optical Features, and Possible Applications. *Polym. Adv. Technol.* **2009**, *20*, 581–588.

(45) Menshikova, A.; Evseeva, T.; Shevchenko, N.; Shabsels, B.; Yakimansky, A.; Ivanchev, S. Monodisperse Particles Based on Copolymers of Methyl Methacrylate or Styrene with N-Vinylformamide. *Macromol. Symp.* **2009**, *281*, 61–68.

(46) Yamamoto, T.; Takahashi, Y. Synthesis of Hydrocolloid through Polymerization of Styrene and N-Vinyl Acetamide by AIBN. *Colloids Surf. Physicochem. Eng. Asp.* **2017**, *516*, 80–84.

(47) Yamamoto, T.; Takahashi, Y. Controlling Porous Hollow Silica Particles through Soap-Free Emulsion Polymerization with Polymer Core Particles. *Chem. Lett.* **2019**, *48*, 1229–1231.

(48) Madl, A.; Spange, S. On the Importance of the Amide-Bonded Hydrogen Atom in the Cationically Induced Oligomerization of N-Vinylamides. *Macromolecules* **2000**, *33*, 5325–5335.

(49) Madl, A.; Spange, S.; Waldbach, T.; Anders, E.; Mahr, N. Mechanistic Aspects of the Cationic Polymerization of Vinylformamide. *Macromol. Chem. Phys.* **1999**, *200*, 1495–1505.

(50) Spange, S.; Madl, A.; Eismann, U.; Utecht, J. Cationic Initiation of Oligomerization of Vinylformamide. *Macromol. Rapid Commun.* **1997**, *18*, 1075–1083.

(51) Otsu, T.; Yoshida, M. Role of Initiator-Transfer Agent-Terminator (Iniferter) in Radical Polymerizations: Polymer Design by Organic Disulfides as Iniferters. *Makromol. Chem. Rapid Commun.* **1982**, *3* (2), 127–132.

(52) Otsu, T. Iniferter Concept and Living Radical Polymerization. *J. Polym. Sci. Part Polym. Chem.* **2000**, *38* (12), 2121–2136.

(53) Chiefari, J.; Chong, Y. K. (Bill); Ercole, F.; Krstina, J.; Jeffery, J.; Le, T. P. T.; Mayadunne, R. T. A.; Meijs, G. F.; Moad, C. L.; Moad, G.; Rizzardo, E.; Thang, S. H. Living Free-Radical Polymerization by Reversible Addition–Fragmentation Chain Transfer: The RAFT Process. *Macromolecules* **1998**, *31* (16), 5559–5562.

(54) Le, T. P.; Moad, G.; Rizzardo, E.; Thang, S. H. Polymerization with Living Characteristics. WO1998001478A1, January 15, 1998.

(55) Destarac, M.; Charmot, D.; Zard, S.; Franck, X. Process for the synthesis of polymers by controlled radical polymerization using halogenated xanthates. FR2794463B1, February 25, 2005.

(56) Perrier, S. 50th Anniversary Perspective: RAFT Polymerization—A User Guide. *Macromolecules* **2017**, *50* (19), 7433–7447.

(57) Destarac, M. On the Critical Role of RAFT Agent Design in Reversible Addition-Fragmentation Chain Transfer (RAFT) Polymerization. *Polym. Rev.* **2011**, *51* (2), 163–187.

(58) Chong,) Y. K.; Krstina, J.; Le, T. P. T.; Moad, G.; Postma, A.; Rizzardo, E.; Thang, S.

H. Thiocarbonylthio Compounds [SC(Ph)S−R] in Free Radical Polymerization with Reversible Addition-Fragmentation Chain Transfer (RAFT Polymerization). Role of the Free-Radical Leaving Group (R). *Macromolecules* **2003**, *36* (7), 2256–2272.

(59) Chiefari, J.; Mayadunne, R. T. A.; Moad, C. L.; Moad, G.; Rizzardo, E.; Postma, A.; Thang, S. H. Thiocarbonylthio Compounds (SC(Z)S−R) in Free Radical Polymerization with Reversible Addition-Fragmentation Chain Transfer (RAFT Polymerization). Effect of the Activating Group Z. *Macromolecules* **2003**, *36* (7), 2273–2283.

(60) Destarac, M.; Charmot, D.; Franck, X.; Zard, S. Z. Dithiocarbamates as Universal Reversible Addition-Fragmentation Chain Transfer Agents. *Macromol. Rapid Commun.* **2000**, *21* (15), 1035–1039.

(61) Destarac, M.; Brochon, C.; Catala, J.-M.; Wilczewska, A.; Zard, S. Z. Macromolecular Design via the Interchange of Xanthates (MADIX): Polymerization of Styrene with O-Ethyl Xanthates as Controlling Agents. *Macromol. Chem. Phys.* **2002**, *203* (16), 2281–2289.

(62) Destarac, M.; Bzducha, W.; Taton, D.; Gauthier-Gillaizeau, I.; Zard, S. Z. Xanthates as Chain-Transfer Agents in Controlled Radical Polymerization (MADIX): Structural Effect of the O-Alkyl Group. *Macromol. Rapid Commun.* **2002**, *23* (17), 1049–1054.

(63) Keddie, D. J.; Guerrero-Sanchez, C.; Moad, G.; Rizzardo, E.; Thang, S. H. Switchable Reversible Addition–Fragmentation Chain Transfer (RAFT) Polymerization in Aqueous Solution, N,N-Dimethylacrylamide. *Macromolecules* **2011**, *44* (17), 6738–6745.

(64) Chen, C.-L.; Lo, Y.-H.; Lee, C.-Y.; Fong, Y.-H.; Shih, K.-C.; Huang, C.-C. Novel W(II) Complexes for Reversible Addition-Fragmentation Chain Transfer (RAFT) Polymerizations. *Inorg. Chem. Commun.* **2010**, *13* (5), 603–605.

(65) Geagea, R.; Ladeira, S.; Mazières, S.; Destarac, M. Chromium and Molybdenum Pentacarbonyl Complexes of Phosphinocarbodithioates: Synthesis, Molecular Structure and Behaviour in RAFT Polymerisation. *Chem. – Eur. J.* **2011**, *17* (13), 3718–3725.

(66) Laus, M.; Papa, R.; Sparnacci, K.; Alberti, A.; Benaglia, M.; Macciantelli, D. Controlled Radical Polymerization of Styrene with Phosphoryl- and (Thiophosphoryl)Dithioformates as RAFT Agents. *Macromolecules* **2001**, *34* (21), 7269–7275.

(67) Kulai, I.; Karpus, A.; Soroka, L.; Valyaev, D. A.; Bourdon, V.; Manoury, E.; Poli, R.;

Destarac, M.; Mazières, S. Manganese Phosphinocarbodithioate for RAFT Polymerisation with Sunlight-Induced Chain End Post-Treatment. *Polym. Chem.* **2018**, *10* (2), 267–277.

(68) Kulai, I.; Brusylovets, O.; Voitenko, Z.; Harrisson, S.; Mazières, S.; Destarac, M. RAFT Polymerization with Triphenylstannylcarbodithioates (Sn-RAFT). *ACS Macro Lett.* **2015**, *4* (8), 809–813.

(69) Demirci, S.; Kinali-Demirci, S.; Caykara, T. A New Selenium-Based RAFT Agent for Surface-Initiated RAFT Polymerization of 4-Vinylpyridine. *Polymer* **2013**, *54* (20), 5345–5350.

(70) Matioszek, D.; Mazières, S.; Brusylovets, O.; Lin, C. Y.; Coote, M. L.; Destarac, M.; Harrisson, S. Experimental and Theoretical Comparison of Addition–Fragmentation Pathways of Diseleno- and Dithiocarbamate RAFT Agents. *Macromolecules* **2019**, *52* (9), 3376–3386.

(71) Zeng, J.; Zhu, J.; Pan, X.; Zhang, Z.; Zhou, N.; Cheng, Z.; Zhang, W.; Zhu, X. Organoselenium Compounds: Development of a Universal "Living" Free Radical Polymerization Mediator. *Polym. Chem.* **2013**, *4* (12), 3453–3457.

(72) Nakamura, Y.; Kitada, Y.; Kobayashi, Y.; Ray, B.; Yamago, S. Quantitative Analysis of the Effect of Azo Initiators on the Structure of α-Polymer Chain Ends in Degenerative Chain-Transfer-Mediated Living Radical Polymerization Reactions. *Macromol. Wash. DC U. S.* **2011**, *44* (21), 8388–8397.

(73) Xu, J.; Shanmugam, S.; Corrigan, N. A.; Boyer, C. Catalyst-Free Visible Light-Induced RAFT Photopolymerization. In *Controlled Radical Polymerization: Mechanisms*; ACS Symposium Series; American Chemical Society, **2015**, *1187*, 247–267.

(74) Quinn, J. F.; Barner, L.; Barner-Kowollik, C.; Rizzardo, E.; Davis, T. P. Reversible Addition–Fragmentation Chain Transfer Polymerization Initiated with Ultraviolet Radiation. *Macromolecules* **2002**, *35* (20), 7620–7627.

(75) Allegrezza, M. L.; DeMartini, Z. M.; Kloster, A. J.; Digby, Z. A.; Konkolewicz, D. Visible and Sunlight Driven RAFT Photopolymerization Accelerated by Amines: Kinetics and Mechanism. *Polym. Chem.* **2016**, *7* (43), 6626–6636.

(76) Xu, J.; Jung, K.; Atme, A.; Shanmugam, S.; Boyer, C. A Robust and Versatile Photoinduced Living Polymerization of Conjugated and Unconjugated Monomers and Its Oxygen Tolerance. *J. Am. Chem. Soc.* **2014**, *136* (14), 5508–5519.

(77) Jung, K.; Xu, J.; Zetterlund, P. B.; Boyer, C. Visible-Light-Regulated Controlled/Living Radical Polymerization in Miniemulsion. *ACS Macro Lett.* **2015**, *4* (10), 1139–1143.

(78) Xu, J.; Jung, K.; Corrigan, N. A.; Boyer, C. Aqueous Photoinduced Living/Controlled Polymerization: Tailoring for Bioconjugation. *Chem. Sci.* **2014**, *5* (9), 3568–3575.

(79) Christmann, J.; Ibrahim, A.; Charlot, V.; Croutxe-Barghorn, C.; Ley, C.; Allonas, X. Elucidation of the Key Role of [Ru(Bpy)3]2+ in Photocatalyzed RAFT Polymerization. *ChemPhysChem* **2016**, *17* (15), 2309–2314.

(80) Shanmugam, S.; Xu, J.; Boyer, C. Exploiting Metalloporphyrins for Selective Living Radical Polymerization Tunable over Visible Wavelengths. *J. Am. Chem. Soc.* **2015**, *137* (28), 9174–9185.

(81) Xu, J.; Shanmugam, S.; Fu, C.; Aguey-Zinsou, K.-F.; Boyer, C. Selective Photoactivation: From a Single Unit Monomer Insertion Reaction to Controlled Polymer Architectures. *J. Am. Chem. Soc.* **2016**, *138* (9), 3094–3106.

(82) Xu, J.; Shanmugam, S.; Duong, H. T.; Boyer, C. Organo-Photocatalysts for Photoinduced Electron Transfer-Reversible Addition–Fragmentation Chain Transfer (PET-RAFT) Polymerization. *Polym. Chem.* **2015**, *6* (31), 5615–5624.

(83) Fu, Q.; McKenzie, T. G.; Tan, S.; Nam, E.; Qiao, G. G. Tertiary Amine Catalyzed Photo-Induced Controlled Radical Polymerization of Methacrylates. *Polym. Chem.* **2015**, *6* (30), 5362–5368.

(84) Chen, M.; MacLeod, M. J.; Johnson, J. A. Visible-Light-Controlled Living Radical Polymerization from a Trithiocarbonate Iniferter Mediated by an Organic Photoredox Catalyst. *ACS Macro Lett.* **2015**, *4* (5), 566–569.

(85) Bai, W.; Zhang, L.; Bai, R.; Zhang, G. A Very Useful Redox Initiator for Aqueous RAFT Polymerization of N-Isopropylacrylamide and Acrylamide at Room Temperature. *Macromol. Rapid Commun.* **2008**, *29* (7), 562–566.

(86) Guinaudeau, A.; Mazières, S.; Wilson, D. J.; Destarac, M. Aqueous RAFT/MADIXpolymerisation of N-Vinyl Pyrrolidone at Ambient Temperature. *Polym. Chem.* **2011**, *3* (1), 81–84.

(87) Martin, L.; Gody, G.; Perrier, S. Preparation of Complex Multiblock Copolymers via Aqueous RAFT Polymerization at Room Temperature. *Polym. Chem.* **2015**, *6* (27), 4875–4886.

(88) McKenzie, T. G.; Colombo, E.; Fu, Q.; Ashokkumar, M.; Qiao, G. G. Sono-RAFT Polymerization in Aqueous Medium. *Angew. Chem. Int. Ed.* **2017**, *56* (40), 12302–12306.

(89) Zhang, B.; Wang, X.; Zhu, A.; Ma, K.; Lv, Y.; Wang, X.; An, Z. Enzyme-Initiated Reversible Addition-Fragmentation Chain Transfer Polymerization. *Macromol. Wash. DC U. S.* **2015**, *48* (21), 7792–7802.

(90) Guégain, E.; Guillaneuf, Y.; Nicolas, J. Nitroxide-Mediated Polymerization of Methacrylic Esters: Insights and Solutions to a Long-Standing Problem. *Macromol. Rapid Commun.* **2015**, *36* (13), 1227–1247.

(91) Qiao, X. G.; Zhou, Z.; Pang, X. C.; Lansalot, M.; Bourgeat-Lami, E. Nitroxide-Mediated Polymerization of Methacrylates in the Presence of 4-Vinyl Pyridine as Controlling Comonomer. *Polymer* **2019**, *172*, 330–338.

(92) Groison, E.; Brusseau, S.; D'Agosto, F.; Magnet, S.; Inoubli, R.; Couvreur, L.; Charleux, B. Well-Defined Amphiphilic Block Copolymer Nanoobjects via Nitroxide-Mediated Emulsion Polymerization. *ACS Macro Lett.* **2012**, *1* (1), 47–51.

(93) Gillies, M. B.; Matyjaszewski, K.; Norrby, P.-O.; Pintauer, T.; Poli, R.; Richard, P. A DFT Study of R–X Bond Dissociation Enthalpies of Relevance to the Initiation Process of Atom Transfer Radical Polymerization. *Macromolecules* **2003**, *36* (22), 8551–8559.

(94) Dommanget, C.; D'Agosto, F.; Monteil, V. Polymerization of Ethylene through Reversible Addition–Fragmentation Chain Transfer (RAFT). *Angew. Chem. Int. Ed.* **2014**, *53* (26), 6683–6686.

(95) Keddie, D. J.; Moad, G.; Rizzardo, E.; Thang, S. H. RAFT Agent Design and Synthesis. *Macromolecules* **2012**, *45* (13), 5321–5342.

(96) Wayland, B. B.; Poszmik, G.; Mukerjee, S. L.; Fryd, M. Living Radical Polymerization of Acrylates by Organocobalt Porphyrin Complexes. *J. Am. Chem. Soc.* **1994**, *116* (17), 7943–7944.

(97) Debuigne, A.; Caille, J.-R.; Jérôme, R. Highly Efficient Cobalt-Mediated Radical Polymerization of Vinyl Acetate. *Angew. Chem. Int. Ed.* **2005**, *44* (7), 1101–1104.

(98) Lu, D.; Weng, Q. Spectral Mixture Analysis of the Urban Landscape in Indianapolis with Landsat ETM+ Imagery. *Photogramm. Eng. Remote Sens.* **2004**, *70* (9), 1053–1062.

(99) Debuigne, A.; Michaux, C.; Jérôme, C.; Jérôme, R.; Poli, R.; Detrembleur, C. Cobalt-Mediated Radical Polymerization of Acrylonitrile: Kinetics Investigations and DFT Calculations. *Chem. – Eur. J.* **2008**, *14* (25), 7623–7637.

(100) Piette, Y.; Debuigne, A.; Jérôme, C.; Bodart, V.; Poli, R.; Detrembleur, C. Cobalt-Mediated Radical (Co)Polymerization of Vinyl Chloride and Vinyl Acetate. *Polym. Chem.* **2012**, *3* (10), 2880–2891.

(101) Kaneyoshi, H.; Matyjaszewski, K. Radical (Co)Polymerization of Vinyl Chloroacetate and N-Vinylpyrrolidone Mediated by Bis(Acetylacetonate)Cobalt Derivatives. *Macromolecules* **2006**, *39* (8), 2757–2763.

(102) Debuigne, A.; Poli, R.; Jérôme, C.; Jérôme, R.; Detrembleur, C. Overview of Cobalt-Mediated Radical Polymerization: Roots, State of the Art and Future Prospects. *Prog. Polym. Sci.* **2009**, *34* (3), 211–239.

(103) Yamago, S.; Miyazoe, H.; Yoshida, J. Reversible Generation of Glycosyl Radicals from Telluroglycosides under Photochemical and Thermal Conditions. *Tetrahedron Lett.* **1999**, *40* (12), 2339–2342.

(104) Takagi, K.; Soyano, A.; Kwon, T. S.; Kunisada, H.; Yuki, Y. Controlled Radical Polymerization of Styrene Utilizing Excellent Radical Capturing Ability of Diphenyl Ditelluride. *Polym. Bull.* **1999**, *43* (2), 143–150.

(105) Yamago, S.; Iida, K.; Yoshida, J. Organotellurium Compounds as Novel Initiators for Controlled/Living Radical Polymerizations. Synthesis of Functionalized Polystyrenes and End-Group Modifications. *J. Am. Chem. Soc.* **2002**, *124* (12), 2874–2875.

(106) Yamago, S.; Iida, K.; Yoshida, J. Tailored Synthesis of Structurally Defined Polymers by Organotellurium-Mediated Living Radical Polymerization (TERP): Synthesis of Poly(Meth)Acrylate Derivatives and Their Di- and Triblock Copolymers. *J. Am. Chem. Soc.* **2002**, *124* (46), 13666–13667.

(107) Yamago, S. Development of Organotellurium-Mediated and Organostibine-Mediated Living Radical Polymerization Reactions. *J. Polym. Sci. Part Polym. Chem.* **2006**, *44* (1), 1–12.

(108) Yamago, S.; Ukai, Y.; Matsumoto, A.; Nakamura, Y. Organotellurium-Mediated Controlled/Living Radical Polymerization Initiated by Direct C–Te Bond Photolysis. *J. Am. Chem. Soc.* **2009**, *131* (6), 2100–2101.

(109) Yusa, S.; Yamago, S.; Sugahara, M.; Morikawa, S.; Yamamoto, T.; Morishima, Y. Thermo-Responsive Diblock Copolymers of Poly(N-Isopropylacrylamide) and Poly(N-Vinyl-2-Pyrroridone) Synthesized via Organotellurium-Mediated Controlled Radical Polymerization (TERP). *Macromolecules* **2007**, *40* (16), 5907–5915.

(110) Kwak, Y.; Goto, A.; Fukuda, T.; Kobayashi, Y.; Yamago, S. A Systematic Study on Activation Processes in Organotellurium-Mediated Living Radical Polymerizations of Styrene, Methyl Methacrylate, Methyl Acrylate, and Vinyl Acetate. *Macromolecules* **2006**, *39* (14), 4671–4679.

(111) Fan, W.; Yamago, S. Synthesis of Poly(N-Vinylamide)s and Poly(Vinylamine)s and Their Block Copolymers by Organotellurium-Mediated Radical Polymerization. *Angew. Chem. Int. Ed.* **2019**, *58* (21), 7113–7116.

(112) Nakabayashi, K.; Mori, H. Recent Progress in Controlled Radical Polymerization of N-Vinyl Monomers. *Eur. Polym. J.* **2013**, *49*, 2808–2838.

(113) Roka, N.; Kokkorogianni, O.; Kontoes-Georgoudakis, P.; Choinopoulos, I.; Pitsikalis, M. Recent Advances in the Synthesis of Complex Macromolecular Architectures Based on Poly(N-Vinyl Pyrrolidone) and the RAFT Polymerization Technique. *Polymers* **2022**, *14* (4), 701.

(114) Peng, H.; Kather, M.; Rübsam, K.; Jakob, F.; Schwaneberg, U.; Pich, A. Water-Soluble Reactive Copolymers Based on Cyclic N-Vinylamides with Succinimide Side Groups for Bioconjugation with Proteins. *Macromolecules* **2015**, *48* (13), 4256–4268.

(115) Peng, H.; Xu, W.; Pich, A. Temperature and PH Dual-Responsive Poly(Vinyl Lactam) Copolymers Functionalized with Amine Side Groups via RAFT Polymerization. *Polym. Chem.* **2016**, *7* (31), 5011–5022.

(116) Peng, H.; Rübsam, K.; Huang, X.; Jakob, F.; Karperien, M.; Schwaneberg, U.; Pich, A. Reactive Copolymers Based on N-Vinyl Lactams with Pyridyl Disulfide Side Groups via RAFT Polymerization and Postmodification via Thiol–Disulfide Exchange Reaction. *Macromolecules* **2016**, *49* (19), 7141–7154.

(117) Moad, G.; Rizzardo, E.; Thang, S. H. Living Radical Polymerization by the RAFT Process. *Aust. J. Chem.* **2005**, *58* (6), 379.

(118) Devasia, R.; Bindu, R. L.; Borsali, R.; Mougin, N.; Gnanou, Y. Controlled Radical Polymerization of N-Vinylpyrrolidone by Reversible Addition-Fragmentation Chain Transfer Process. *Macromol. Symp.* **2005**, *229* (1), 8–17.

(119) Postma, A.; Davis, T. P.; Li, G.; Moad, G.; O'Shea, M. S. RAFT Polymerization with Phthalimidomethyl Trithiocarbonates or Xanthates. On the Origin of Bimodal Molecular Weight Distributions in Living Radical Polymerization. *Macromolecules* **2006**, *39* (16), 5307–5318.

(120) Wan, D.; Satoh, K.; Kamigaito, M.; Okamoto, Y. Xanthate-Mediated Radical Polymerization of N-Vinylpyrrolidone in Fluoroalcohols for Simultaneous Control of Molecular Weight and Tacticity. *Macromolecules* **2005**, *38* (25), 10397–10405.

(121) Guinaudeau, A.; Coutelier, O.; Sandeau, A.; Mazières, S.; Nguyen Thi, H. D.; Le Drogo, V.; Wilson, D. J.; Destarac, M. Facile Access to Poly(N-Vinylpyrrolidone)-Based Double Hydrophilic Block Copolymers by Aqueous Ambient RAFT/MADIX Polymerization. *Macromolecules* **2014**, *47* (1), 41–50.

(122) Wang, Y.; Wang, M.; Bai, L.; Zhang, L.; Cheng, Z.; Zhu, X. Facile Synthesis of Poly(N-Vinyl Pyrrolidone) Block Copolymers with "'more-Activated'" Monomers by Using Photoinduced Successive RAFT Polymerization. *Polym. Chem.* **2020**, *11* (12), 2080–2088.

(123) Góis, J. R.; Costa, J. R. C.; Popov, A. V.; Serra, A. C.; Coelho, J. F. J. Synthesis of Well-Defined Alkyne Terminated Poly(N-Vinyl Caprolactam) with Stringent Control over the LCST by RAFT. *RSC Adv.* **2016**, *6* (21), 16996–17007.

(124) Wan, D.; Zhou, Q.; Pu, H.; Yang, G. Controlled Radical Polymerization of N-Vinylcaprolactam Mediated by Xanthate or Dithiocarbamate. *J. Polym. Sci. Part Polym. Chem.* **2008**, *46* (11), 3756–3765.

(125) Shao, L.; Hu, M.; Chen, L.; Xu, L.; Bi, Y. RAFT Polymerization of N-Vinylcaprolactam and Effects of the End Group on the Thermal Response of Poly(N-Vinylcaprolactam). *React. Funct. Polym.* **2012**, *72* (6), 407–413.

(126) Li, R.; An, Z. Achieving Ultrahigh Molecular Weights with Diverse Architectures for Unconjugated Monomers through Oxygen-Tolerant Photoenzymatic RAFT Polymerization. *Angew. Chem. Int. Ed.* **2020**, *59* (49), 22258–22264.

(127) Etchenausia, L.; Rodrigues, A. M.; Harrisson, S.; Deniau Lejeune, E.; Save, M. RAFT Copolymerization of Vinyl Acetate and N-Vinylcaprolactam: Kinetics, Control, Copolymer Composition, and Thermoresponsive Self-Assembly. *Macromol. Wash. DC U. S.* **2016**, *49* (18), 6799–6809.

(128) Hurtgen, M.; Liu, J.; Debuigne, A.; Jerome, C.; Detrembleur, C. Synthesis of Thermo-Responsive Poly(N-Vinylcaprolactam)-Containing Block Copolymers by Cobalt-Mediated Radical Polymerization. *J. Polym. Sci. Part Polym. Chem.* **2012**, *50* (2), 400–408.

(129) Kermagoret, A.; Fustin, C.-A.; Bourguignon, M.; Detrembleur, C.; Jerome, C.; Debuigne, A. One-Pot Controlled Synthesis of Double Thermoresponsive N-Vinylcaprolactam-Based Copolymers with Tunable LCSTs. *Polym. Chem.* **2013**, *4*, 2575–2583.

(130) Miao, X.; Zhu, W.; Zhang, Z.; Zhang, W.; Zhu, X.; Zhu, J. Photo-Induced Cobalt-Mediated Radical Polymerization of Vinyl Acetate. *Polym. Chem.* **2014**, *5* (2), 551–557.

(131) Fan, W.; Nakamura, Y.; Yamago, S. Synthesis of Multivalent Organotellurium Chain-Transfer Agents by Post-Modification and Their Applications in Living Radical Polymerization. *Chem. – Eur. J.* **2016**, *22* (47), 17006–17010.

(132) Yamago, S.; Ukai, Y.; Matsumoto, A.; Nakamura, Y. Organotellurium-Mediated Controlled/Living Radical Polymerization Initiated by Direct C–Te Bond Photolysis. *J. Am. Chem. Soc.* **2009**, *131* (6), 2100–2101.

(133) Singh, P.; Srivastava, A.; Kumar, R. Synthesis of Amphiphilic Poly(N-Vinylcaprolactam) Using ATRP Protocol and Antibacterial Study of Its Silver Nanocomposite. *J. Polym. Sci. Part Polym. Chem.* **2012**, *50* (8), 1503–1514.

(134) Vivek M.; Rajesh K. Cyclic Polymer of N-Vinylpyrrolidone via ATRP Protocol: Kinetic Study and Concentration Effect of Polymer on Click Chemistry in Solution. *Polym. Sci. Ser. B Polym. Chem.* **2019**, *61* (6), 753–761.

(135) Shi, L.; Chapman, T. M.; Beckman, E. J. Poly(Ethylene Glycol)-Block-Poly(N-Vinylformamide) Copolymers Synthesized by the RAFT Methodology. *Macromolecules* **2003**, *36* (7), 2563–2567.

(136) Lou, Y.; Shi, D. J.; Dong, W. F.; Chen, M. Q. Synthesis and Self-Assemble Behavior of Block Copolymerization of Vinyl Acetate and N-Vinylacetamide. *Adv. Mater. Res.* **2013**, *645*, 10–14.

(137) Peng, H.; Xu, W.; Pich, A. Temperature and PH Dual-Responsive Poly(Vinyl Lactam) Copolymers Functionalized with Amine Side Groups via RAFT Polymerization. *Polym. Chem.* **2016**, *7* (31), 5011–5022.

(138) Kawatani, R.; Kelland, M. A.; Ajiro, H. Design of a Rigid Side Chain for Poly(N-Vinylamide) Derivatives Bearing an Alkenyl Group and Evaluation of Their Ability to Inhibit Tetrahydrofuran Hydrate Crystal Growth. *J. Appl. Polym. Sci.* **2020**, *137* (38), 49154.

(139) Dréan, M.; Guégan, P.; Detrembleur, C.; Jérôme, C.; Rieger, J.; Debuigne, A. Controlled Synthesis of Poly(Vinylamine)-Based Copolymers by Organometallic-Mediated Radical Polymerization. *Macromolecules* **2016**, *49* (13), 4817–4827.

(140) Stiernet, P.; Dréan, M.; Jérôme, C.; Midoux, P.; Guégan, P.; Rieger, J.; Debuigne, A. Tailor-Made Poly(Vinylamine)s via Thermal or Photochemical Organometallic Mediated Radical Polymerization. In *Reversible Deactivation Radical Polymerization: Mechanisms and Synthetic Methodologies*; ACS Symposium

Series; American Chemical Society, **2018**, *1284*, 349–363.

(141) Fan, W.; Yamago, S. Synthesis of Poly(N-Vinylamide)s and Poly(Vinylamine)s and Their Block Copolymers by Organotellurium-Mediated Radical Polymerization. *Angew. Chem. Int. Ed.* **2019**, *58* (21), 7113–7116.

CHAPTER 1.

RAFT POLYMERIZATION OF *N*-METHYL-*N*-VINYLACETAMIDE AND RELATED DOUBLE HYDROPHILIC BLOCK COPOLYMERS

1.1 INTRODUCTION

N-methyl-*N*-vinylacetamide (NMVA) is one of the three commercially available acyclic *N*-vinylamide monomers, along with *N*-vinylformamide (NVF) and *N*-vinylacetamide (NVA). Its resulting polymer, PNMVA, is used as kinetic hydrate inhibitor,[1–4] in optical lenses,[5] in biomedical fields,[6–9] or in batteries as polyelectrolyte multilayers.[10] However, as stated earlier in the general introduction, the controlled radical polymerization of acyclic *N*-vinylamides has been successfully reported, but on a much smaller scale compared to their cyclic counterparts.

In the case of NMVA, the first report on its controlled radical polymerization was by the team of Prof. Debuigne and coworkers using Cobalt-Mediated Radical Polymerization (CMRP) in 2012.[11] The polymerization of NMVA was conducted in bulk and a satisfying control was obtained with molecular weight M_n values up until 25 kg mol^{-1} while maintaining dispersity $Đ$ values below 1.3 for monomer conversion going up to around 60% after 14h. More recently, Prof. Debuigne's team went further to the hydrolysis of NMVA-based polymers and copolymers to give polymers containing secondary amines, poly(*N*-methylvinylamine), in addition to the successful control of NVA polymerization.[12,13] The polymerization of NMVA, NVA, and NVF for the first time have recently also been successfully conducted and

reported by the team of Prof. Yamago using Tellurium-mediated Radical Polymerization (TERP).[14] Excellent control over the polymerization of NMVA was achieved for low M_n with a $M_{n,NMR}$ of 9700 g mol^{-1} ($M_{n,th}$ = 9500 g mol^{-1}) and $Đ$ of 1.08 and for the very high monomer conversion of 95% after 7h. Despite a deviation in measured $M_{n,SEC}$ values compared to expected, probably due to analysis conditions according to the authors, the good control is very likely to have been kept for higher molecular weights up until 43 kg mol^{-1} with dispersities maintained below 1.3.

Surprisingly, no study on the reversible addition-fragmentation chain transfer (RAFT) polymerization of NMVA can be found in the literature, despite the technique being very user-friendly and suitable for the synthesis of block copolymers. This opportunity drove me to choose NMVA as the first example for my study on the controlled polymerization of acyclic *N*-vinylamides.

In this chapter, using size-exclusion chromatography (SEC), ^{1}H NMR spectroscopy and mass spectrometry, I establish that conditions for an efficient control of molar masses (M_n) and dispersities ($Đ$) of poly(*N*-methyl-*N*-vinylacetamide) (PNMVA) can be obtained by means of appropriate xanthate and dithiocarbamate RAFT agents, provided that suitable concentrations of initiator and RAFT agent and polymerization temperature are chosen. Consequently, two types of PNMVA-based double hydrophilic copolymers are synthesized, namely poly(ethylene oxide)-*b*-poly(*N*-methyl-*N*-vinylacetamide) (PEO-b-PNMVA) and poly(*N*-isopropylacrylamide)-*b*-poly(*N*-methyl-*N*-vinylacetamide) (PNIPAAm-*b*-PNMVA). Finally, the temperature-induced assembly of PNIPAAm-*b*-PNMVA in water is discussed.

1.2 RESULTS AND DISCUSSION

1.2.1 Homopolymerization of NMVA

1.2.1.1 Reaction conditions

I first explored the scope and limitations of the RAFT polymerization of NMVA with two xanthates and two dithiocarbamate chain transfer agents (CTA) of general formula R-S(C=S)-Z (Scheme 1-1).

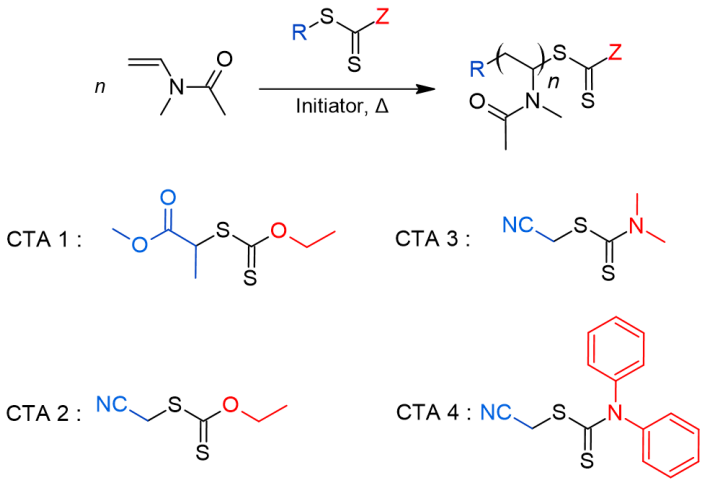

Scheme 1-1. General scheme of RAFT polymerization of NMVA using xanthate and dithiocarbamate CTAs

In an ideal RAFT polymerization, the CTA regulates the molar masses of polymers without noticeable impact on the overall rate of polymerization. However, it is common to observe some retardation effect and slower kinetics when the concentration in CTA is increased.[15–17] Therefore, I decided to study the impact of the CTA concentration on monomer conversion using methyl 2-((ethoxycarbonothioyl)thio)propanoate (CTA1), a well-known xanthate used to control the polymerization of *N*-vinyllactams.[18–20] Polymerizations of NMVA were performed in bulk, at 65°C in presence of AIBN (29 mmol L^{-1}) for 16 h as a reference, with five different concentrations of CTA1 ranging from 19.2 to 521 mmol L^{-1} (respectively corresponding to theoretical M_n ($M_{n,th}$) of 50000 and 2000 g mol^{-1}), as

represented in Figure 1-1a. CTA1 was found to have a marked impact on monomer conversion, which decreased significantly when increasing CTA1 concentration. While the acyclic *N*-vinylamide NMVA conversion reached 63% conversion when working at $[CTA1]_0$= 19.2 mmol L^{-1}, which is a bit lower compared to the 78% conversion obtained without CTA, only 10% conversion was obtained with $[CTA1]_0$ = 521 mmol L^{-1}. In contrast, the polymerization of the cyclic *N*-vinylamide NVP under the same conditions was much faster and reached ~80% conversion after only 1h without or with CTA1 in the range of 19.2-48.3 mmol L^{-1} (Figure 1-1b). Compared to NVP, the more pronounced retardation observed with NMVA and its lower intrinsic reactivity are mainly responsible for the difficulties encountered to establish suitable conditions for a RAFT study. Indeed, k_p^2/k_t values for bulk polymerization are virtually 50 times lower for NMVA polymerization than for NVP based on the works of Fischer[21] and Lacik [22,23] In addition to these factors, a low value of 0.25 was reported for the AIBN efficiency (*f*) in bulk polymerization of NMVA at 65°C.[21] Based on results shown in Figure 1-1a, under typical concentration conditions for RAFT polymerization ($[AIBN]_0/[CTA1]_0$=0.1), NMVA conversion should lie in the 10-15% range after 16h. From this observation, the only possibility to overcome this drawback and reach an acceptable rate of polymerization was to keep a low CTA1 concentration of 19.2 mmol L^{-1}, corresponding to $M_{n,th}$ = 50000 g mol^{-1} and an abnormally high [initiator]/[CTA] ratio of 1.49/1 in order to compensate the slow overall kinetics of polymerization and low initiator efficiency.

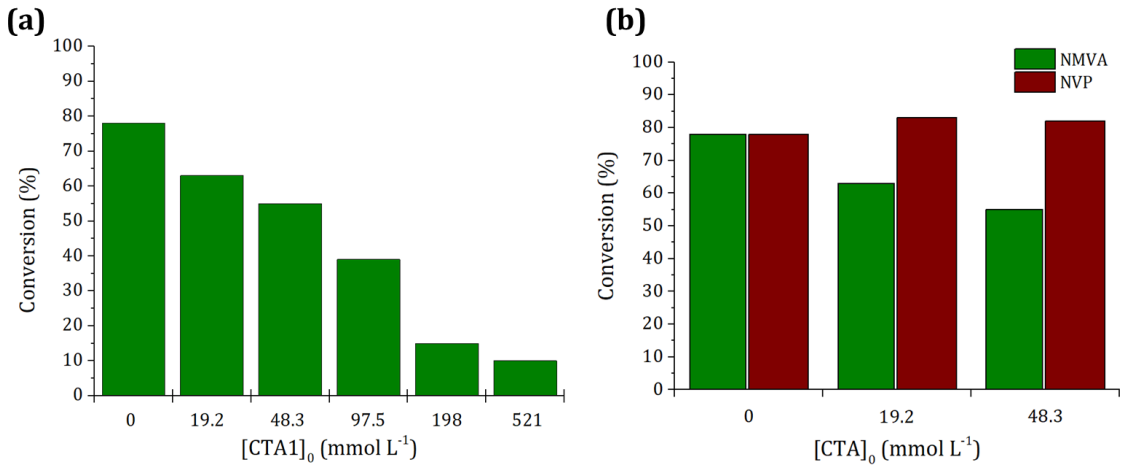

Figure 1-1. Effect of CTA1 concentration on monomer conversion in bulk RAFT polymerization of **(a)** NMVA after 16 h at 65°C and **(b)** its comparison with bulk RAFT polymerization of NVP after 1h at 65°C.

Under these polymerization conditions, I followed the evolution of M_n and dispersity $Đ$ with conversion. As it can be observed in Figure 1-2a, M_n increased linearly in the first 20% of NMVA conversion, but with values approximately twice as high as expected for a controlled RAFT process, before a slight downward change of slope occurred between 20 and 30% conversion. At this stage, the reaction was intentionally stopped due to the observed lack of control of M_n. $Đ$ values were kept below 1.3 up to 30% conversion (Figure 1-2a and Table 1-1). The observed deviations of M_n values suggested that CTA1 was either only partially reacted, or partially degraded at an early stage of the polymerization. All my attempts to detect possibly remaining CTA1 by SEC analysis of the crude mixture with RI or UV detector failed, as well as with ^{1}H NMR analysis, considering the low CTA1 concentration in the reaction mixture.

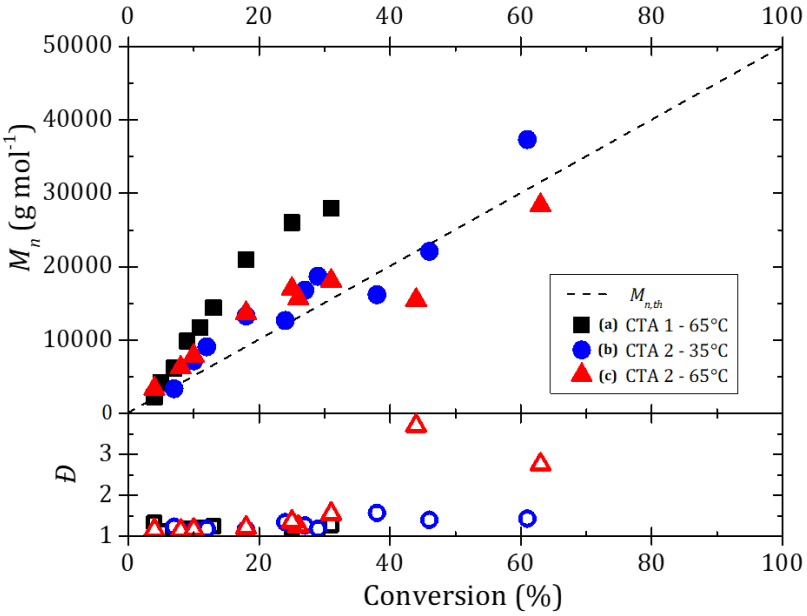

Figure 1-2. Evolution of M_n and $Đ$ for the RAFT polymerization of NMVA in bulk, using **(a)** CTA1 at 65°C (AIBN initiation), **(b)** CTA2 at 65°C, and **(c)** CTA2 at 35°C (V-70 initiation) for $M_{n,th}$ = 50 kg mol^{-1}. $[NMVA]_0$= 9.69 mol L^{-1}; $[Initiator]_0$= 29 mmol L^{-1} and $[CTA]_0$= 19 mmol L^{-1}.

Table 1-1. RAFT polymerization of NMVA with CTA1 at 65°C

Entry	CTA	Targeted M_n (g mol^{-1})	Conversion [a] (%)	$M_{n,th}$ [b] (g mol^{-1})	$M_{n,SEC}$ [c] (g mol^{-1})	$Đ$
1	CTA 1	50000	4	2206	2300	1.33
2			5	2706	4200	1.12
3			7	3705	6200	1.16
4			9	4704	9900	1.18
5			11	5703	11700	1.21
6			13	6702	14400	1.25
7			18	9199	21000	1.09
8			25	12695	26000	1.20
9			31	15692	28000	1.27

[a]calculated by ^{1}H NMR, [b]$M_{n,th}$ = $[NMVA]_0/[CTA]_0 \times M_{NMVA} \times conv. + M_{CTA}$, [c]$M_{n,SEC}$ measured with a RI-MALS detection. M_{CTA1}=208 g mol^{-1}.

I considered a second xanthate with a cyanomethyl leaving group (CTA2, namely *S*-cyanomethyl *O*-ethyl carbonodithioate), to help me understand whether the selected R-group could be responsible for this poor control. The obtained $M_{n,SEC}$ values using CTA2 were comparatively much closer to theory with slightly higher values than expected below 30% and slightly lower ones above (Figure 1-2b and Table 1-2, entries 11-19) compared to CTA1. From these results, I concluded that CTA2 acted a better suited RAFT agent than CTA1 (Figure 1-2). At this stage, it is not yet clear why the R-group of the xanthate had such an impact on the regulation of M_n, apart from the possibly greater propensity of the cyanomethyl group to start polymer chains during the reinitiation process compared to the 2-ethylpropanoate group of CTA1. Dispersities were less than 1.4 below 30% conversion before an abrupt rise up to 3.7 with the concomitant formation of a bimodal population as observed on SEC traces (Figure 1-3). The terminal xanthate group of RAFT-derived polyvinylpyrrolidone (PVP) is known to be thermally unstable.[16] Because NMVA is structurally similar to VP, it is likely that PNMVA chains also face thermal degradation of the xanthate-end group for prolonged polymerization times, leading to an increase of dispersity. In an attempt to minimize side reactions, NMVA was polymerized at 35°C with CTA2 and 2,2'-azobis(4-methoxy-2,4-dimethylvaleronitrile) as initiator (V-70) (Figure 1-2c and Table 1-2 entries 1-10).

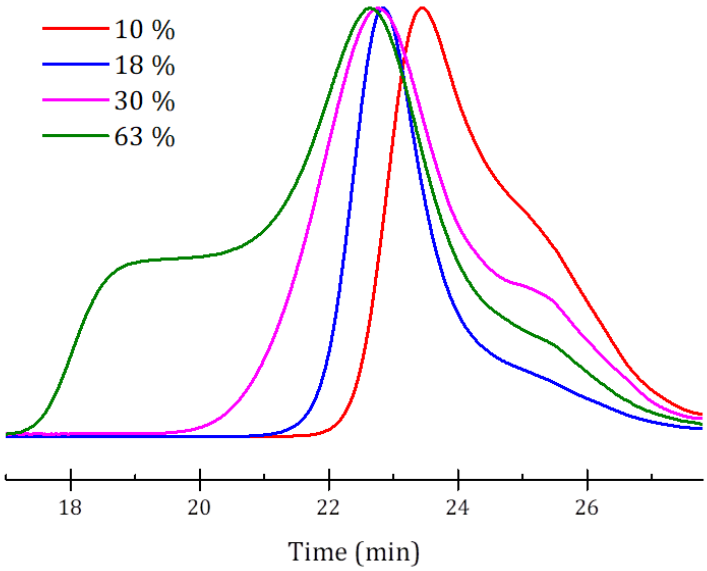

Figure 1-3. Evolution of SEC-RI traces of PNMVA with NMVA conversion for a RAFT polymerization with CTA2 at 65°C.

Below 30% conversion, I observed a similar evolution of $M_{n,SEC}$ and $Đ$ at 35 and 65°C (Figure 1-2 and Table 1-2). At higher conversion, in contrast with results observed at 65°C, $Đ$ values were maintained below 1.5 at 35°C with a gradual increase over the course of the polymerization, mainly due to an increased proportion of azo-derived chains. At the same time, $M_{n,SEC}$ continued to increase with NMVA conversion and still fitted reasonably well the expected values. These results highlighted the beneficial selection of a lower temperature of 35°C.

Table 1-2. RAFT polymerization of NMVA with CTA2 at 35°C (V-70 initiator) and 65°C (AIBN initiation)

Entry	Targeted M_n (g mol^{-1})	Temperature (°C)	Conversion [a] (%)	$M_{n,th}$ [b] (g mol^{-1})	$M_{n,SEC}$ [c] (g mol^{-1})	$Đ$
1	50000	35°C	7	3658	3400	1.23
2			10	5156	7200	1.16
3			12	6155	9100	1.18
4			18	9152	13300	1.17
5			24	12149	12700	1.34
6			27	13647	16800	1.26
7			29	14646	18700	1.18
8			38	19142	16200	1.57
9			46	23138	22100	1.40
10			61	30630	37300	1,43
11	50000	65°C	4	2159	3400	1.15
12			8	4157	6300	1.14
13			10	5156	7900	1.16
14			18	9152	13700	1.21
15			25	12648	17000	1.36
16			26	13148	15700	1.24
17			31	15645	18100	1.55
18			44	22139	15500	3.71
19			63	31629	28400	2.76

[a]calculated by ^{1}H NMR, [b]$M_{n,th}$ = $[NMVA]_0/[CTA]_0 \times M_{NMVA} \times conv. + M_{CTA}$, [c]$M_{n,SEC}$ measured with a RI-MALS detection. M_{CTA2}=161 g mol^{-1}.

The controlled character of the polymerization was also illustrated with SEC traces shifted towards lower elution time with conversion (Figure 1-4a). At 35°C, the shape of the chromatograms was monomodal all along the polymerization (Figure 1-4a) while at 65°C, the shape of the chromatograms rapidly evolved with monomer conversion to become bimodal and very broad (Figure 1-3). In Figure 1-4b, the clear differences of SEC traces for a similar conversion of around 60% (Table

1-2, entries 10 and 19) for 35°C and 65°C polymerization can be observed, once again highlighting a better control at low temperature.

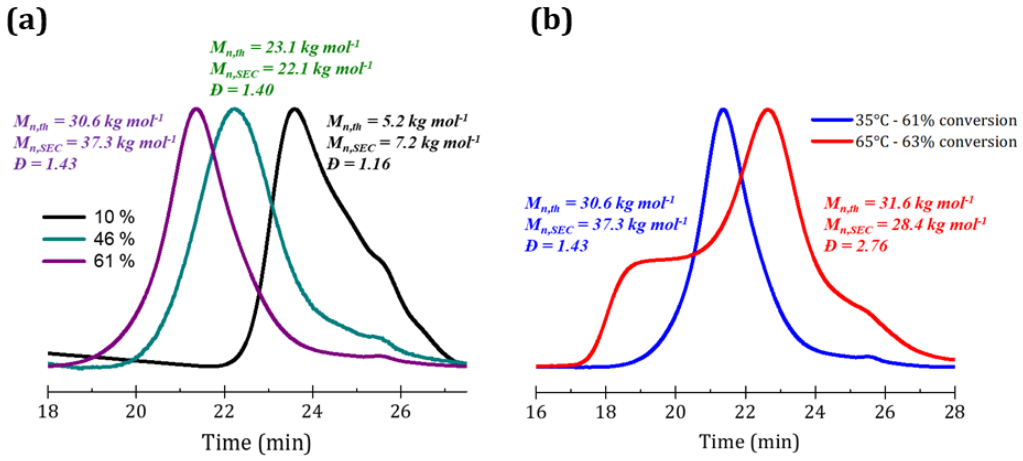

Figure 1-4. SEC traces of **(a)** NMVA polymerization at 35°C using CTA2 and **(b)** the comparison of PNMVA obtained at 35°C and 65°C for similar monomer conversions using CTA2.

At this point, I decided to compare all CTAs 1-4 at 35°C in RAFT bulk polymerization of NMVA for a $M_{n,th}$ = 50000 g mol^{-1} with $[V\text{-}70]_0$ = 29 mmol L^{-1}. Similarly to the previous observations at 65°C, the evolution of $M_{n,SEC}$ with conversion for CTA1 deviated rapidly from the expected values. Dispersities were slightly lower than the ones obtained with CTA2 (Figure 1-5a and Table 1-3).

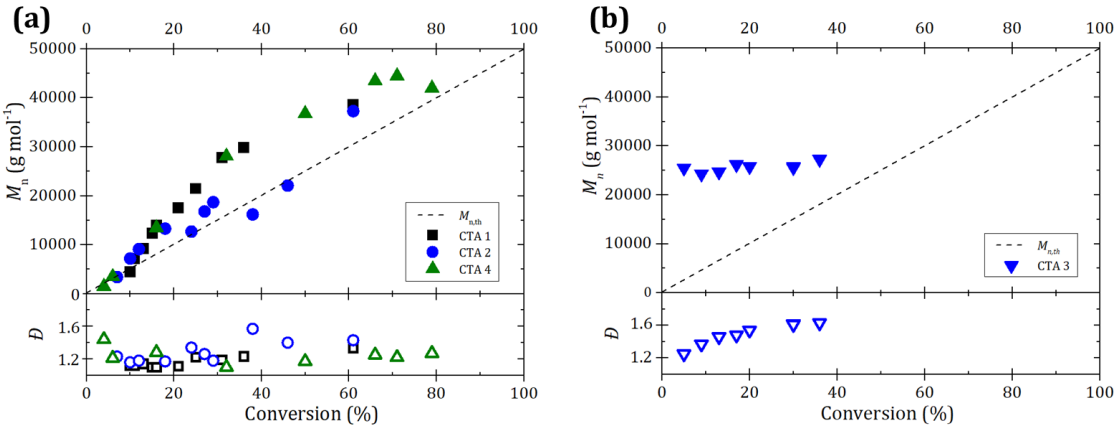

Figure 1-5. Evolution on M_n and Đ with NMVA conversion at 35°C for **(a)** CTA1, CTA2, CTA4 and **(b)** CTA3.

Table 1-3. RAFT polymerization of NMVA at 35°C with xanthate CTAs 1 and 2

Entry	CTA	Targeted M_n (g mol^{-1})	Time (h)	Conversion [a] (%)	$M_{n,th}$ [b] (g mol^{-1})	$M_{n,SEC}$ [c] (g mol^{-1})	$Đ$
1	-	-	2	26	-	350000 [d]	2.36 [d]
2			4	46		285000 [d]	3.13 [d]
3			8	50		136000 [d]	2.86 [d]
4			24	57		156000 [d]	2.94 [d]
5	CTA1	50000	0.5	10	5155	4500	1.12
6			1	11	5654	7200	1.12
7			1,5	13	6653	9200	1.14
8			2	15	7652	12400	1.10
9			2.5	16	8152	14000	1.10
10			3	21	10649	17500	1.11
11			4	25	12647	21500	1.22
12			6	31	15644	27800	1.19
13			8	36	18141	29900	1.23
14			16	61	30629	38600	1.33
15	CTA2	50000	2	7	3658	3400	1.23
16			3	10	5156	7200	1.16
17			4	12	6155	9100	1.18
18			6	18	9152	13300	1.17
19			8	24	12149	12700	1.34
20			16	27	13647	16800	1.26
21			24	29	14646	18700	1.18
22			32	38	19142	16200	1.57
23			40	46	23138	22100	1.40
24			48	61	30630	37300	1.43

[a]calculated by ^{1}H NMR, [b]$M_{n,th}$ = $[NMVA]_0/[CTA]_0 \times M_{NMVA} \times conv. + M_{CTA}$, [c]$M_{n,SEC}$ measured with a RI-MALS detection. [d]Measured with a set of two KD-804 and KD-805L (SHODEX) columns; M_{CTA1}=208 g mol^{-1}; M_{CTA2}=161 g mol^{-1}.

In addition to xanthate CTAs, I considered dithiocarbamates due to their known ability to control RAFT polymerization of *N*-vinyllactams.[24] With cyanomethyl dimethylcarbamodithioate (CTA3) (Figure 1-5b and Table 1-4 entries 1-8), no control was observed on the molar masses and dispersities due to a too low chain transfer constant (C_{tr}). In contrast, cyanomethyl diphenylcarbodithioate (CTA4) led to a much better control of NMVA polymerization, with very similar results to the ones obtained with CTA1. The evolution of M_n with NMVA conversion almost perfectly fitted the ones obtained with CTA1, with dispersities less than 1.3 between 6% and 79% monomer conversion (Figure 1-5a and Table 1-4 entries 9-16). As previously reported,[25] replacing Z = NMe_2 (CTA3) by Z = $N(Ph)_2$ (CTA4) allows an increase of C_{tr} of the dithiocarbamate CTA thanks to the delocalization of the nitrogen's lone pair on the aromatic rings, increasing the C=S double bond character of the RAFT agent as observed for other monomers.

Table 1-4. RAFT polymerization of NMVA at 35°C with dithiocarbamate CTAs 3 and 4

Entry	CTA	Targeted M_n (g mol^{-1})	Time (h)	Conversion [a] (%)	$M_{n,th}$ [b] (g mol^{-1})	$M_{n,SEC}$ [c] (g mol^{-1})	$Đ$
1	CTA3	50000	1	5	2658	25500	1.25
2			1.5	9	4656	24300	1.37
3			2	13	6654	24700	1.46
4			3	17	8652	26200	1.48
5			4	20	10150	25800	1.54
6			6	30	15145	25800	1.62
7			8	30	15145	25600	1.61
8			16	36	18142	27300	1.63
9	CTA4	50000	1	4	2306	1500	1.44
10			2	6	3305	3500	1.21
11			4	16	8300	13500	1.28
12			6	32	16292	28100	1.10
13			8	50	25283	36800	1.17
14			16	66	33275	43500	1.25
15			24	71	35772	44500	1.22
16			40	79	39768	42000	1.27

[a]calculated by ^{1}H NMR, [b]$M_{n,th}$ = $[NMVA]_0/[CTA]_0 \times M_{NMVA} \times conv. + M_{CTA}$, [c]$M_{n,SEC}$ measured with a RI-MALS detection. M_{CTA3}=160 g mol^{-1}; M_{CTA4}=284 g mol^{-1}.

During the RAFT polymerization of NMVA with CTA1 at 35°C, I observed a higher rate of polymerization than for CTA2, with 61% NMVA conversion obtained after 16 h while CTA2 only led to 27% conversion (Table 1-3, entries 14 and 20, and Figure 1-6). With CTA4, the rate of polymerization in the first four hours was similar to that obtained with CTA2, before an unexpected and unexplained acceleration was observed (Figure 1-6).

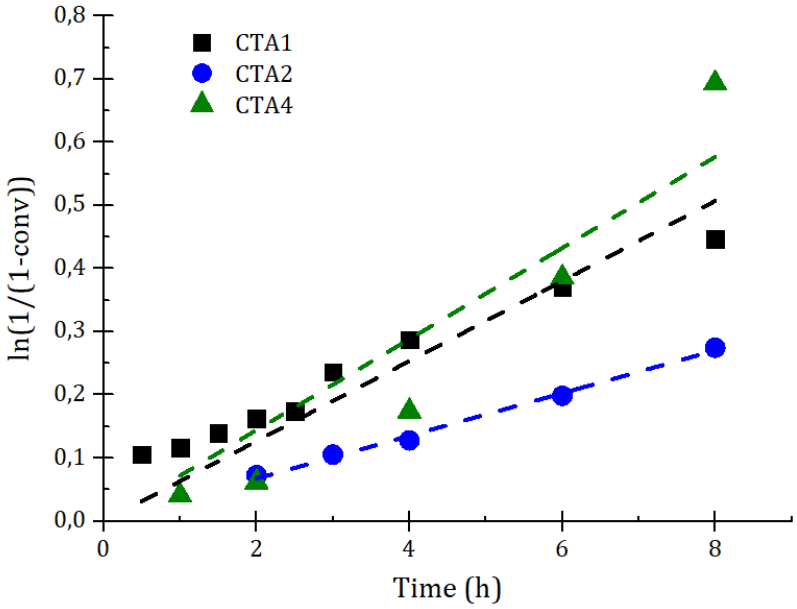

Figure 1-6. Semi-logarithmic kinetic plot for CTA1, CTA2 and CTA4 at 35°C.

1.2.1.2 Chain-end fidelity

One of the key features of RAFT polymerization is its capacity to be used in block copolymerization, with an excellent chain-end fidelity as a prerequisite. In order to confirm this, I synthesized a series of low molar mass PNMVA with a theoretical mass of 50000 g moL^{-1} and stopped the reaction after short reaction times (which corresponded to polymer samples in the conversion range of 6-15%). These different PNMVA-CTAs were analyzed by ^{1}H NMR and mass spectrometry and used as macro-CTAs in chain extension experiments (*vide infra*).

In order to get further insight of the behavior of CTA1 at 65°C, I first synthesized a PNMVA-CTA1 at 65°C with $[AIBN]_0$= 29 mmol L^{-1} and stopped the polymerization after 10% conversion to get a polymer with M_n of about 5000 g mol^{-1} for a $M_{n,th}$ of 50000 g mol^{-1}. A precipitated PNMVA-CTA1 of $M_{n,SEC}$ = 7000 g mol^{-1} and $Đ$ = 1.05 was analyzed by ^{1}H NMR and MALDI-TOF MS to observe the chain-end groups. On the ^{1}H NMR spectrum (Figure 1-7), it was possible to detect the alpha methylene protons relative to oxygen of the xanthate terminal group at 4.6-4.7 ppm, but not the CH proton of the terminal NMVA next to sulfur, presumably due to the too high M_n value of the polymer.

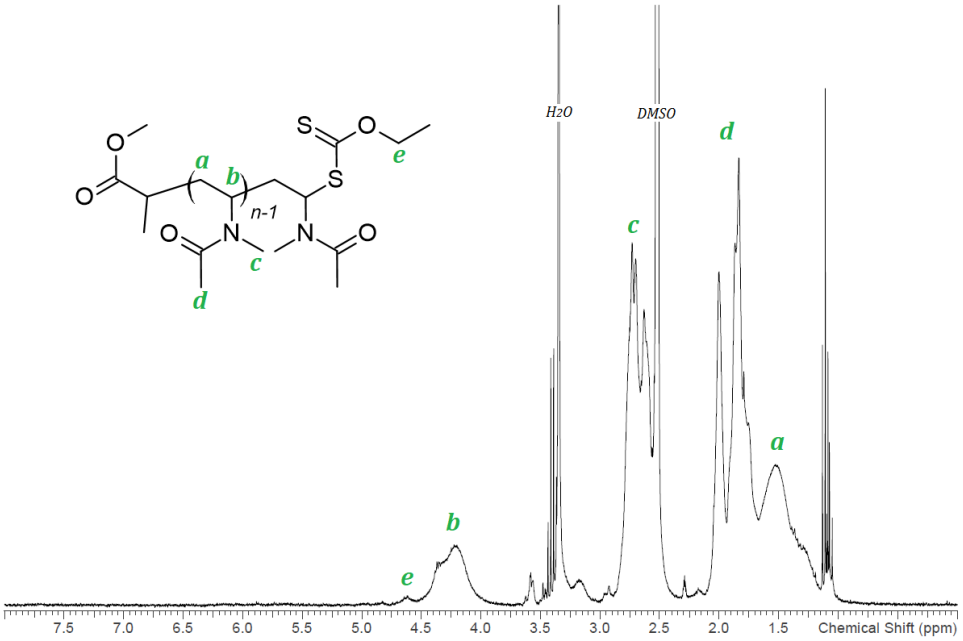

Figure 1-7. ^{1}H NMR spectrum of PNMVA-CTA1. $M_{n,SEC}$ = 7000 g mol^{-1}, $Đ$ = 1.05. Measured on a 300MHz apparatus.

Hence, I turned to MALDI-TOF MS analysis (Figure 1-8a) to observe the different populations obtained at the end of the polymerization and detected 4 populations, with a main population A with a general formula $C_4H_7O_2$-$(C_5H_9NO)_n$-C_5H_8NO,Na^+ corresponding to the sodium adduct of a PNMVA initiated by the R-group of CTA1, but terminated by a double bond, presumably from the degradation of the xanthate chain-end during the analysis, as often observed on PVP controlled with a xanthate.[3] A second population B was identified with a general formula of C_4H_6N-$(C_5H_9NO)_n$-C_5H_8NO,Na^+ corresponding to the sodium adduct of a PNMVA initiated by an AIBN fragment and also terminated by a double bond, which is not surprising considering the relatively high [AIBN]/[CTA1] required in those experimental conditions. The two other populations could not be identified and did not correspond to the combination of PNMVA initiated by either the R-group of CTA1 or AIBN-derived cyanoisopropyl and terminated by SH, H or the xanthate group that can be expected form a RAFT polymerization.

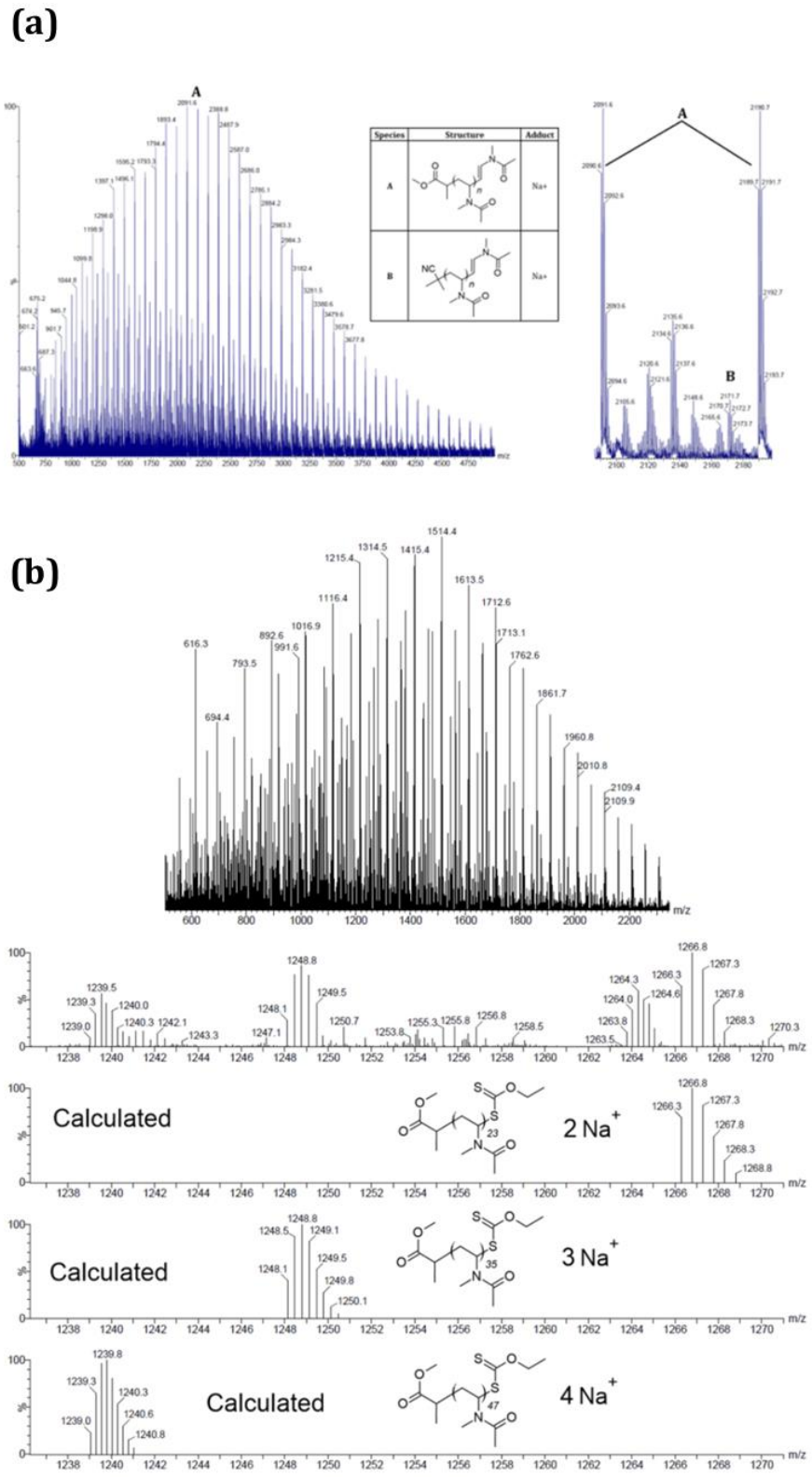

Figure 1-8. (a) MALDI-TOF MS spectrum of PNMVA-CTA1 **(b)** ESI-MS spectrum (top) and comparison of a zoom portion with calculated structures (bottom).

I decided to turn to ESI-MS analysis (Figure 1-8b), which was established as an overall better technique to reveal Z end-groups of RAFT polymers than MALDI-TOF MS.[26] ESI-MS spectrum was very complex to analyze with an overlap of several populations. However, upon careful analysis and simulated MS spectra, I was able to observe the same $C_4H_7O_2$-$(C_5H_9NO)_n$-$C_3H_5S_2O$ population as mainly a bis-Na^+ cation, and also as tris-, and tetra Na^+ cations overlapping, confirming this time the presence of a xanthate at the end of the main PNMVA population, as expected for a RAFT polymerization. Surprisingly the population initiated by cyanoisopropyl radicals detected by MALDI-TOF MS could not be detected among the other small populations on the spectrum, but considering the complexity of the spectrum it is possible that this population also overlaps with other signals making its detection virtually impossible.

Then, I synthesized and characterized after precipitation a PNMVA-CTA4 of lower molar mass obtained by bulk polymerization of NMVA in presence of CTA4 at 35°C with $[V\text{-}70]_0$= 29 mmol L^{-1}, for which the polymerization was stopped after 6% conversion with $M_{n,th}$ = 50000 g mol^{-1}. With 10 aromatic protons easily detected by ^1H NMR (Figure 1-9), the Z-group of CTA4 was clearly observed through the aromatic signals between 7.2 and 7.5 ppm. By relative integration of the aromatic signals compared with the methylene protons of the polymer chain (*b*) at 4.5 ppm I measured a $M_{n,NMR}$ = 2100 g mol^{-1} in agreement with $M_{n,th}$ = 2500 g mol^{-1} calculated from NMVA conversion and $M_{n,SEC}$ = 2200 g mol^{-1}. ESI-MS analysis of PNMVA-CTA4 (Figure 1-10) presented one main population A corresponding to the expected Na^+ adduct of a PNMVA capped by CH_2CN and $S(C=S)NPh_2$ groups from CTA4. Its corresponding bis-Na^+ charged population (Figure 1-10, population B) was observed as well. A small secondary population C corresponding to PNMVA capped by CH_2CN on one side, and terminated by a double bond (Figure 1-10, population C) was also detected. Some other populations of smaller intensity were observed, but their nature could not be determined. Again, PNMVA chains initiated by V-70 radicals were expected, but not detected.

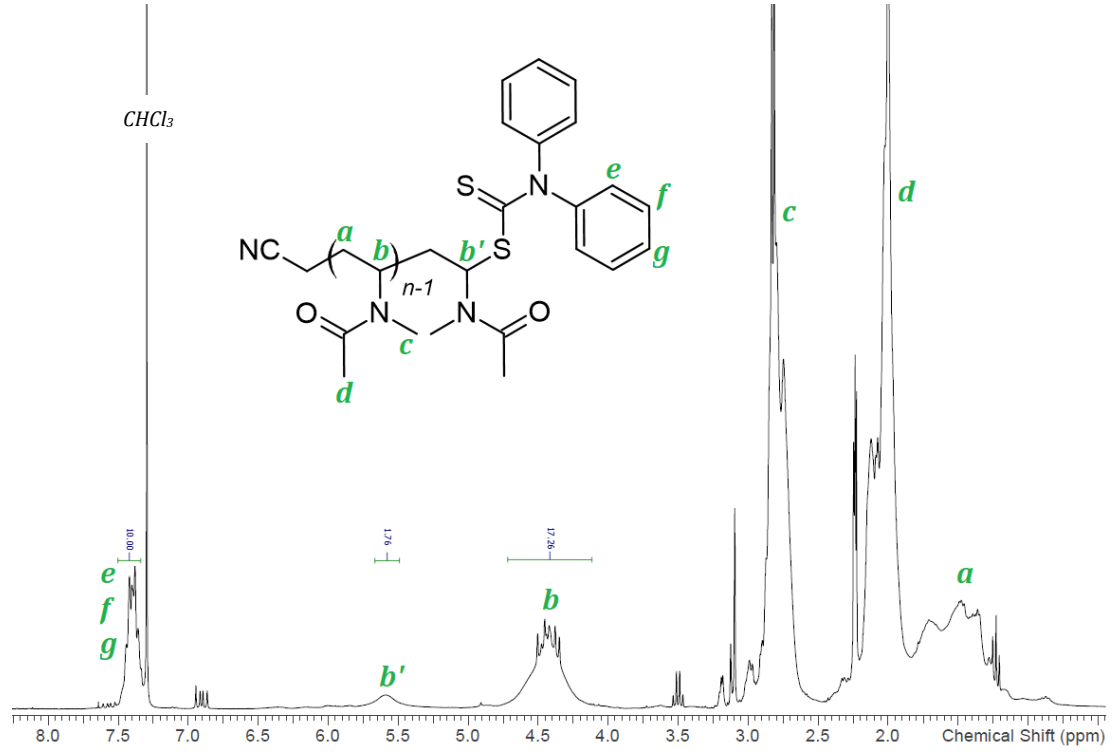

Figure 1-9. ^{1}H NMR spectrum of PNMVA-CTA4. $M_{n\,NMR} = M_{CTA4} + \frac{10*(b+b')}{(e+f+g)} \times M_{NMVA}$ with $M_{CTA4} = 284$ g mol^{-1}; $M_{NMVA} = 99$ g mol^{-1}. Measured on a 300MHz apparatus

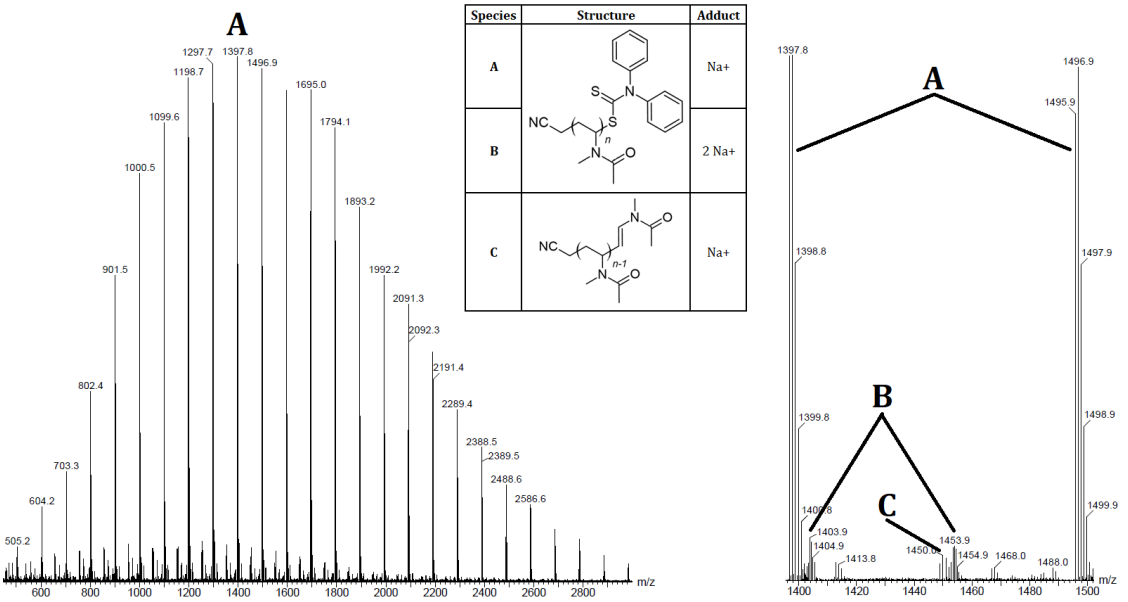

Figure 1-10. ESI-MS spectrum of PNMVA-CTA4.

Finally, to further confirm the chain-end fidelity of RAFT groups, I performed a chain extension from PNMVA-CTA2 and PNMVA-CTA4 obtained after polymerization of NMVA with CTA2 and CTA4 respectively, according to the aforementioned synthetic strategy to obtain well-defined macro-CTAs

In the case of PNMVA-CTA2, SEC analysis of the crude mixture gave a $M_{n,SEC}$ = 5300 g mol^{-1} in close agreement with the expected value ($M_{n,th}$ = 4600 g mol^{-1}), and a $Đ$ of 1.11. PNMVA-CTA2 was purified by precipitation in diethyl ether to remove unreacted monomer prior use as a macro-CTA. SEC analysis of PNMVA-CTA2 after precipitation highlighted a fractionation of the molar mass distribution, with a new value of $M_{n,SEC}$ = 7000 g mol^{-1} and a $Đ$ = 1.18. The precipitated polymer was also analyzed by ESI-MS spectroscopy, but considering the relatively high molar mass of the polymer, the MS spectrum was very complex to analyze with multi-charged populations (bis, tris and tetra Na^+ cations). Nevertheless, I was able to get the confirmation, by simulating the expected structure of a PNMVA capped with a $CNCH_2$ and SC(S)OEt, in a bis, tris and tetra charged version, of its presence as main species. This evidenced the formation of a xanthate end-capped prepolymer with the identification of populations A to D (Figure 1-11a and b). Deconvolution of the MS-spectrum to extract the mono cationic population gave a spectrum centered around 7000 Da, in agreement with the M_n obtained by SEC (Figure 1-11c).

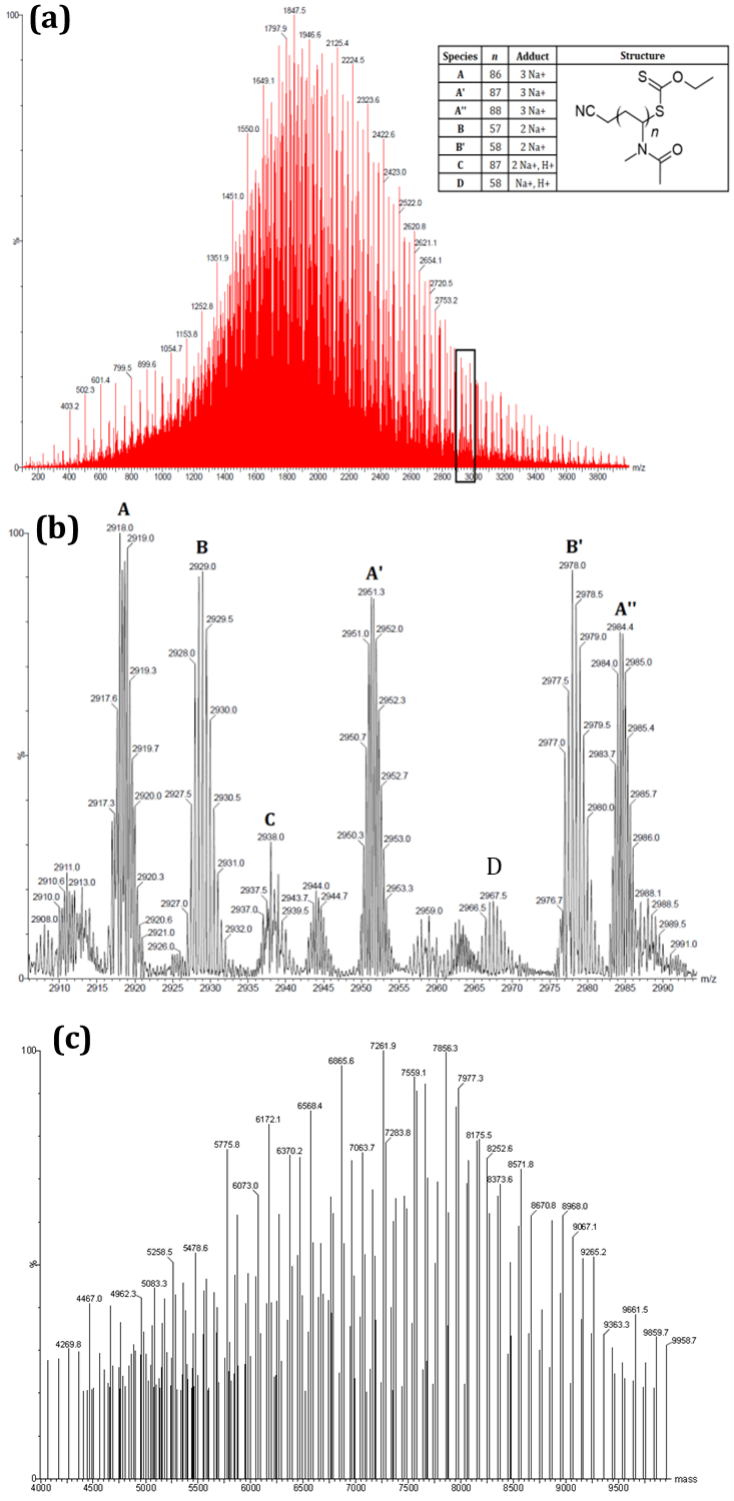

Figure 1-11. (a) ESI-MS analysis of PNMVA-CTA2. $M_{n,SEC}$ = 7000 g mol^{-1}, $Đ$ = 1.18 (Table 1-5, entry 1) and **(b)** a zoomed part. **(c)** Deconvolution to access the monoisotopic mono-charged populations.

Then, PNMVA-CTA2 was used as a macro-CTA in the bulk polymerization of NMVA at 35°C in presence of $[V\text{-}70]_0$ = 29 mmol L^{-1}. SEC analysis of samples withdrawn during the polymerization confirmed the chain extension, with SEC traces shifted towards higher molar masses with conversion, and the disappearance of the initial PNMVA-CTA2 (Figure 1-12 and Table 1-5). At the same time, a tailing in the low molar mass area was revealed, and suggested the presence of a fraction of dead chains. $M_{n,SEC}$ measured during polymerization (Table 1-5, entries 1-5) were close but lower than theoretical values calculated based on monomer conversion, and the dispersities gradually increased from 1.18 to 1.39 after 16 h which is understandable considering the high concentration of V-70 required a second time for the chain extension.

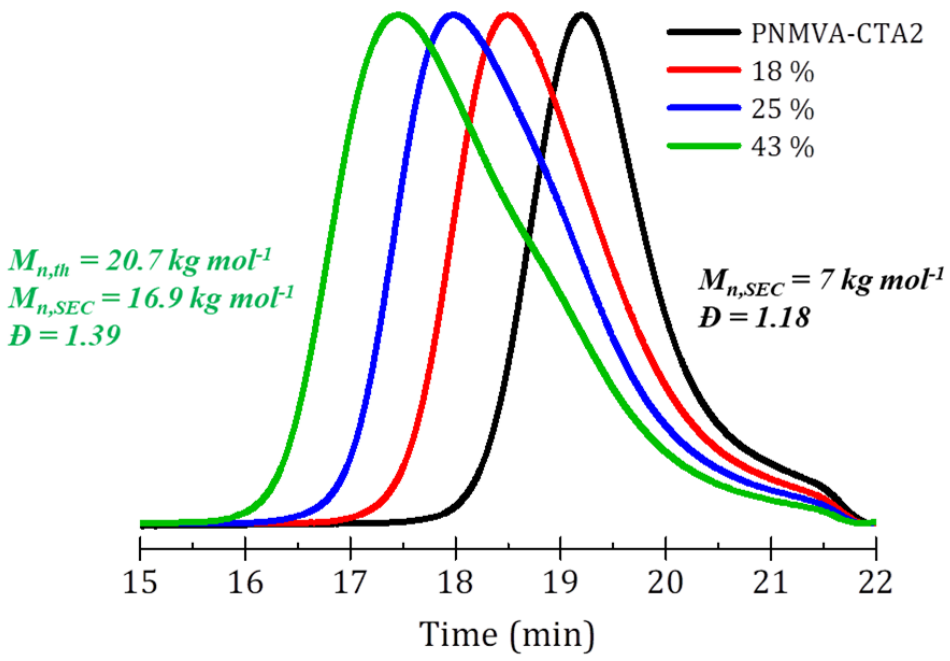

Figure 1-12. Evolution of SEC traces with NMVA conversion during the PNMVA-CTA2 chain extension at 35°C.

Table 1-5. RAFT polymerization of NMVA at 35°C using a PNMVA-CTA2 and PNMVA-CTA4 macro-RAFT agent. V-70 initiation

Entry	CTA	Targeted M_n (g mol^{-1})	Time (h)	Conversion[a] (%)	$M_{n,th}$[b] (g mol^{-1})	$M_{n,SEC}$[c] (g mol^{-1})	$Đ$
1	PNMVA-CTA2	39000	0	0	-	7000	1.18
2			2	13	11142	7700	1.18
3			4	18	12735	8900	1.34
4			8	25	14965	12400	1.34
5			16	43	20700	16900	1.39
6	PNMVA-CTA4	65000	0	0	-	3500	1.41
7			2	5	6574	5200	1.42
8			4	12	10877	10100	2.14
9			8	31	22557	42800	1.30
10			16	59	39770	47300	1.70

[a]calculated by ^{1}H NMR, [b]$M_{n,th}$ = [NMVA]$_0$/[PNMVA-CTAx]$_0$×M$_{NMVA}$×conv.+$M_{n,PNMVA\text{-}CTAx}$, with $M_{n,PNMVA\text{-}CTA2}$ = 7000 g mol^{-1} and $M_{n,PNMVA\text{-}CTA4}$ = 3500 g mol^{-1}, [c]$M_{n,SEC}$ measured with a RI-MALS detection.

In contrast to PNMVA-CTA2, I surprisingly did not observe any marked fractionation after purification by precipitation of PNMVA-CTA4; with an agreement between $M_{n,SEC}$ = 3500 g mol^{-1}, $M_{n,NMR}$ = 2700 g mol^{-1} and $M_{n,th}$ = 3000 g mol^{-1}, and a $Đ$ = 1.41. Chain extension from PNMVA-CTA4 with NMVA in bulk with [V-70]$_0$ = 29 mmol L^{-1} showed a clear shift of the SEC traces towards higher molar masses with conversion (Figure 1-13 and Table 1-5) but with much higher $M_{n,SEC}$ values than expected above 30% conversion. The corresponding dispersities fluctuated between1.3 and 2.14 during polymerization (Table 1-5, entries 6-10). The observed lack of control of M_n is in accordance with my results of NMVA polymerization with CTA4 shown in Figure 1-5a. From these results, it appears that xanthates are better suited for RAFT polymerization of NMVA and the preparation of corresponding block copolymers.

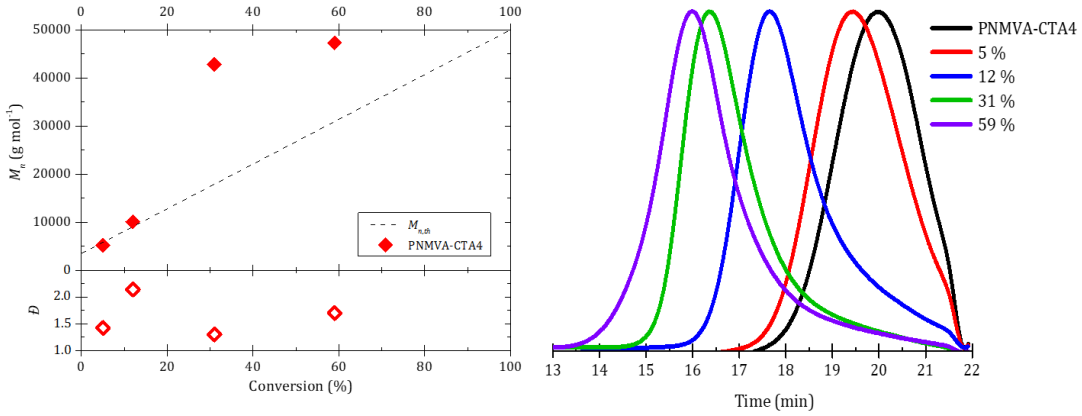

Figure 1-13. (left) Evolution of M_n and dispersity and (right) SEC-RI traces with NMVA conversion during chain extension of PNMVA-CTA4 at 35°C.

1.2.2 PNMVA-based double hydrophilic block copolymers

In order to illustrate the advantage of RAFT polymerization on the control of polymers architectures, two double hydrophilic diblock copolymers (DHBC) containing a PNMVA segment were synthesized by RAFT polymerization of NMVA with two different macro-CTAs. The first one, a O-ethyl xanthate end-functionalized poly(ethylene oxide) (PEO-xanthate) ($M_{n,NMR}$ = 2200 g mol^{-1}, $Đ$ = 1.19) was prepared from a commercially available PEO-OH ($M_{n,NMR}$ = 2000 g mol^{-1}) following a previously described protocol.[27] The second macro-RAFT agent, PNIPAAm-CTA1 ($M_{n,SEC}$ = 3200 g mol^{-1}, $Đ$ = 1.15) was obtained by RAFT polymerization of NIPAAm with CTA1 in presence of AIBN at 70°C, targeting a $M_{n,th}$ = 2000 g mol^{-1}.

1.2.2.1 PEO-b-PNMVA

At first, a PEO-*b*-PNMVA DHBC, with a targeted M_n = 22000 g mol^{-1} was synthesized by RAFT polymerization of NMVA in bulk at 35°C in presence of [V-70]$_0$= 26 mmol L^{-1} and a PEO-xanthate. The conversion reached 63% after 16 h and the SEC traces of the DHBC during polymerization clearly shifted towards higher molar masses with the concomitant disappearance of the initial PEO-xanthate (Figure 1-14a), confirming the successful formation of the DHBC. M_n values

increased linearly with NMVA conversion and remained slightly lower the than expected values throughout polymerization (Figure 1-14b and Table 1-6). Dispersity values increased slowly during polymerization but remained relatively low ($Đ$ = 1.36 for the longest reaction times, Figure 1-14b and Table 1-6). The SEC-RI chromatograms are not symmetrical and present a shoulder in the lower molar mass region. Although it is difficult to ascertain the origin of this population, I believe this corresponds to the combined contribution of dead PNMVA chains and a fraction of unreactivated PEO.

Table 1-6. Block polymerization of NMVA at 35°C using a PEO-X and PNIPAAm-CTA1 macro-RAFT agent. V-70 initiation

Entry	CTA	Targeted M_n (g mol^{-1})	Time (h)	Conversion[a] (%)	$M_{n,th}$[b] (g mol^{-1})	$M_{n,SEC}$[c] (g mol^{-1})	$Đ$
1	PEO-X	22000	2	15	5222	4200	1.11
2			4	25	7237	5400	1.24
3			8	41	10460	7700	1.36
4			16	63	14893	10500	1.36
5	PNIPAAm-CTA1	20000	2	12	5040	4400	1.18
6			4	22	6741	6900	1.18
7			8	29	7931	7700	1.54
8			16	64	13882	11300	1.47

[a]calculated by ^{1}H NMR, [b]$M_{n,th}$ = $[NMVA]_0/[CTA]_0 \times M_{NMVA} \times conv. + M_{n,first\ block}$. $M_{n,PEG\text{-}X}$ = 2200 g mol^{-1}, $M_{n,PNIPAAm\text{-}CTA1}$ = 3200 g mol^{-1} , [c]$M_{n,SEC}$ measured with a RI-MALS detection.

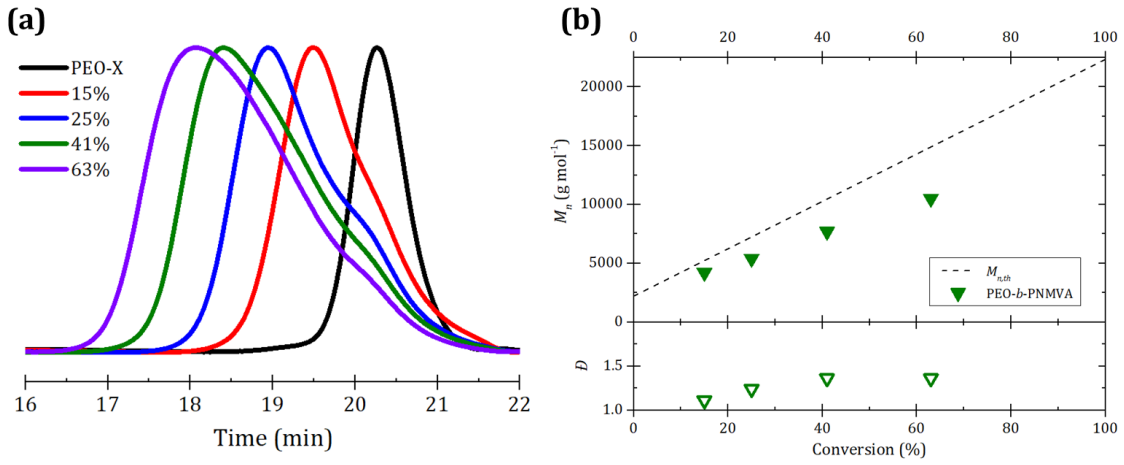

Figure 1-14. Evolution of **(a)** SEC traces **(b)** M_n and $Đ$ with NMVA conversion during PEO-*b*-PNMVA synthesis at 35°C.

1.2.2.2 PNIPAAm-b-PNMVA

For the second diblock copolymer, I targeted a thermoresponsive PNIPAAm-*b*-PNMVA with a M_n = 20000 g mol^{-1} obtained by RAFT polymerization of NMVA in bulk, at 35°C with $[V\text{-}70]_0$ = 29 mmol L^{-1}, from a PNIPAAm-CTA1 prepolymer with $M_{n,SEC}$ = 3200 g mol^{-1}. NMVA conversion reached 64% after 16h polymerization and the SEC analysis of the final diblock copolymer suggested the successful formation of the DHBC, with a clear shift of the measured molar masses (Figure 1-15a and Table 1-6, entry 9). A $M_{n,SEC}$ = 11300 g mol^{-1} was in close agreement with the expected $M_{n,th}$ = 13900 g mol^{-1}. The dispersity was measured at $Đ$ = 1.47 at the end of the polymerization with a step increase between 20% and 30% conversion ($Đ$ = 1.18 and 1.54, respectively. Figure 1-15b, and Table 1-6, entries 5-8).

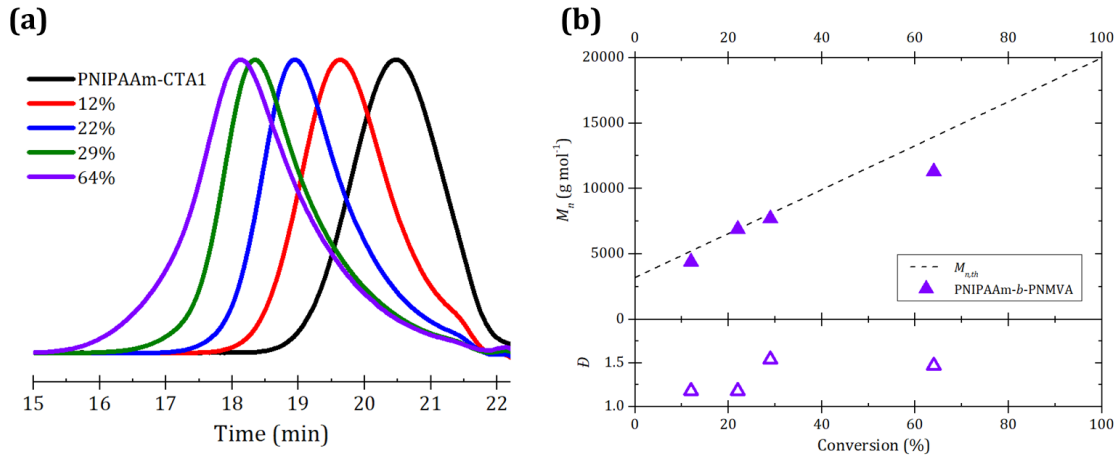

Figure 1-15. Evolution of **(a)** SEC traces **(b)** M_n and $Đ$ with NMVA conversion during the synthesis of PNIPAAm-*b*-PNMVA at 35°C.

PNIPAAm is a well-known thermoresponsive polymer exhibiting a lower critical solution temperature (LCST) phase transition at ca. 32°C. PNIPAAm-containing DHBCs are expected to display higher LCST as studies reported that hydrophilic non-thermoresponsive blocks lead to an increase of LCST.[28] Another PNIPAAm-*b*-PNMVA copolymer of $M_{n,SEC}$ = 19600 g mol^{-1} and $Đ$ = 1.58 (Figure 1-16), was synthesized and purified from a first PNIPAAm-CTA1 prepolymer with a $M_{n,SEC}$ = 2600 g mol^{-1}, following the same process as before with this time 89% NMVA conversion, with a calculated $M_{n,th}$ of 18100 g mol^{-1} for such conversion.

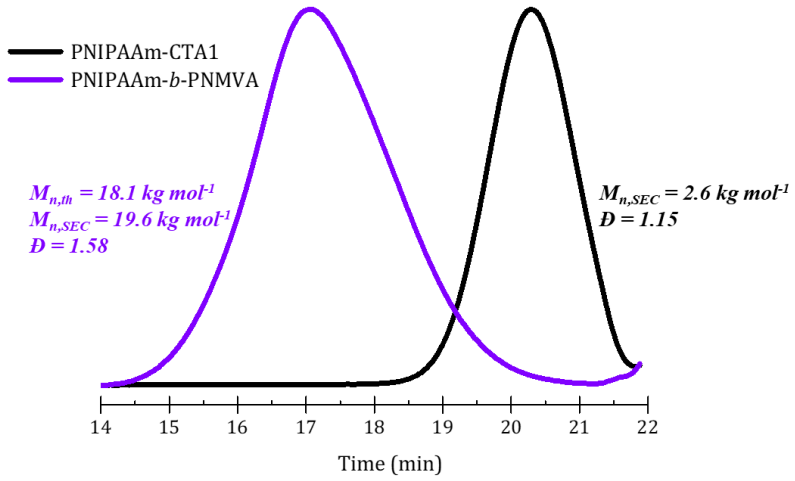

Figure 1-16. SEC chromatograms of PNIPAAm-CTA1 versus PNIPAAm-b-PNMVA.

The copolymer composition determined by ^{1}H NMR (NIPAAm/NMVA=8/92 mol%, Figure 1-17) after precipitation was in agreement with expected values predefined by experimental conditions (NIPAAm/NMVA = 11/89 mol%).

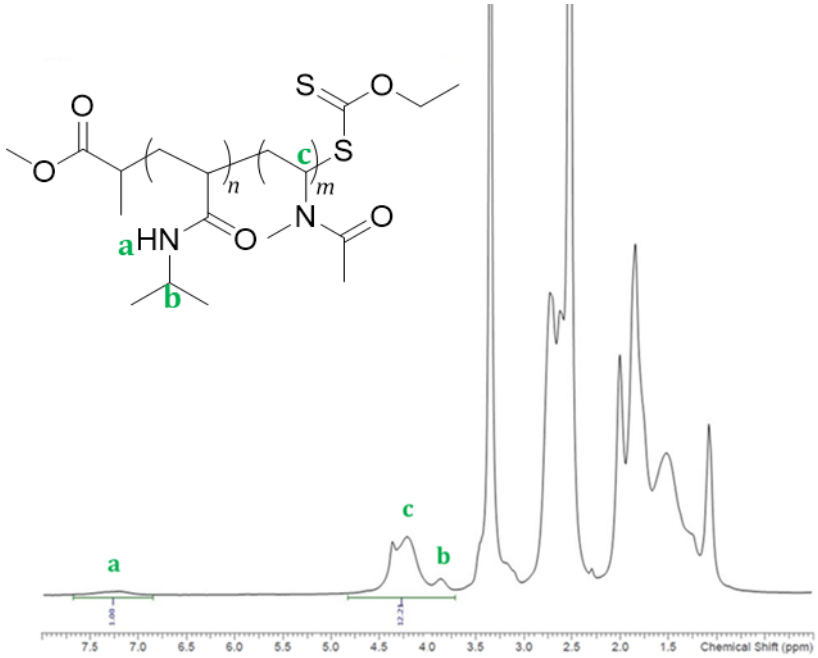

Figure 1-17. ^{1}H NMR spectrum of PNIPAAm-b-PNMVA. $M_{n,SEC}$ = 19600 g mol^{-1}, $Đ$ = 1.58. $\%_{NMVA} = \frac{(b+c)-a}{(b+c)} \times 100$. Measured on a 300MHz apparatus.

Light scattering experiments were carried over a range of temperature from 25°C to 50°C to determine the cloud point temperature (T_{cp}) of said PNIPAAm-*b*-PNMVA aqueous solution at 1%$_{w/v}$ (pH 7.2) and evaluate the evolution of the size of the objects formed during the process. T_{cp} was determined as onset value of D_h versus temperature plot during heating phase and was 36.5°C (Figure 1-18), consistent with expectations. Below T_{cp}, PNIPAAm-*b*-PNMVA was most probably as unimer state with D_h neighboring 10 nm. When temperature was raised beyond T_{cp}, the PNIPAAm block underwent a coil-to-globule transition, resulting in PNIPAAm-*b*-PNMVA diblock self-assembly with a likely core/shell structure made of a hydrophobic PNIPAAm core and a hydrophilic PNMVA shell. Such transition

reflected in D_h increasing drastically. Significant D_h differences at 50°C were observed whether it was measured at the end of the heating ramp or at the beginning of the cooling one. A kinetic effect may explain it since the copolymer solution from the cooling ramp was directly heated to 50°C, minimizing the aggregation of amphiphilic self-assembled objects. Regardless, LCST phase-transition was fully reversible and PNIPAAm-*b*-PNMVA diblock regained its unimer state at room temperature.

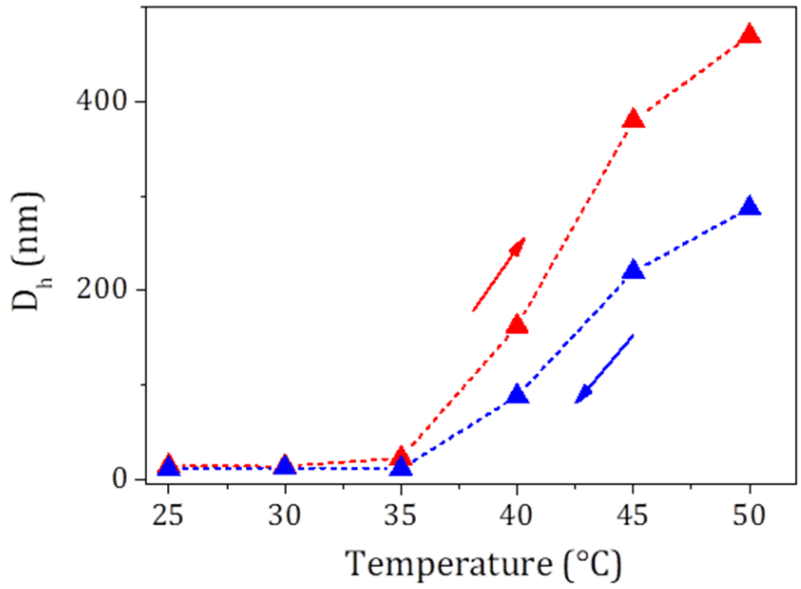

Figure 1-18. Average hydrodynamic diameter from DLS measurements of copolymer PNIPAAm-*b*-PNMVA at 1%$_{w/v}$ during heating from 25 °C to 50 °C (red) and cooling from 50°C to 25°C (blue).

1.3 CONCLUSION

NMVA was successfully controlled for the first time by RAFT polymerization with xanthate and dithiocarbamate CTAs. Typical [initiator]/[CTA] concentration ratios for RAFT polymerization led to poor monomer conversions due to the combined effects of low initiator efficiency, moderate reactivity of NMVA and RAFT retardation. To counterbalance this effect and obtain satisfactory conversions, an unusually high [initiator]/[CTA] ratio of 1.49/1 was applied. The appearance of bimodality in molar mass distributions of PNMVA-CTA1 at 65°C for prolonged reaction times was attributed to thermal degradation of the RAFT end-group, which prompted us to carry on the study at 35°C. Quite unexpectedly, the selected concentration and temperature conditions allowed a controlled growth of PNMVA chains with CTAs 2 and 4, and to a lesser extent with CTA1. Complementary synthetic methodologies (synthesis of low molar mass PNMVA-CTA, chain extension experiment, block copolymerization) and analytical techniques (^{1}H NMR, MALDI-TOF and ESI MS, SEC) helped to conclude on the effective presence of the RAFT terminal groups, with a far less significant contribution of initiator-derived chains than predicted based on $[initiator]_0/[RAFT]_0$, which can be related to low initiator efficiency. Original PEO-*b*-PNMVA and PNIPAAm-*b*-PNMVA DHBCs were successfully synthesized. The latter showed thermoresponsive behavior in water with formation of block copolymer aggregates above 36.5°C, with a fully reversible LCST phase transition.

Thanks to all the results of this first chapter on NMVA, I gained a better understanding on its RAFT polymerization, of its difficulties and some of its limits. This knowledge will serve as the starting point for the following chapter, which deals with another acyclic *N*-vinylamide monomer, *N*-vinylformamide (NVF), which can provide a convenient way to obtain polyvinylamine.

1.4 EXPERIMENTAL SECTION

1.4.1 Characterization

NMR analysis.

^{1}H NMR spectra were recorded at 298 K on a Bruker Avance 300 MHz instrument at an operating frequency of 300.13 MHz. Coupling constants (*J*) are reported to ± 0.5 Hz. The resonance multiplicities are described as s (singlet), d (doublet), t (triplet), q (quartet) or m (multiplet). Chemical shifts δ are reported in parts per million (ppm) and are referenced to the residual solvent peak (DMSO: H = 2.5 ppm or $CDCl_3$: H = 7.26 ppm). The NMVA conversion was determined by ^{1}H NMR spectroscopy.

Size-exclusion chromatography.

Size-exclusion chromatography (SEC) analysis in DMF/LiBr (10 mM) were performed on a system composed of an Agilent technologies guard column (PLGel20 µm, 50 × 7.5 mm) and a set of three TSKgel Alpha-2500, Alpha-3000, Alpha-3500 (TOSOH BIOSCIENCE) for PNMVAs obtained with CTAs 1-4. Another set of two KD-804 and KD-805L (SHODEX) columns was used for the analysis of PNMVA-CTA2 and PNMVA-CTA4 prepolymers, PNMVAs obtained from chain extension experiments and diblock copolymers.

Detections were conducted using a Wyatt Optilab® rEX refractive index detector, a Varian ProStar UV detector (dual wavelength analysis at 290 and 254 nm) and a Wyatt MiniDawn TREOS multi-angle light scattering detector. Analyses were performed at 55°C and a flow rate of 1.0 mL min^{-1}. $(dn/dc)_{PNMVA}$ = 0.077 mL g^{-1} was measured with a PSS DnDc-2010 differential refractometer.

Matrix-assisted laser desorption/ionization–time of flight mass spectrometry (MALDI-TOF-MS) and Electron spray ionization- time of flight mass spectrometry (ESI-TOF-MS).

MALDI-TOF-MS analyses were performed on Waters MALDI-TOF Micro MX equipped with a nitrogen laser emitting at λ = 337 nm. All analyses were carried out

with 1,8-dihydroxy-9(10H)-anthracenone (Dithranol) as matrix and NaI salt for polymer samples as cationizing agents. ESI-TOF mass spectra were acquired with a QTOF Premier mass spectrometer (Waters) and a Xevo G2 QTOF mass spectrometer (Waters) in electrospray ionization in positive mode. Samples of PNMVA were dissolved in chloroform, diluted at 1/10 with acetonitrile and then an acetone solution of NaI (10 mg mL^{-1}) was added. On the QTOF Premier, the resulting samples are directly infused in the source. The source temperature and desolvation temperature were 110 °C and 200 °C, respectively, and the cone voltage was optimized at 30 V. On the Xevo G2 QTOF, the injection was made in Flow Injection Analysis (FIA). The source temperature and desolvation temperature were 110 °C and 350 °C, respectively, and the cone voltage was optimized at 60 V. For both techniques, the acquisition software was Masslynx (Waters) and the spectra were processed by using Masslynx and Polymerix 3.0 (Sierra Analytics).

Dynamic light scattering.

Dynamic Light Scattering (DLS) measurements were acquired on a Malvern ZetaSizer Nano ZS with a He-Ne laser at 633 nm. then five measurements were recorded every 1 °C after 120 s equilibration time from 25 °C to 50 °C during heating phase and from 50 °C to 25 °C during cooling phase. Samples were prepared at $1\%_{w/v}$ in ultrapure water. Average apparent hydrodynamic diameter D_h was determined according to the Stokes-Einstein equation from intensity-weighted mean diameter derived from the cumulative analysis.

1.4.2 Materials

Cyanomethyl dimethylcarbamodithioate (CTA3, Sigma-Aldrich, 97%), 2,2'-Azobis(4-methoxy-2,4-dimethylvaleronitrile) (V-70, Wako), 1,4-dioxane (Sigma-Aldrich, 99.8%), Methyl-2-bromopropionate (Sigma-Aldrich, 98%), potassium ethylxanthogenate (Sigma-Aldrich, 96%), ethanol (Sigma-Aldrich, 96%), 2-bromopropionylbromide (97%, Sigma-Aldrich), dichloromethane (Sigma-Aldrich, 99.8%), trimethylamine (Sigma-Aldrich, ≥99%), anhydrous magnesium sulphate

(Sigma-Aldrich), bromoacetonitrile (Sigma-Aldrich, 97%), diethyl ether (Sigma-Aldrich, 99.9%), silica gel pore size 60 Å 220-440 mesh particle size, 35-75 mm particle size (Sigma-Aldrich), ethyl acetate (Sigma-Aldrich, 99.7%), petroleum ether (Sigma-Aldrich), potassium hydroxide (Sigma-Aldrich, 85%), diphenylamine (Sigma-Aldrich, 99%), carbon disulfide (Sigma-Aldrich, 99%), chloroacetonitrile, (Sigma-Aldrich, 99%), tetrahydrofuran (THF, (Sigma-Aldrich, 99.9%), Polyethylene glycol monomethylether (Fluka, 2000 g mol^{-1}) were used as received. *N*-methyl-*N*-vinylacetamide (NMVA, Sigma-Aldrich, 98%) was distilled under reduced pressure before use. *N*-isopropylacrylamide (NIPAAm, Sigma-Aldrich, 97%). was recrystallized twice from hexane before use. 2,2′-Azobis(2-methylpropionitrile) (AIBN, Sigma-Aldrich, 98%) was recrystallized from methanol before use.

1.4.3 Synthesis of RAFT agents CTA1-4.

Methyl 2-((ethoxycarbonothioyl)thio)propanoate (CTA1) was synthesized according to a previously published procedure from our group.[29] The synthesis of *S*-(cyanomethyl) *O*-ethyl carbonodithioate (CTA2) synthesis was repeated from past works.[30]

Cyanomethyl N,N-diphenylamine carbodithioate (CTA4). To a solution of potassium hydroxide (1.75 g, 31.3 mmol) in THF (100 mL) in an ice-water bath, was added *N,N*-diphenylamine (5 g, 295 mmol). The mixture was stirred for 10 min in the ice-water bath and carbon disulfide (2.925 g, 38.4 mmol) was then added slowly. The reaction mixture was stirred for 5 min in the ice-water bath, then overnight at room temperature. The mixture was filtered and potassium N,N-diphenylamine carbodithioate was obtained as an orange solid, which was washed with diethyl ether, dried under vacuum, and used in the next step without purification. Potassium *N,N*-diphenylamine carbodithioate (2 g, 7.1 mmol) was dissolved in deionized water (100 mL) and then cooled in an ice-water bath. Chloroacetonitrile (0.559 g, 7.4 mmol) was then added and the reaction mixture was stirred in the ice-water bath for 5 min and then at room temperature for 3h. The mixture was then

cooled in an ice-water bath for 15 min and filtered. The dark yellow solid was collected, washed with ice-cold water, and dried under vacuum.

^{1}H NMR (300.13 MHz, DMSO d6, 298K) δ = 7.40 – 7.64 (m, 10H, Ph), 4.28 (s, 2H, NCC$\underline{H_2}$SC(S)NPh$_2$) (Figure 19)

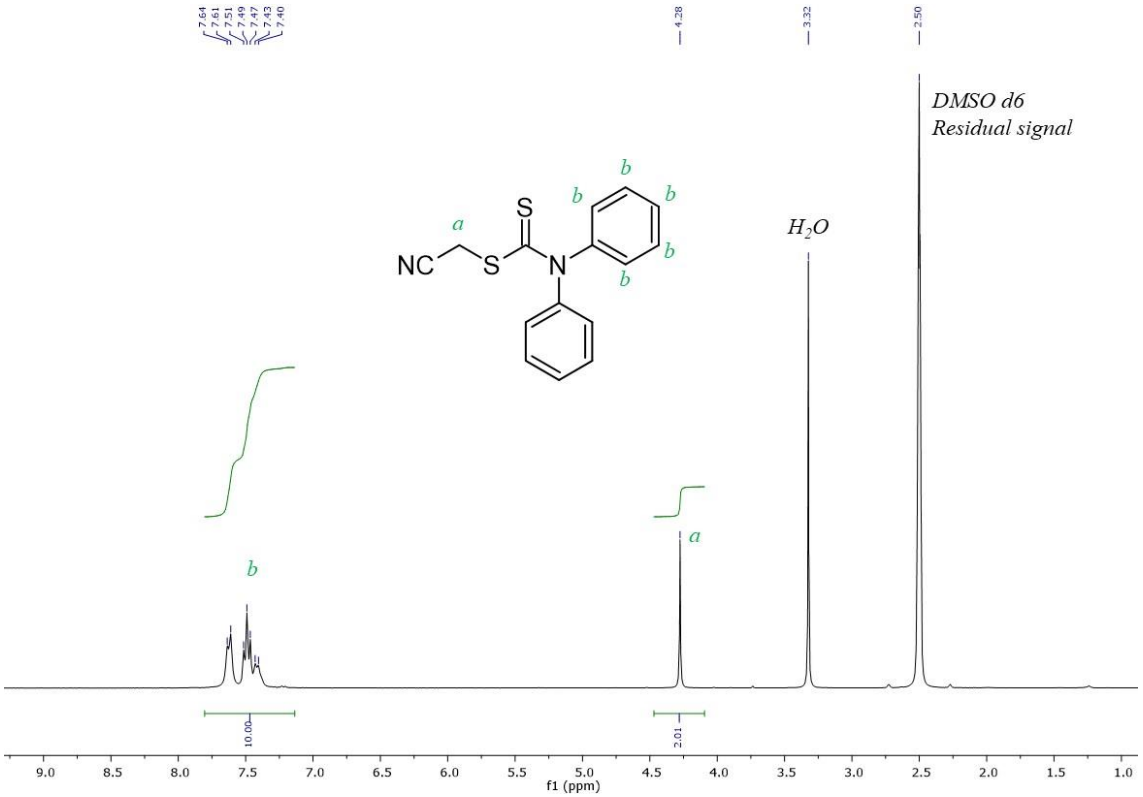

Figure 1-19. ^{1}H NMR spectrum of cyanomethyl *N,N*-diphenylamine carbodithioate (CTA4). Measured on a 300MHz apparatus.

1.4.4 General procedure for the polymerization of NMVA with CTA1-4 for a targeted M_n = 50000 g mol^{-1}.

Typically, NMVA (10 g, 0.10 mol), V-70 (92 mg, 0.30 mmol), and either CTA1 (42 mg, 0.20 mmol), CTA2 (32 mg, 0.20 mmol), CTA3 (32 mg, 0.20 mmol) or CTA4 (57 mg, 0.20 mmol), were added to 50 ml round bottom flask and stirred. 1 ml of the reaction mixture was added to each sealing tube. After degassing by three freeze-pump-thaw cycles, the tubes were sealed under acetylene/oxygen flame. The tubes were immersed into an oil bath at 35°C for different times.

For the kinetic studies, sample were rapidly cooled down in liquid nitrogen and directly analyzed by ^{1}H NMR and SEC without purification. Dry polymers were obtained after purification by three cycles of solubilization in ethanol, precipitation in cold diethyl ether and filtration, and then was dried under vacuum.

1.4.5 Procedure for chain extension experiment with PNMVA-CTA2.

Synthesis of PNMVA-CTA2. NMVA (12 g, 0.12 mol), CTA2 (65 mg, 0.40 mmol) and V-70 (185 mg, 0.60 mmol) were added to a Schlenk tube, degassed by three freeze-pump-thaw cycles, and immersed into an oil bath at 35°C for 4 h. The polymerization was stopped by rapidly cooling down the reaction mixture with liquid nitrogen and a sample was withdrawn and analyzed by ^{1}H NMR to determine a 15% conversion ($M_{n,th}$ = 4635 g mol^{-1}) and by SEC ($M_{n,SEC}$ = 5330 g mol^{-1} , $Đ$ = 1.11). PNMVA-CTA2 was purified by 3 cycles of solubilization in ethanol, precipitation in cold diethyl ether and filtration, and then was dried under vacuum. Dry PNVA-CTA2 was analyzed by SEC ($M_{n,SEC}$ = 7000 g mol^{-1} , $Đ$ = 1.18) and ESI-TOF MS spectrometry.

Chain extension from PNMVA-CTA2. NMVA (6 g, 60.6 mmol), PNMVA-CTA2 (1.317 g, 0.146 mmol) and V-70 (67 mg, 0.218 mmol) were added to 50 mL round bottom flask and stirred. 1 mL of the reaction mixture was added to each sealing tube. After degassing by three freeze-pump-thaw cycles, the tubes were sealed under acetylene/oxygen flame. Sealed tubes were immersed into an oil bath at 35°C for different times. The polymerization was stopped by rapidly cooling down the reaction mixture with liquid nitrogen and the samples directly analyzed by ^{1}H NMR to determine a conversion and by SEC.

1.4.6 Procedure for chain extension experiment with PNMVA-CTA4.

Synthesis of PNMVA-CTA4. NMVA (20 g, 0.202 mol), CTA4 (0.114 g, 0.402 mmol) and V-70 (0.185 g, 0.600 mmol) were added to a Schlenk tube, degassed by three freeze-pump-thaw cycles, and immersed into an oil bath at 35°C for 2 h. The polymerization

was stopped by rapidly cooling down the reaction mixture with liquid nitrogen and a sample was withdrawn and analyzed by ^{1}H NMR to determine a conversion of 6%. PNMVA-CTA4 was purified by 3 cycles of solubilization in ethanol, precipitation in cold diethyl ether and filtration, and then was dried under vacuum. Dry PNMVA-CTA4 was analyzed by SEC ($M_{n,SEC}$ = 3500 g mol^{-1} , $Đ$ = 1.41) and ESI-TOF MS spectrometry.

Chain extension from PNMVA-CTA4. NMVA (5 g, 50.5 mmol), PNMVA-CTA2 (0.285 g, 0.106 mmol) and V-70 (49 mg, 0.158 mmol) were added to a 50 mL round-bottom flask and stirred. 1 mL of the reaction mixture was added to each sealing tube. After degassing by three freeze-pump-thaw cycles, the tubes were flame sealed. Sealed tubes were immersed into an oil bath at 35°C for different times. The polymerization was stopped by rapidly cooling down the reaction mixture with liquid nitrogen and the samples were directly analyzed by ^{1}H NMR to determine monomer conversion and by SEC.

1.4.7 Synthesis of PNIPAAm-*b*-PNMVA diblock copolymer.

Synthesis of PNIPAAm-CTA1. NIPAAm (5 g, 44.2 mmol), CTA1 (0.581 g, 2.79 mmol), AIBN (69 mg, 0.418 mmol), and dioxane (5.78 g) were added to a Schlenk tube and degassed by bubbling argon for 30 min and immersed into an oil bath at 70°C for 6 h. The polymerization was stopped by cooling down the reaction mixture with cold water, and a sample withdrawn to determine a conversion of 94% by ^{1}H NMR. The polymer was purified by precipitation in cold diethyl ether, filtration, dried under vacuum, and analyzed by SEC ($M_{n,SEC}$ = 3200 g mol^{-1}, $Đ$ = 1.12.

PNIPAAm-b-PNMVA. NMVA (5 g, 50.5 mmol), PNIPAAm-CTA1 (0.882 g, 0.294 mmol), and V-70 (0.136g, 0.439 mmol) were added to 50 mL round bottom flask and stirred. 1 mL of the reaction mixture was added to each sealing tube. After degassing by three freeze-pump-thaw cycles, the tubes were sealed under acetylene/oxygen flame. Sealed tubes were immersed into an oil bath at 35°C for different times. The polymerization was stopped by rapidly cooling down the reaction mixture with

liquid nitrogen and the samples directly analyzed by ^{1}H NMR to determine a conversion and by SEC. Polymers were purified by 3 cycles of solubilization in ethanol, precipitation in cold diethyl ether, filtrated, then dried under vacuum. dn/dc values were calculated for each copolymer following the equation:

$$(dn/dc)_{PNIPAAm-b-PNMVA} = W_{PNIPAAm} \times (dn/dc)_{PNIPAAm} + W_{PNMVA} \times (dn/dc)_{PNMVA}$$

where $W_{PNIPAAm}$ and W_{PNMVA} correspond to the weight fractions of the PNIPAAm block and the PNMVA block, respectively. $(dn/dc)_{PNIPAAm}$ = 0.087.[31]

1.4.8 Synthesis of PEO-*b*-PNMVA diblock copolymer.

A xanthate-terminated poly(ethylene oxide) (PEO-X) was synthesized from an OH-terminated PEO (M_n = 2012 g mol^{-1}) according to a previously published procedure from our group.[32]

PEO-b-PNMVA. NMVA (4.24 g, 42.9 mmol) PEO-X (0.46 g, 0.232 mmol), and V-70 (36 mg, 0.115 mmol) were added to 50 mL round bottom flask and stirred. 1 mL of the reaction mixture was added to each sealing tube. After degassing by three freeze-pump-thaw cycles, the tubes were sealed under acetylene/oxygen flame. and immersed into an oil bath at 35°C for different times. The polymerization was stopped by rapidly cooling down the reaction mixture with liquid nitrogen and the samples directly analyzed by ^{1}H NMR to determine a conversion and by SEC. Polymers were purified by 3 cycles of solubilization in a 50/50 (v/v) of methanol/ethanol mixture, precipitation in cold diethyl ether, filtration, and dried under vacuum. dn/dc values were calculated for each copolymer following the equation:

$$(dn/dc)_{PEO-b-PNMVA} = W_{PEO} \times (dn/dc)_{PEO} + W_{PNMVA} \times (dn/dc)_{PNMVA}$$

where W_{PEO} and W_{PNMVA} correspond to the weight fractions of the PEO block and the PNMVA block, respectively. $(dn/dc)_{PEO}$=0.057.[33]

1.5 REFERENCES

(1) Ajiro, H.; Takemoto, Y.; Akashi, M.; Chua, P. C.; Kelland, M. A. Study of the Kinetic Hydrate Inhibitor Performance of a Series of Poly(N-Alkyl-N-Vinylacetamide)s. *Energy Fuels* **2010**, *24*, 6400–6410.

(2) Kawatani, R.; Kawata, Y.; Yusa, S.; Kelland, M. A.; Ajiro, H. Synthesis of Thermosensitive Poly(N-Vinylamide) Derivatives Bearing Oligo Ethylene Glycol Chain for Kinetic Hydrate Inhibitor. *Macromol. Wash. DC U. S.* **2018**, *51*, 7845–7852.

(3) Reyes, F. T.; Kelland, M. A. First Investigation of the Kinetic Hydrate Inhibitor Performance of Polymers of Alkylated N-Vinyl Pyrrolidones. *Energy Fuels* **2013**, *27*, 3730–3735.

(4) Zhang, Q.; Kawatani, R.; Ajiro, H.; Kelland, M. A. Optimizing the Kinetic Hydrate Inhibition Performance of N-Alkyl-N-Vinylamide Copolymers. *Energy Fuels* **2018**, *32*, 4925–4931.

(5) Lee, M.-J.; Sung, A.-Y. Polymerization and Physical Property Assessment of Optical Lens Materials Containing Amide Group. *J. Korean Chem. Soc.* **2018**, *62*, 113–117.

(6) Fischer, J. P.; Becker, U.; Von Halasz, S. P.; Mueck, K. F.; Pueschner, H.; Roesinger, S.; Schmidt, A.; Suhr, H. H. The Preparation and Characterization of Surface-Grafted Plastic Materials Designed for the Evaluation of Their Tissue and Blood Compatibility. *J. Polym. Sci. Polym. Symp.* **1979**, *66*, 443–463.

(7) Eeckman, F.; Moees, A. J.; Amighi, K. Synthesis and Characterization of Thermosensitive Copolymers for Oral Controlled Drug Delivery. *Eur. Polym. J.* **2004**, *40*, 873–881.

(8) Panarin, E. F. N-Vinylamides and Related Polymers as Delivery Agents of Biologically Active Compounds. *Russ. Chem. Bull.* **2015**, *64*, 15–23.

(9) Nazarova, O. V.; Anan'eva, E. P.; Zarubaev, V. V.; Sinegubova, E. O.; Zolotova, Yu. I.; Bezrukova, M. A.; Panarin, E. F. Synthesis and Antibacterial and Antiviral Properties of Silver Nanocomposites Based on Water-Soluble 2-Dialkylaminoethyl Methacrylate Copolymers. *Pharm. Chem. J.* **2020**, *53*, 1076–1080.

(10) Neff, P. A.; Wunderlich, B. K.; von Klitzing, R.; Bausch, A. R. Formation and Dielectric Properties of Polyelectrolyte Multilayers Studied by a Silicon-on-Insulator Based Thin Film Resistor. *Langmuir* **2007**, *23*, 4048–4052.

(11) Debuigne, A.; Morin, A. N.; Kermagoret, A.; Piette, Y.; Detrembleur, C.; Jerome, C.; Poli, R. Key Role of Intramolecular Metal Chelation and Hydrogen Bonding in the Cobalt-Mediated Radical Polymerization of N-Vinyl Amides. *Chem. - Eur. J.* **2012**, *18*, 12834–12844,

(12) Dréan, M.; Guégan, P.; Detrembleur, C.; Jérôme, C.; Rieger, J.; Debuigne, A. Controlled Synthesis of Poly(Vinylamine)-Based Copolymers by Organometallic-Mediated Radical Polymerization. *Macromolecules* **2016**, *49* (13), 4817–4827.

(13) Stiernet, P.; Drean, M.; Jerome, C.; Midoux, P.; Guegan, P.; Rieger, J.; Debuigne, A. Tailor-Made Poly(Vinylamine)s via Thermal or Photochemical Organometallic Mediated Radical Polymerization. *ACS Symp. Ser.* **2018**, *1284*, 349–363.

(14) Fan, W.; Yamago, S. Synthesis of Poly(N-Vinylamide)s and Poly(Vinylamine)s and Their Block Copolymers by Organotellurium-Mediated Radical Polymerization. *Angew. Chem. Int. Ed.* **2019**, *58*, 7113–7116.
(15) Wan, D.; Satoh, K.; Kamigaito, M.; Okamoto, Y. Xanthate-Mediated Radical Polymerization of N-Vinylpyrrolidone in Fluoroalcohols for Simultaneous Control of Molecular Weight and Tacticity. *Macromolecules* **2005**, *38* (25), 10397–10405.
(16) Pound, G.; Eksteen, Z.; Pfukwa, R.; McKenzie, J. M.; Lange, R. F. M.; Klumperman, B. Unexpected Reactions Associated with the Xanthate-Mediated Polymerization of N-Vinylpyrrolidone. *J. Polym. Sci. Part Polym. Chem.* **2008**, *46* (19), 6575–6593.
(17) Stenzel, M. H.; Cummins, L.; Roberts, G. E.; Davis, T. P.; Vana, P.; Barner-Kowollik, C. Xanthate Mediated Living Polymerization of Vinyl Acetate: A Systematic Variation in MADIX/RAFT Agent Structure. *Macromol. Chem. Phys.* **2003**, *204* (9), 1160–1168.
(18) Guinaudeau, A.; Mazières, S.; Wilson, D. J.; Destarac, M. Aqueous RAFT/MADIXpolymerisation of N-Vinyl Pyrrolidone at Ambient Temperature. *Polym. Chem.* **2011**, *3* (1), 81–84.
(19) Guinaudeau, A.; Coutelier, O.; Sandeau, A.; Mazières, S.; Nguyen Thi, H. D.; Le Drogo, V.; Wilson, D. J.; Destarac, M. Facile Access to Poly(N-Vinylpyrrolidone)-Based Double Hydrophilic Block Copolymers by Aqueous Ambient RAFT/MADIX Polymerization. *Macromolecules* **2014**, *47* (1), 41–50.
(20) Zhao, X.; Coutelier, O.; Nguyen, H. H.; Delmas, C.; Destarac, M.; Marty, J.-D. Effect of Copolymer Composition of RAFT/MADIX-Derived N-Vinylcaprolactam/N-Vinylpyrrolidone Statistical Copolymers on Their Thermoresponsive Behavior and Hydrogel Properties. *Polym. Chem.* **2015**, *6* (29), 5233–5243.
(21) Fischer, J. P.; Rösinger, S. Kinetik Der Radikalischen Polymerisation Und Copolymerisation von N-Vinyl-N-Methylacetamid. *Makromol. Chem.* **1983**, *184* (6), 1247–1254.
(22) Uhelská, L.; Chorvát, D.; Hutchinson, R. A.; Santanakrishnan, S.; Buback, M.; Lacík, I. Radical Propagation Kinetics of N-Vinylpyrrolidone in Organic Solvents Studied by Pulsed-Laser Polymerization–Size-Exclusion Chromatography (PLP–SEC). *Macromol. Chem. Phys.* **2014**, *215* (23), 2327–2336.
(23) Schrooten, J.; Buback, M.; Hesse, P.; Hutchinson, R. A.; Lacík, I. Termination Kinetics of 1-Vinylpyrrolidin-2-One Radical Polymerization in Aqueous Solution. *Macromol. Chem. Phys.* **2011**, *212* (13), 1400–1409.
(24) Stace, S. J.; Moad, G.; Fellows, C. M.; Keddie, D. J. The Effect of Z-Group Modification on the RAFT Polymerization of N-Vinylpyrrolidone Controlled by "Switchable" N-Pyridyl-Functional Dithiocarbamates. *Polym. Chem.* **2015**, *6* (40), 7119–7126.
(25) Destarac, M.; Charmot, D.; Franck, X.; Zard, S. Z. Dithiocarbamates as Universal Reversible Addition-Fragmentation Chain Transfer Agents. *Macromol. Rapid Commun.* **2000**, *21* (15), 1035–1039.
(26) Ladavière, C.; Lacroix-Desmazes, P.; Delolme, F. First Systematic MALDI/ESI Mass Spectrometry Comparison to Characterize Polystyrene Synthesized by

Different Controlled Radical Polymerizations. *Macromolecules* **2009**, *42* (1), 70–84.

(27) Markiewicz, K. H.; Seiler, L.; Misztalewska, I.; Winkler, K.; Harrisson, S.; Wilczewska, A. Z.; Destarac, M.; Marty, J.-D. Advantages of Poly(Vinyl Phosphonic Acid)-Based Double Hydrophilic Block Copolymers for the Stabilization of Iron Oxide Nanoparticles. *Polym. Chem.* **2016**, *7* (41), 6391–6399.

(28) Chee, C. K.; Rimmer, S.; Shaw, D. A.; Soutar, I.; Swanson, L. Manipulating the Thermoresponsive Behavior of Poly(N-Isopropylacrylamide). 1. On the Conformational Behavior of a Series of N-Isopropylacrylamide−Styrene Statistical Copolymers. *Macromolecules* **2001**, *34* (21), 7544–7549.

(29) Liu, X.; Coutelier, O.; Harrisson, S.; Tassaing, T.; Marty, J.-D.; Destarac, M. Enhanced Solubility of Polyvinyl Esters in ScCO2 by Means of Vinyl Trifluorobutyrate Monomer. *ACS Macro Lett.* **2015**, *4* (1), 89–93.

(30) Chiefari, J.; Mayadunne, R. T.; Moad, G.; Rizzardo, E.; Thang, S. H. Polymerization Process with Living Characteristics and Polymers Made Therefrom. US6747111B2, June 8, 2004.

(31) Read, E.; Guinaudeau, A.; Wilson, D. J.; Cadix, A.; Violleau, F.; Destarac, M. Low Temperature RAFT/MADIX Gel Polymerisation: Access to Controlled Ultra-High Molar Mass Polyacrylamides. *Polym. Chem.* **2014**, *5* (7), 2202–2207.

(32) Markiewicz, K. H.; Seiler, L.; Misztalewska, I.; Winkler, K.; Harrisson, S.; Wilczewska, A. Z.; Destarac, M.; Marty, J.-D. Advantages of Poly(Vinyl Phosphonic Acid)-Based Double Hydrophilic Block Copolymers for the Stabilization of Iron Oxide Nanoparticles. *Polym. Chem.* **2016**, *7* (41), 6391–6399.

(33) Dwyer, A. B.; Chambon, P.; Town, A.; Hatton, F. L.; Ford, J.; Rannard, S. P. Exploring the Homogeneous Controlled Radical Polymerisation of Hydrophobic Monomers in Anti-Solvents for Their Polymers: RAFT and ATRP of Various Alkyl Methacrylates in Anhydrous Methanol to High Conversion and Low Dispersity. *Polym. Chem.* **2015**, *6* (41), 7286–7296.

CHAPTER 2.

RAFT POLYMERIZATION OF *N*-VINYLFORMAMIDE AND CORRESPONDING DOUBLE HYDROPHILIC BLOCK COPOLYMERS

2.1 INTRODUCTION

Polyvinylamine (PVAm) is the cationic water-soluble polymer with the highest content of primary amine groups, which makes it a candidate of choice for surface engineering.[1,2] In recent years, PVAm gained a lot of interest for diverse applications in biomedicine,[3–7] textiles,[8,9] adhesives,[10] oil field chemicals[11] or environmental remediation.[12–16] As PVAm cannot be produced from the direct polymerization of vinyl amine as monomer, typical synthetic pathways involve the modification of precursor polymers, i.e. via the Hofmann modification of polyacrylamide[17] or through hydrazinolysis of poly(*N*-vinylphthalimide).[18–20] A more appealing strategy consists in the polymerization of *N*-vinylformamide (NVF), the structurally simplest vinyl amide monomer,[21] followed by hydrolysis of the resulting poly(*N*-vinylformamide) (PNVF) in aqueous acidic or basic medium.[22,23]

Unlike NMVA (studied in chapter 1), not many techniques achieved the controlled polymerization of NVF as of today. Prof. Yamago and coworkers successfully used organotellurium-mediated radical polymerization (TERP) to control PNVF synthesis to an excellent level for the first time.[24] Indeed, they synthesized PNVFs of determined molecular weights up to $M_{n,SEC}$ = 27700 g mol^{-1} ($M_{n,th}$ = 28900 g mol^{-1}) while maintaining dispersities below 1.2, and with up to 80∼90% monomer conversion after 30h of reaction.

In contrast, reports on the reversible addition-fragmentation chain transfer (RAFT) polymerization of NVF are scarce. Beckman and coworkers described the synthesis of poly(ethylene oxide)-*b*-poly(*N*-vinylformamide) (PEO-*b*-PNVF) block copolymers using a xanthate-terminated PEO as macro-RAFT agent.[25] However, the reported copolymers showed high dispersities (1.7 to 2.3) with low NVF conversions. Pich and coworkers also used RAFT polymerization to synthesize a series of statistical copolymers pairing NVF with VCL, VPI or VP.[26] Though the obtained copolymers showed relatively low dispersity with compositions close to the expected ones, the authors mainly focused on low molar mass copolymers (M_n~10 kg mol^{-1}) with a maximum fraction of NVF of 50%. Kawatani and coworkers performed the random copolymerization of NVF with NVF derivatives monomers bearing alkenyl groups at their amide's Nitrogen side.[27] Using two different CTAs, one xanthate and one dithiocarbamate, they synthesized copolymers of M_n of 1 to 6 kg mol^{-1}. However, the authors reported relatively high dispersity values, going from 1.5 to 3.3 and for relatively long reaction time (7 days).

In this chapter, my motivation is to better reveal the potential of NVF monomer for RAFT polymerization through a thorough study of its homopolymerization and related block copolymerization using xanthate RAFT agents. In a first part, I will establish the optimal polymerization conditions and apply them to the synthesis of controlled PNVFs over a wide range of average molar masses. In a second part, I will proceed to the synthesis of PNVF-based double hydrophilic block copolymers (DHBC) such as poly(*N*,*N*-dimethylacrylamide)-*b*-poly(*N*-vinylformamide) (PDMA-*b*-PNVF), poly(*N*-vinylcaprolactam)-*b*-poly(*N*-vinylformamide) (PVCL-*b*-PNVF) and poly(*N*-isopropylacrylamide)-*b*-poly(*N*-vinylformamide) (PNIPAAm-*b*-PNVF). Asymmetrical Flow Field Flow Fractionation (AF4) and ^{1}H DOSY NMR analyses will be used to characterize diblock copolymers and confirm their effective synthesis. Finally, an example of the selective hydrolysis of the PNVF block will be given for PVCL-*b*-PNVF, to illustrate the ease of access to stimuli-responsive PVAm-based materials with controlled architecture.

2.2 RESULTS AND DISCUSSION

2.2.1 Homopolymerization of NVF.

2.2.1.1 Reaction conditions

In order to set up the best experimental conditions for the RAFT polymerization of NVF, all polymerizations were performed in DMSO at 35°C using 2,2'-azobis(4-methoxy-2,4-dimethylvaleronitrile) (V-70) (Scheme 2-1). Based on my previous chapter on NMVA, I globally chose the same reaction conditions (CTA, initiator, temperature), with the addition of DMSO as suitable low transferring organic solvent able to solubilize PNVF. In their respective works, Beckman and coworkers,[25] Kawatani and coworkers,[27] and Pich and coworkers[26] used xanthate CTAs. In the latter case, showing the most promising results, CTA1 (same as in my first chapter) was used. However, as I concluded in chapter 1, the xanthate CTA2 is better suited for the polymerization of NMVA. Thus, I chose CTA2 as the CTA in this chapter.

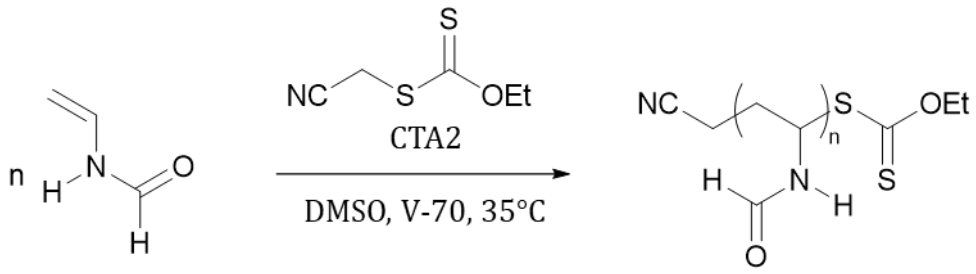

Scheme 2-1. General scheme of RAFT polymerization of NVF at 35°C in DMSO using CTA2.

At first, I studied the effect of three different concentrations of *S*-cyanomethyl-*O*-ethylcarbonodithioate (CTA2) on the kinetics and regulation of molar masses of PNVF (Scheme 2-1). While in a free-radical polymerization a conversion of 95% was already obtained after 16h, I observed a retardation effect when increasing $[CTA2]_0$, with conversions of respectively 93%, 80% and 66% after 24h for $[CTA2]_0$ = 6.5,

16.2 and 55.1 mmol L^{-1} (Figure 2-1), a common phenomenon in RAFT polymerization of *N*-vinylamides with xanthate CTAs.[28]

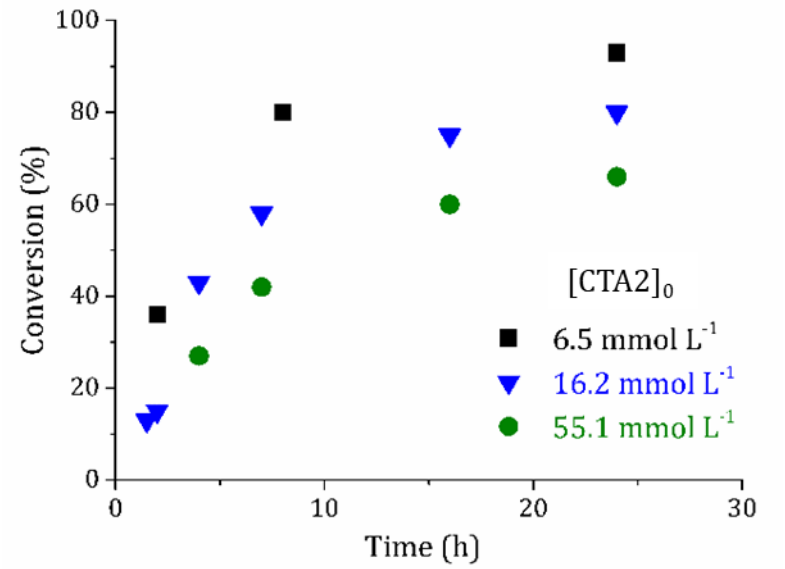

Figure 2-1. Effect of CTA2 initial concentration on monomer conversion at 35°C in RAFT polymerization of NVF in DMSO. $[NVF]_0$ = 4.5 mol L^{-1}; $[V\text{-}70]_0$ = 5.4 mmol L^{-1}.

These three concentrations correspond to $[V\text{-}70]_0/[CTA2]_0$ ratios of 0.83, 0.33 and 0.10, respectively. While the highest conversion (93%) was obtained with $[V\text{-}70]_0/[CTA2]_0$ = 0.83, the important amount of initiator relative to CTA2 used could have decreased the quality of the control by generating a high proportion of dead chains.[29] On the other hand, with $[V\text{-}70]_0/[CTA2]_0$ = 0.10, 66% conversion after 24h was considered as not satisfactory enough. Therefore, for the rest of the study, I decided to work with $[V\text{-}70]_0/[CTA2]_0$ = 0.33 as the best compromise in terms of conversion (80% after 24h) and initiator concentration. Preliminary SEC analysis of the PNVFs indicated a regulation of M_n with values inversely proportional to $[CTA2]_0$ and monomodal SEC traces (Figure 2-2). Compared to $M_{n,SEC}$ = 200000 g mol^{-1} and $Đ$ = 1.82 obtained via CTA-free radical polymerization, $M_{n,SEC}$ = 47800 g mol^{-1}, 18200 g mol^{-1} and 5100 g mol^{-1} were respectively obtained for the three increasing concentrations of CTA2, in agreement with theoretical values, and with dispersities all below $Đ$ = 1.3 (Table 2-1).

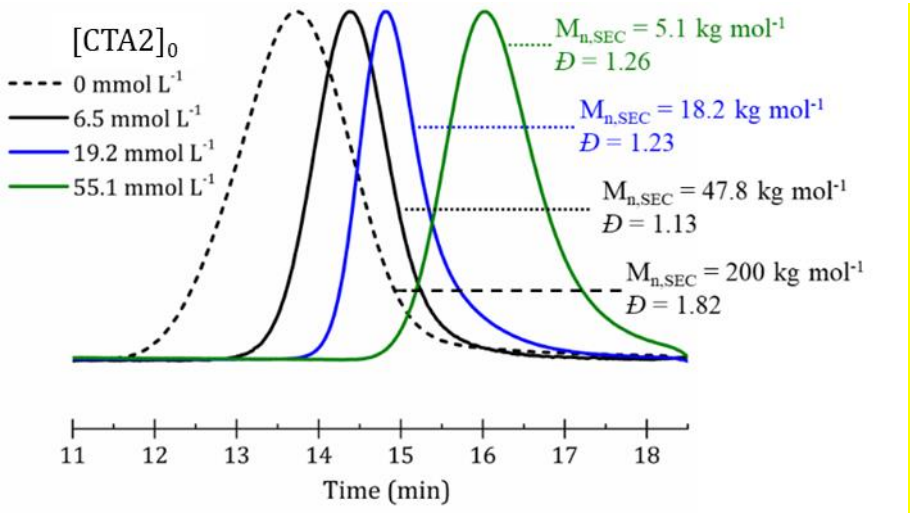

Figure 2-2. Evolution of PNVF SEC-RI traces after 24h reaction for different $[CTA2]_0$. Conditions of Figure 2-1.

These encouraging results led me to delve deeper into the RAFT polymerization of NVF by targeting five different molar masses ranging from 5000 to 100000 g mol^{-1}, with a fixed $[V\text{-}70]_0/[CTA2]_0$ ratio of 0.33. The evolutions of M_n and $Đ$ with monomer conversion are presented in Figure 2-3 with corresponding data in Table 2-1 (entries 9-14) and Table 2-2.

Table 2-1. RAFT polymerization of NVF in DMSO with CTA2 at different initial concentrations at 35°C. $[NVF]_0$ = 4.5 mol L^{-1}, $[V\text{-}70]_0$ = 5.4 mmol L^{-1}.

Entry	Targeted M_n (g mol^{-1})	Time (h)	Conversion [a] (%)	$M_{n,th}$ [b] (g mol^{-1})	$M_{n,SEC}$ [c] (g mol^{-1})	$Đ$
1	-	2	22	-	192000	1.62
2		4	30	-	183000	1.44
3		8	80	-	221000	1.36
4		16	95	-	225000	1.40
5		24	95	-	200000	1.82
6	50000	2	36	18000	22100	1.03
7		8	80	39800	40100	1.03
8		24	93	46200	47800	1.13
9	20000	1.5	13	2500	4700	1.21
10		2	15	3100	6300	1.18
11		4	43	8700	10400	1.17
12		7	58	11700	13200	1.15
13		16	75	15100	14800	1.33
14		24	80	16100	18200	1.23
15	6000	4	27	1700	5100	1.14
16		7	42	2600	4000	1.19
17		16	60	3700	5100	1.19
18		24	66	4000	5100	1.26

[a]calculated by ^{1}H NMR, [b]$M_{n,th}=[NVF]_0/[CTA2]_0\times M_{NVF}\times Conv.+M_{CTA2}$, [c]$M_{n,SEC}$ measured with RI-MALS detection. M_{NVF} =71 g mol^{-1}; M_{CTA2} =161 g mol^{-1}.

Table 2-2. RAFT polymerization of NVF at 35°C in DMSO for different $M_{n,th}$. $[V\text{-}70]_0/[CTA2]_0 = 0.33$. $[NVF]_0 = 4.5$ mol L^{-1} (30% wt NVF in DMSO).

Entry	Targeted M_n (g mol^{-1})	Time (h)	Conversion [a] (%)	$M_{n,th}$ [b] (g mol^{-1})	$M_{n,SEC}$ [c] (g mol^{-1})	$Đ$
1	100000	4	20	20300	17300	1.34
2		8	33	33300	29100	1.32
3		16	42	42400	43600	1.28
4		24	58	58500	53200	1.38
5	50000	2	14	7100	10700	1.18
6		4	24	12000	14600	1.19
7		8	43	21400	23300	1.12
8		16	57	28400	29600	1.19
9		24	66	32800	34300	1.19
10	10000	2	27	2800	5300	1.12
11		4	46	4700	5400	1.11
12		8	70	7100	8400	1.07
13		16	84	8400	9300	1.13
14		24	89	8900	8400	1.23
15	5000	2	35	1900	2600	1.12
16		4	57	2900	4300	1.01
17		8	79	4000	5900	1.10
18		16	90	4500	6200	1.05
19		24	92	4600	5300	1.03

[a]calculated by ^{1}H NMR, [b] $M_{n,th}=[NVF]_0/[CTA2]_0\times M_{NVF}\times Conv.+M_{CTA2}$, [c] $M_{n,SEC}$ measured with a RI-MALS detection. $M_{NVF}=71$ g mol^{-1}; $M_{CTA2}=161$ g mol^{-1}.

For all polymerizations, I observed a linear evolution of $M_{n,SEC}$ with conversion in agreement with $M_{n,th}$. Dispersities tended to increase when reducing $[CTA2]_0$ but remained under $Đ$ = 1.4 (Figure 2-3 and Table 2-2). The maximum NVF conversion decreased when targeting higher molecular weight PNVF, which was expected given the fixed $[V\text{-}70]_0/[CTA2]_0$ ratio and decreasing concentration of CTA2. The evolution of SEC-RI traces with conversion also confirmed the controlled character of the RAFT polymerization with monomodal distributions and a gradual shift of molar mass distributions of PNVF towards lower elution times (Figure 2-4).

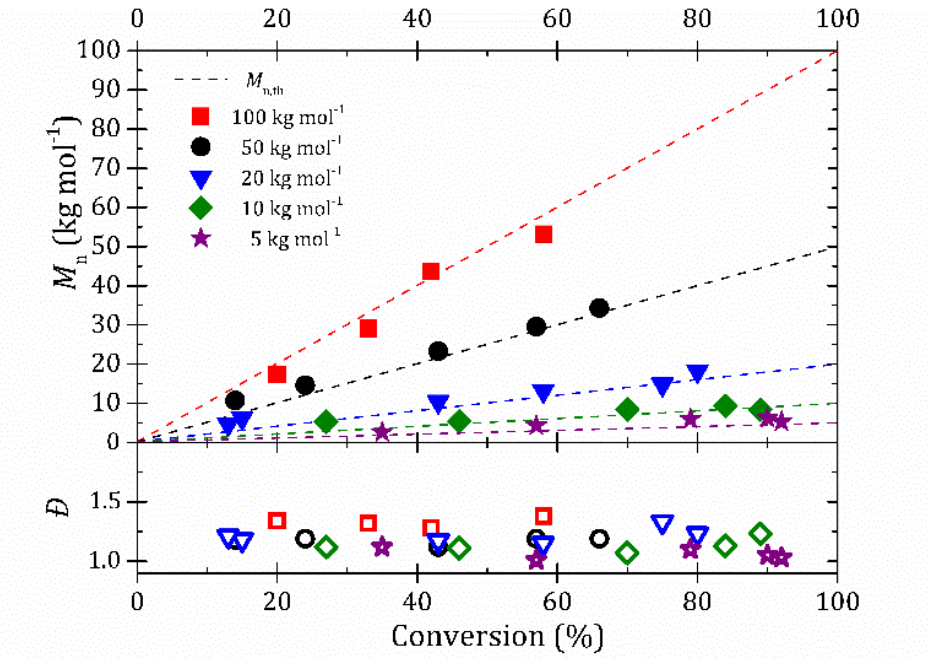

Figure 2-3. Evolution of $M_{n,SEC}$ and $Đ$ with NVF conversion using CTA2 at 35°C for $M_{n,th}$ ranging from 5000 to 100000 g mol^{-1}. $[NVF]_0$ = 4.5 mol L^{-1}. Solvent: DMSO.

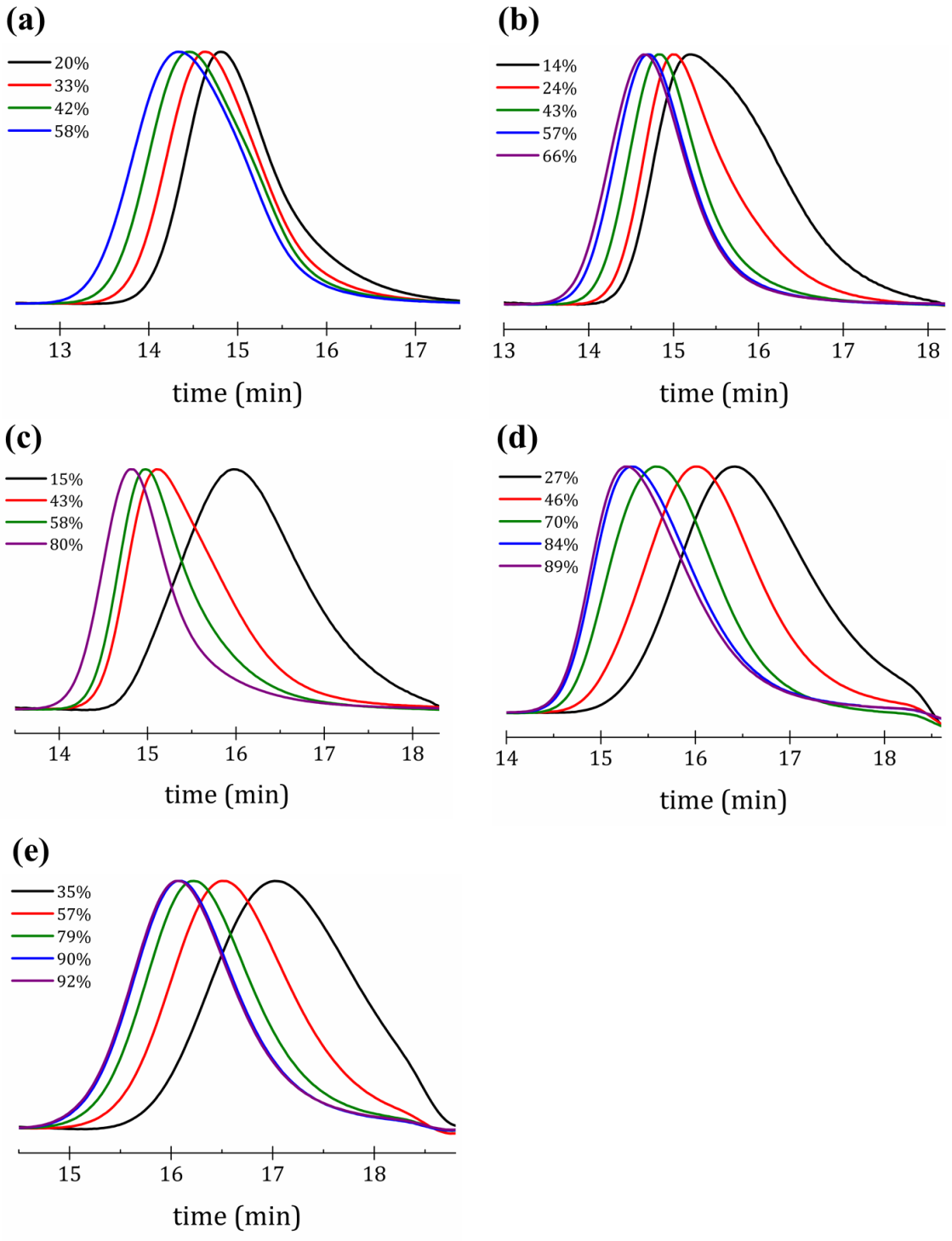

Figure 2-4. Evolution of SEC-RI traces of PNVF with NVF conversion for RAFT polymerization with CTA2 at 35°C (V-70 initiation) aiming for different $M_{n,th}$: **(a)** 100 kg mol^{-1}, **(b)** 50 kg mol^{-1}, **(c)** 20 kg mol^{-1}, **(d)** 10 kg mol^{-1} and **(e)** 5 kg mol^{-1}.

The limited NVF conversion (58%) for the highest targeted M_n of 100000 g mol^{-1} (Table 2-2 entry 4) prompted me to increase the V-70 concentration. As expected, a 2.5-fold increase resulted in a much higher conversion of 87% after 24h (Table 2-3 entry 5). At the same time, the polymerization still exhibited a satisfying level of control (Figure 2-5) as evidenced by predetermined molar masses increasing linearly up to ~80000 g mol^{-1} with conversion, and with dispersities no higher than 1.3 (Table 2-3). This result was relatively unexpected when considering that these reaction conditions correspond to an initiator to CTA2 ratio of 0.83, which is way higher than for classical RAFT conditions. A similar phenomenon was encountered in my previous chapter on NMVA where polymerizations unexpectedly showed a satisfying control of molar masses for an abnormally high [V-70]/[CTA] ratio of 1.49/1. This result may be ascribed to the low efficiency of V-70 in NVF polymerization. In the literature, a low efficiency factor *f* between 0.2 and 0.3 was reported for the polymerization of other *N*-vinyl monomers such as NMVA,[52] VP[53] and VCL[53].

Table 2-3. RAFT polymerization of NVF at 35°C in DMSO aiming for $M_{n,th.}$= 100 kg mol^{-1}. $[NVF]_0$ = 4.5 mol L^{-1}, $[CTA2]_0$ = 3.2 mmol L^{-1}, $[V\text{-}70]_0$ = 2.7 mmol L^{-1}.

Entry	Targeted M_n (g mol^{-1})	Time (h)	Conversion [a] (%)	$M_{n,th}$ [b] (g mol^{-1})	$M_{n,SEC}$ [c] (g mol^{-1})	$Đ$
1	100000	2	18	18100	20700	1.31
2		4	32	32100	39200	1.19
3		8	51	51100	53900	1.18
4		16	79	79000	74300	1.22
5		24	87	87000	79500	1.22

[a]calculated by ^{1}H NMR, [b] $M_{n,th}=[NVF]_0/[CTA2]_0\times M_{NVF}\times Conv.+M_{CTA2}$, [c]$M_{n,SEC}$ measured with a RI-MALS detection. M_{NVF}=71 g mol^{-1}; M_{CTA2}=161 g mol^{-1}.

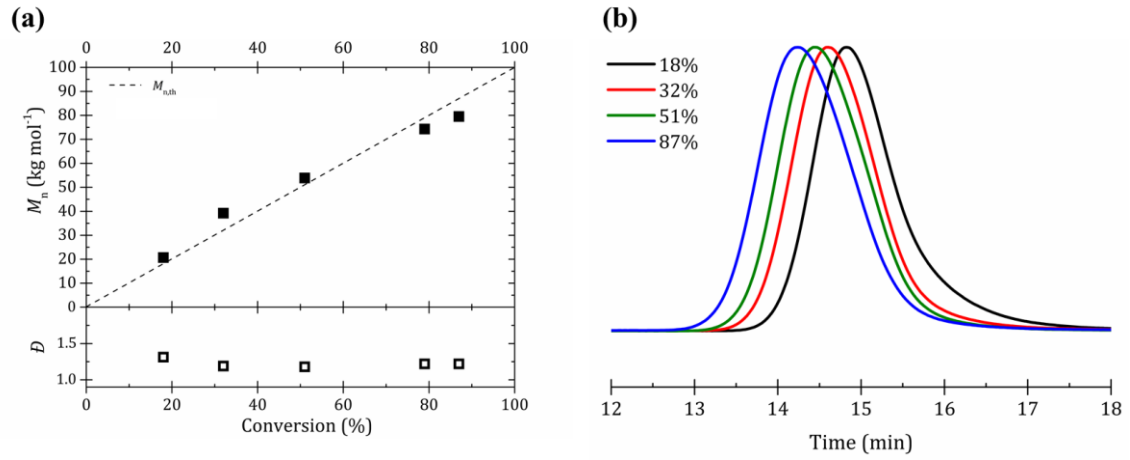

Figure 2-5. Evolution of **(a)** $M_{n,SEC}$, $Đ$ and **(b)** SEC-RI traces with monomer conversion for the RAFT polymerization of NVF in DMSO (data taken from Table 2-3).

2.2.1.2 Chain-end fidelity

To attest the effective presence of the xanthate at the chain-end of PNVFs, electrospray ionization time of flight mass spectrometry (ESI-TOF-MS) analysis was conducted on a low molar mass PNVF$_{5k}$-CTA2 ($M_{n,SEC}$ = 4700 g mol^{-1} and $Đ$ =1.21, Table 2-1 entry 9). ESI–TOF-MS analysis (Figure 2-6) showed three main overlapping populations corresponding to mono-, bis- and tris-charged PNVF chains capped with the xanthate functionality and of general formula C_2H_2N-$(C_3H_5NO)_n$-$C_3H_5OS_2$,xNa^+ (x = 1, 2 and 3) confirming the presence of the xanthate on the majority of the polymer chains. Other populations of smaller intensities were also observed but could not be identified.

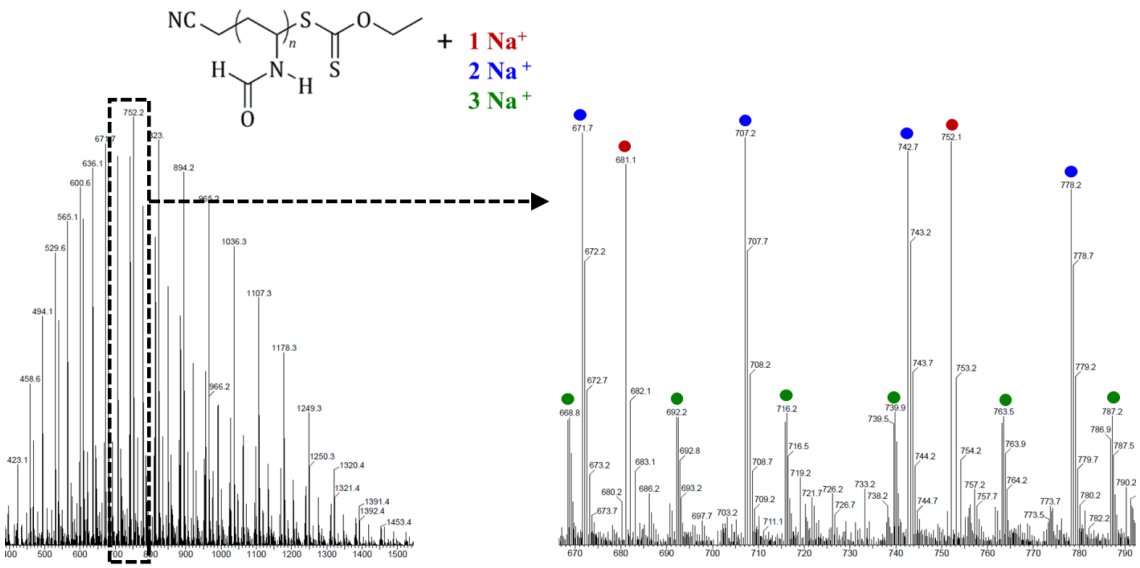

Figure 2-6. (left) ESI-TOF-MS spectrum of PNVF-CTA2 and (right) a zoomed portion with attributions of populations.

To further show the livingness of the obtained polymer chains, I conducted the chain extension of a PNVF-CTA2 polymer, starting from a polymer of M_n = 4700 g mol^{-1} and targeting a M_n = 50000 g mol^{-1} (Figure 2-7 and Table 2-4). A relatively linear evolution of molar masses with NVF conversion was observed (Figure 2-7a), with values a bit higher but close to what was expected, and dispersities maintained below 1.3 throughout the experiment. Looking at the SEC-RI traces, a clear shift was observed towards lower elution times, with monomodal distributions (Figure 2-7b).

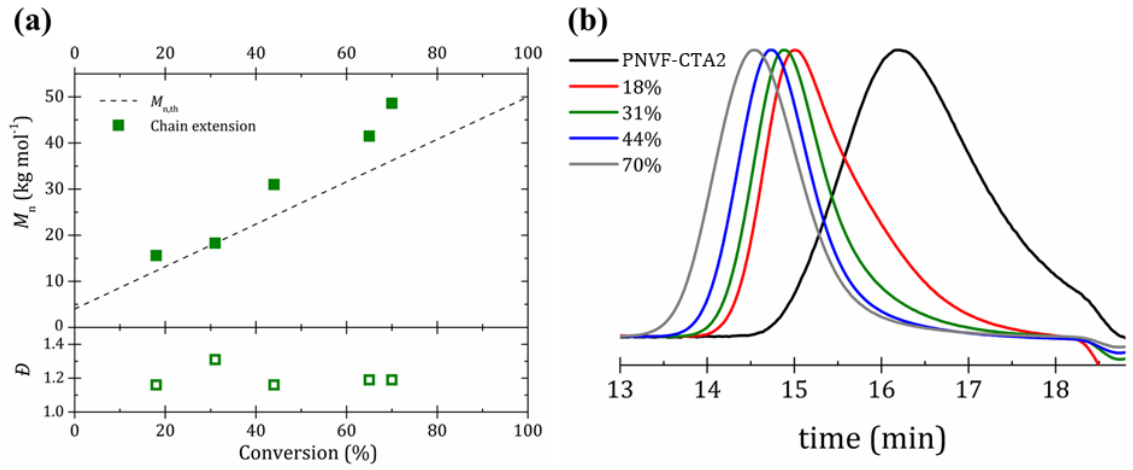

Figure 2-7. Evolution of **(a)** $M_{n,SEC}$, $Đ$ and **(b)** SEC-RI traces with monomer conversion for the chain extension of PNVF-CTA2 at 35°C. $[NVF]_0$ = 4.5 mol L^{-1}, $[PNVF\text{-}CTA2]_0$ = 7.0 mmol L^{-1}, $[V\text{-}70]_0$ = 2.3 mmol L^{-1}.

Table 2-4. RAFT polymerization of NVF at 35°C (V-70 initiation) using a PNVF-CTA2 macro-RAFT agent. $[NVF]_0$ = 4.5 mol L^{-1}, $[PNVF\text{-}CTA2]_0$ = 7.0 mmol L^{-1}, $[V\text{-}70]_0$ = 2.3 mmol L^{-1}.

Entry	Targeted M_n (g mol^{-1})	Time (h)	Conversion [a] (%)	$M_{n,th}$ [b] (g mol^{-1})	$M_{n,SEC}$ [c] (g mol^{-1})	$Đ$
1	50000	2	18	12300	15600	1.16
2		4	31	18300	18300	1.31
3		8	44	24200	31000	1.16
4		16	65	33900	41500	1.19
5		24	70	36200	48600	1.19

[a]calculated by ^{1}H NMR, [b]$M_{n,th}=[NVF]_0/[PNVF\text{-}CTA2]_0\times M_{NVF}\times conv.+M_{n,PNVF\text{-}CTA2}$, with $M_{n,PNVF\text{-}CTA2}$ = 4700 g mol^{-1}; [c]$M_{n,SEC}$ measured with a RI-MALS detection

These results allowed me to conclude that NVF can be efficiently controlled by RAFT polymerization, paving the way to the synthesis of PNVF-based block copolymers.

2.2.2 Poly (*N*-vinylformamide)-based double hydrophilic block copolymers

A strength of the RAFT polymerization technique is its ability to produce copolymers of controlled architectures. A series of PNVF-based double hydrophilic block copolymers (DHBC) were synthesized via RAFT polymerization of NVF from PDMA-CTA1, PVCL-CTA1 and PNIPAAm-CTA1 precursors, respectively leading to PDMA-*b*-PNVF, PVCL-*b*-PNVF and PNIPAAm-*b*-PNVF (Scheme 2-2).

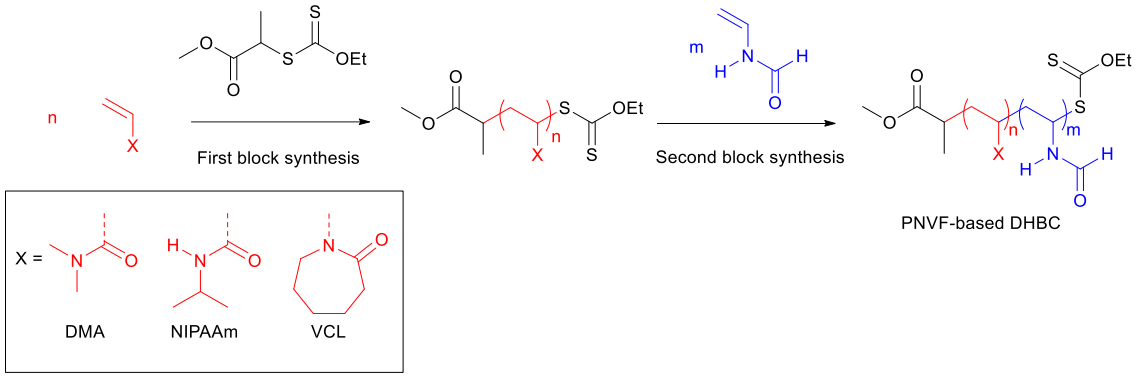

Scheme 2-2. General scheme for synthesis of PNVF-based DHBCs

To better highlight the effective formation of DHBCs, I targeted PDMA, PNIPAAm and PVCL first blocks of low molar mass ($M_{n,th}$ = 5000 g mol^{-1}) via RAFT polymerization using xanthate CTA1, a well-known versatile control agent for monomers of disparate reactivities.[30,31] PDMA-CTA1 ($M_{n,SEC}$ = 6200 g mol^{-1}, $Đ$ = 1.30), PVCL-CTA1 ($M_{n,SEC}$ = 6400 g mol^{-1}, $Đ$ = 1.11) and PNIPAAm-CTA1 ($M_{n,SEC}$ = 6300 g mol^{-1}, $Đ$ = 1.31) were obtained with $M_{n,SEC}$ slightly higher than expected but still close to the expected values, and low dispersities (Table 2-5 entries 1, 3, 5). Then, RAFT polymerization of NVF at 35°C was performed in the presence of the previously synthesized CTA1-capped polymers as macro-CTAs. Diblock copolymers of around 30000 g mol^{-1} were targeted. All polymerizations occurred with a satisfying conversion of 80% achieved after 16h (Table 2-5 entries 2, 4, 6).

Table 2-5. Block polymerization of NVF at 35°C in DMSO for 16h using PDMA-CTA1, PVCL-CTA1 and PNIPAAm-CTA1 as macro-RAFT agents. $[NVF]_0$ = 4.5 mol L^{-1}. $[V\text{-}70]_0/[\text{macro-CTA}]_0$ = 0.33.

Entry	Polymer	Target. M_n (g mol^{-1})	Conv.[a] (%)	$M_{n,th}$ [b] (g mol^{-1})	$M_{n,SEC}$ [c] (g mol^{-1})	$Đ_{SEC}$	$M_{n,A4F}$ [c] (g mol^{-1})	$Đ_{AF4}$
1	PDMA-CTA1	5000	99	5000	6200	1.30	9900	1.23
2	PDMA-*b*-PNVF	32700	83	28100	-	-	28900	1.21
3	PVCL-CTA1	5000	99	5000	6400	1.11	6000	1.04
4	PVCL-*b*-PNVF	36000	82	30600	-	-	37200	1.27
5	PNIPAAm-CTA1	5000	99	5000	6300	1.31	9800	1.28
6	PNIPAAm-*b*-PNVF	40300	81	33800	-	-	46800	1.18

[a]calculated by ^{1}H NMR. [b]$M_{n,th}=[\text{Monomer}]_0/[\text{macro-CTA}]_0\times M_{Monomer}\times\text{conv.}+M_{n,macro\text{-}CTA}$; [c]measured with a RI-MALS detection.

The complex nature of these DHBCs, composed of one block that can only be eluted in organic SEC and the other PNVF block that can only be eluted in aqueous SEC, made all my attempts to measure accurate M_n and dispersities by SEC unsuccessful. In aqueous SEC, only PDMA-CTA1 and PDMA-*b*-PNVF were both eluted with a shift of SEC traces between the first block and the DHBC (Figure 2-8a), but with strong interactions with the SEC columns preventing any precise molar mass measurement. As for the other two DHBCs, both PNIPAAm-CTA1 and PVCL-CTA1 could not be eluted in aqueous SEC, with no signal from the RI detector (Figure 2-8b and c). Their corresponding DHBCs were eluted in aqueous SEC thanks to the high proportion of PNVF, but still with strong interactions with the SEC columns and therefore no accurate values for M_n and dispersities could be obtained.

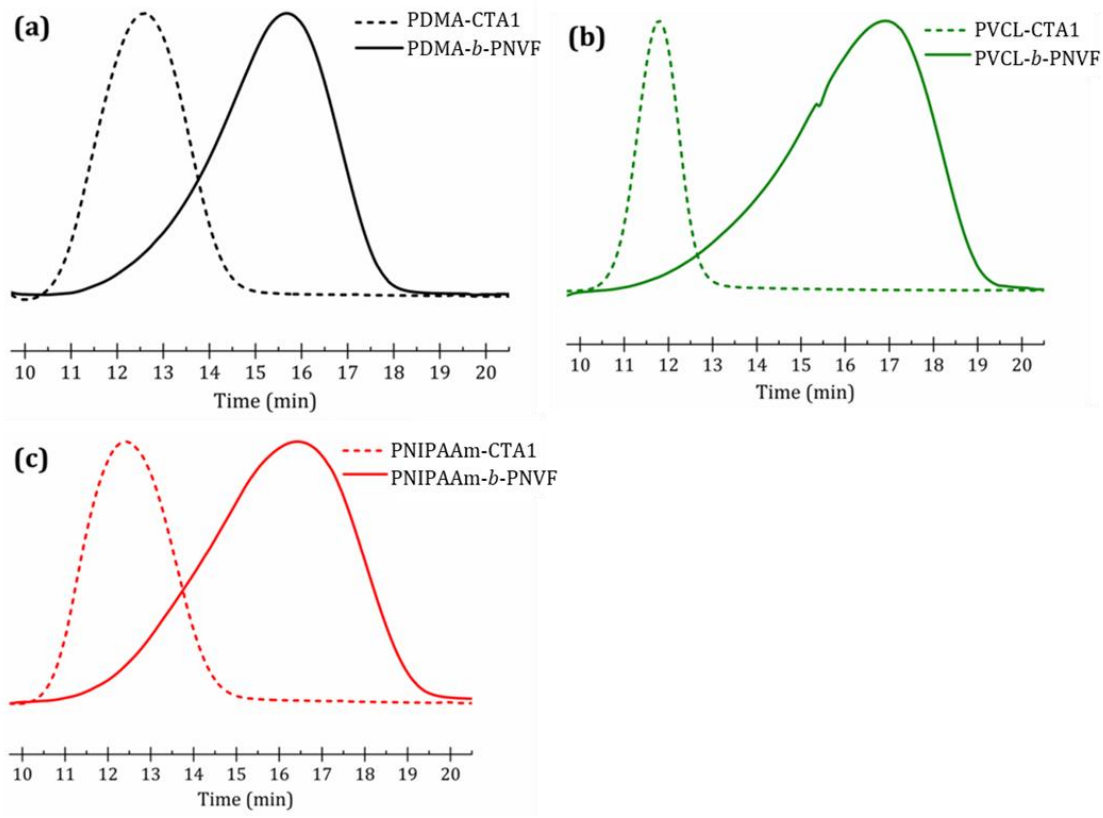

Figure 2-8. SEC-RI traces of **(a)** PDMA-*b*-PNVF, **(b)** PVCL-*b*-PNVF, **(c)** PNIPAAm-*b*-PNVF and corresponding first blocks.

Thus, I turned to alternative characterization techniques such as asymmetrical flow field flow fractionation (AF4) and diffusion-ordered spectroscopy NMR (DOSY-NMR). With AF4, it is possible to separate macromolecules based on their diffusion coefficients in the parabolic flow of an eluent, without the need of a stationary phase. Therefore, it eliminates the problem of column interactions and gives the possibility to analyze PNVF-based DHBCs and measure their molar masses. Indeed, during the analysis a crossflow is applied in the channel, through a membrane, to the injected sample and macromolecules are first separated with the bigger ones diffusing closer to the membrane. Then, a parabolic flow is applied to elute the sample. As the macromolecules of lower molecular weight diffused closer to the center, they will be faster eluted than the macromolecules of higher molecular weights. Fractograms of DHBCs and their corresponding first blocks were clearly

detected at different elution times, with lower ones for the smaller first blocks and higher ones for the DHBCs, with no significant sign of residual first blocks, attesting the successful synthesis of the diblock copolymers. (Figure 2-9). Molar mass determination was in agreement with theoretical values for PDMA-*b*-PNVF ($M_{n,AF4}$ = 28900 g mol^{-1}, $Đ$= 1.21; $M_{n,th}$ = 28100 g mol^{-1}) and PVCL-*b*-PNVF ($M_{n,AF4}$ = 37200 g mol^{-1}, $Đ$= 1.27; $M_{n,th}$ = 30600 g mol^{-1}) (Table 2-5, entries 2 and 4). However, in the case of PNIPAAm-*b*-PNVF a $M_{n,AF4}$ = 46800 g mol^{-1} and $Đ$ = 1.18 were measured, way higher than the expected value ($M_{n,th}$ = 33800 g mol^{-1}) (Table 2-5, entry 6) compared to the other two.

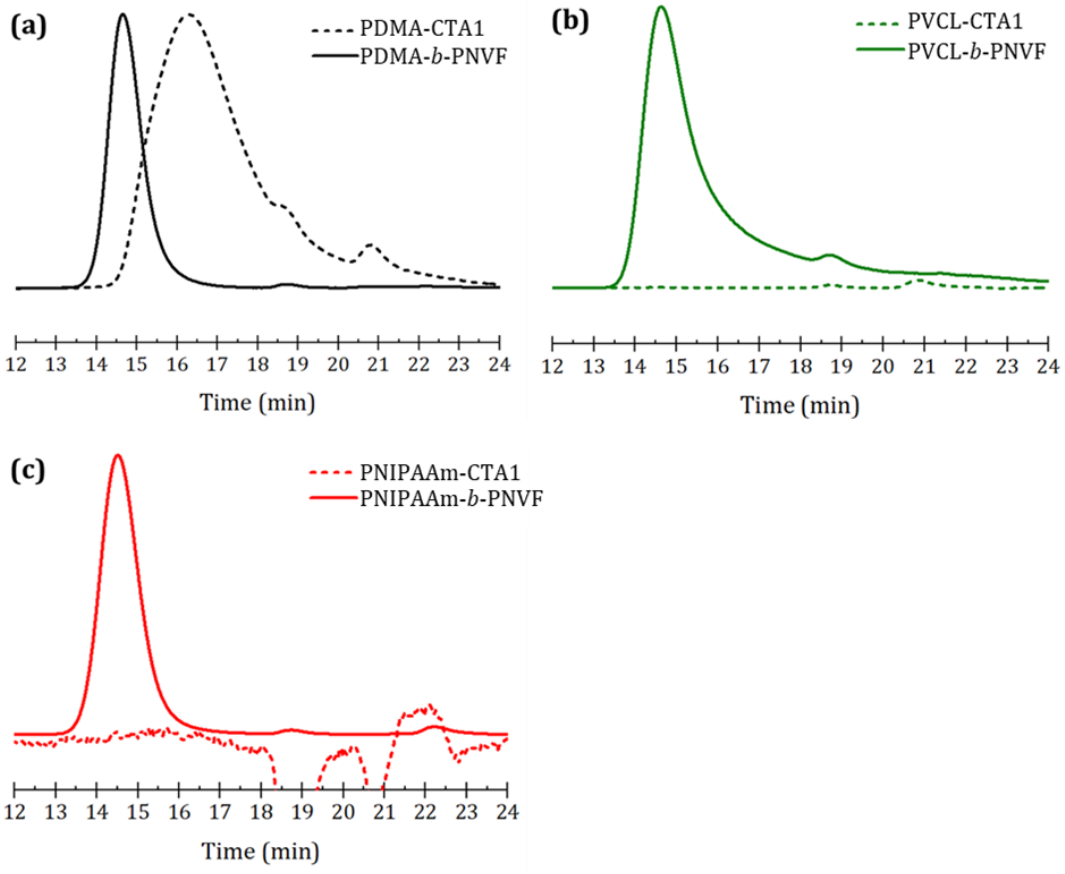

Figure 2-9. AF4-RI fractograms of **(a)** PDMA-*b*-PNVF **(b)** PVCL-*b*-PNVF **(c)** PNIPAAm-*b*-PNVF copolymers with corresponding first blocks.

The fact that no significant residual PNIPAAm first block was detected after DHBC synthesis rules out the possibility of the formation of a diblock of much higher M_n than expected which would result from partial reactivation of PNIPAAm-CTA1. I rather thought that this higher molar mass may result from the partial self-aggregation of the PNIPAAm-*b*-PNVF copolymer in water that can't be dissociated by the very low shear forces in AF4, resulting in the detection of larger objects. To support this hypothesis, I analyzed by dynamic light scattering (DLS) a 0.5 mg mL^{-1} aqueous solution of PNIPAAm-*b*-PNVF and observed the formation of 10 nm diameter objects in the 25-35°C range, corresponding to the temperature range of the AF4 equipment and detectors, explaining the apparent high molar mass detected in AF4. (Figure 2-10)

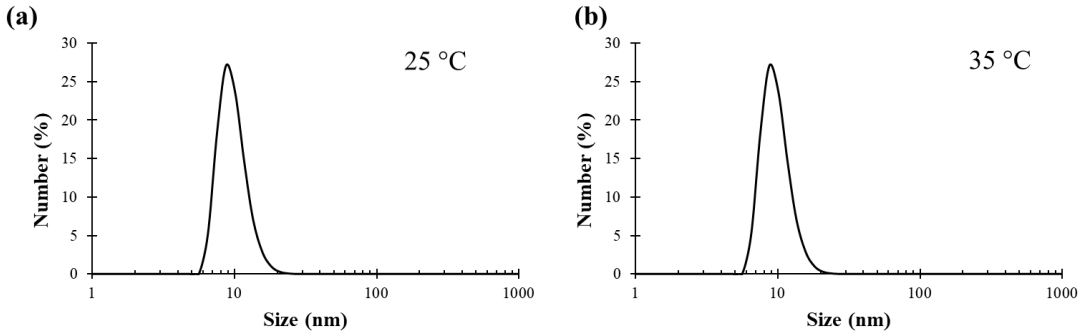

Figure 2-10. Dynamic light scattering measurements at **(a)** 25°C and **(b)** 35°C of PNIPAAm-*b*-PNVF block copolymer at a concentration of 0.5 mg mL^{-1} in ultrapure water.

To support the AF4 analysis, I performed ^1H DOSY-NMR on the DHBCs and their corresponding first blocks. This NMR technique allows the determination of the diffusion coefficients of molecules. By mapping in two dimensions the ^1H NMR spectrum against the diffusion coefficient, it becomes possible to visualize the efficiency of block copolymerization and detect the presence -or not- of residual first block in a diblock copolymer. With no surprise and confirming the results obtained with AF4, no residual first blocks were found in the DHBCs, with a significant

difference in their diffusion coefficients (Figure 2-11 and Table 2-6). As illustrated in Figure 2-11 with PDMA-CTA1 and PDMA-*b*-PNVF, ^{1}H NMR signals of the first block are detected at a diffusion coefficient of 33 $\mu m^2\ s^{-1}$, and in the DHBC the same ^{1}H NMR signals now shifted to a lower diffusion coefficient at 4 $\mu m^2\ s^{-1}$, with the ^{1}H NMR signals of the NVF units newly incorporated (Table 2-6 entries 1-2, Figure 2-11).

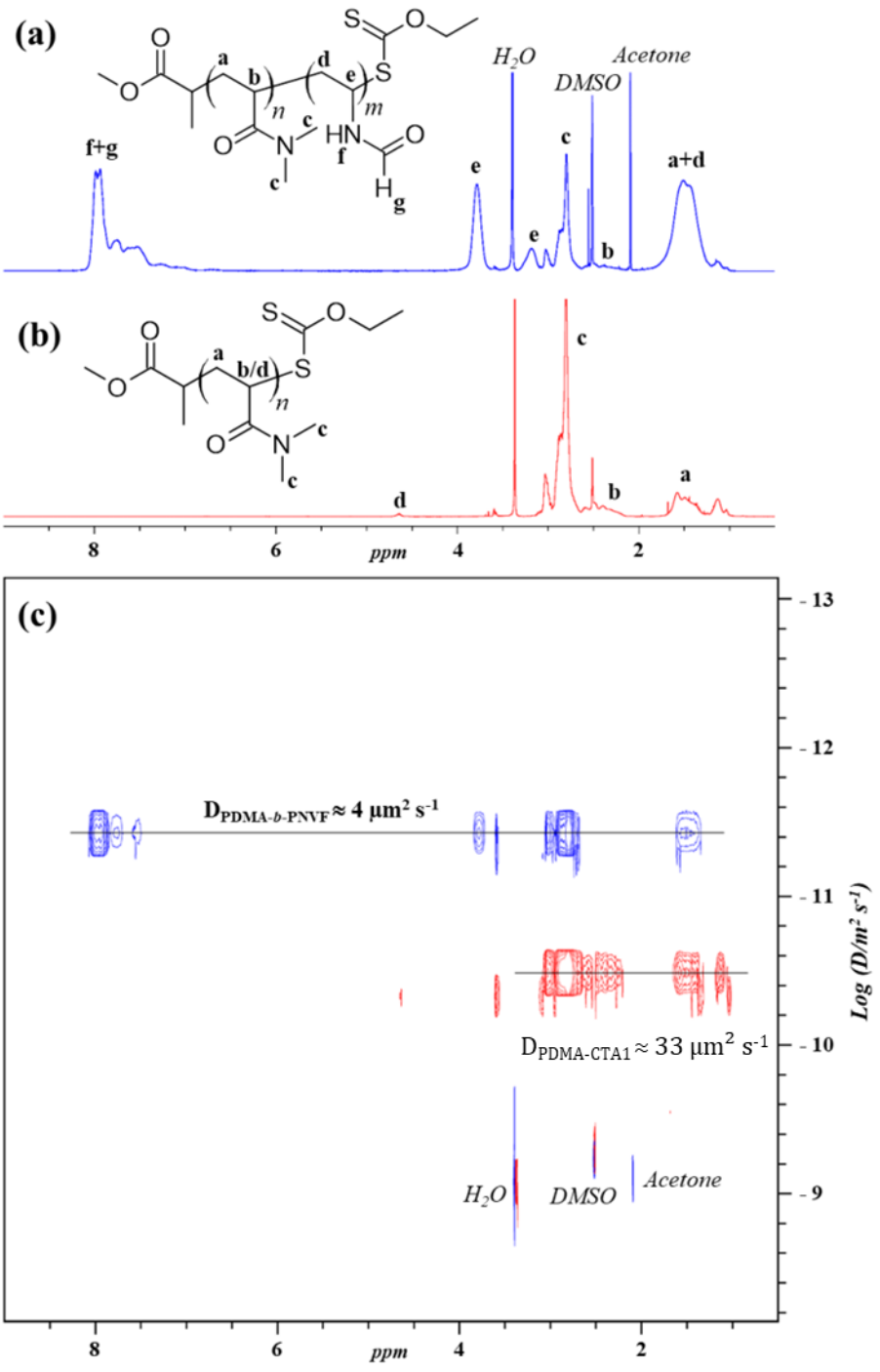

Figure 2-11. ^{1}H NMR spectra of **(a)** PDMA-*b*-PNVF and **(b)** PDMA-CTA1, measured on a 500MHz apparatus. **(c)** Superposition of ^{1}H DOSY NMR of PDMA-CTA1 in red and copolymer PDMA-*b*-PNVF in blue.

Table 2-6. ^{1}H DOSY-NMR analysis data of the block copolymers and their first block.

Entry	Polymer	$M_{n,SEC}$[a] ($M_{n,A4F}$[a]) (g mol^{-1})	Diffusion coefficient of first block[b] (μm^2 s^{-1})	Diffusion coefficient of second block[b] (μm^2 s^{-1})
1	PDMA-CTA1	6200 (9900)	33.2 ± 0.4 (c)	-
2	PDMA-*b*-PNVF	(28900)	4.0 ± 0.6 (c)	3.8 ± 0.4 (f+g)
3	PVCL-CTA1	6400 (6000)	58 ± 3 (c)	-
4	PVCL-*b*-PNVF	(37200)	2.5 ± 0.3 (a+e+f)	2.5 ± 0.3 (h+i)
5	PNIPAAm-CTA1	6300 (9800)	32.6 ± 0.5 (e)	-
6	PNIPAAm-*b*-PNVF	(46800)	3.4 ± 0.6 (e)	2.9 ± 0.4 (h+i+c)

[a] measured with a RI-MALS detection; [b] determined by DOSY-NMR technique applied on the attributed ^{1}H NMR signals of Fig. 2-11 for PDMA-CTA1 and PDMA-*b*-PNVF and of Fig. 2-12 for the two other copolymers.

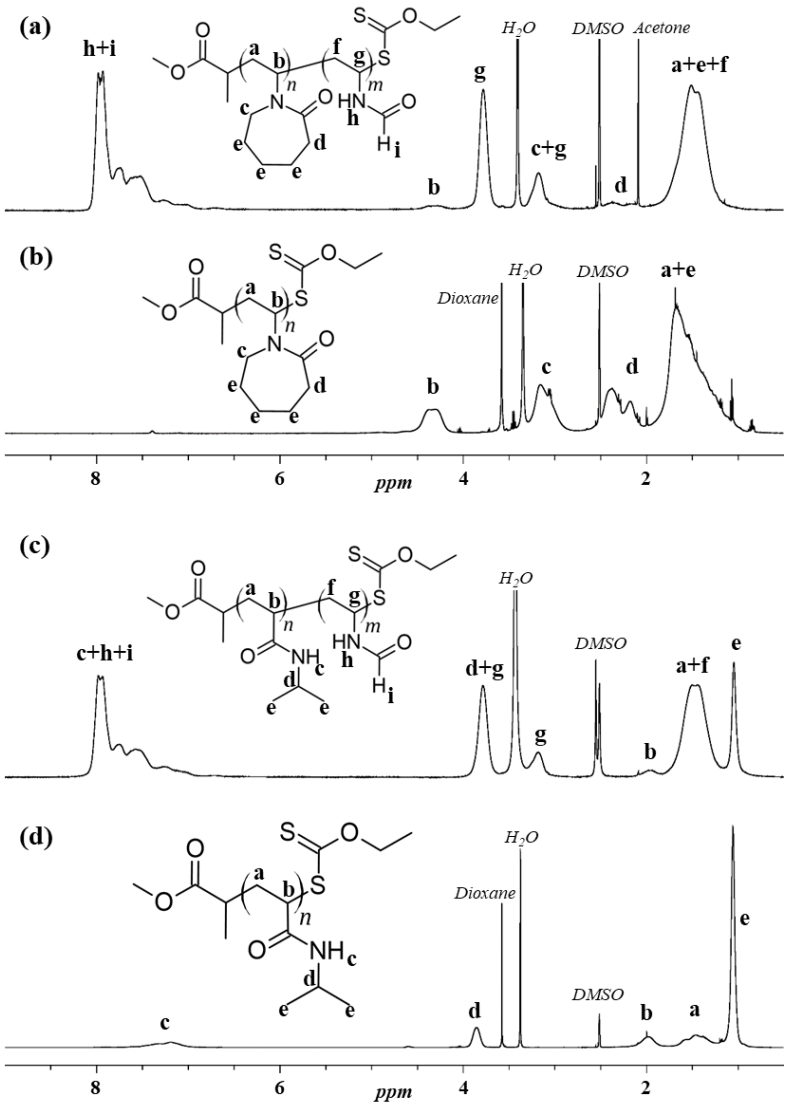

Figure 2-12. ^{1}H NMR spectra of **(a)** PVCL-*b*-PNVF, **(b)** PVCL-CTA1, **(c)** PNIPAAm-*b*-PNVF and **(d)** PNIPAAm-CTA1 analyzed via DOSY-NMR (Table 2-6). Measured in DMSO-*d6* on a 500MHz apparatus.

2.2.4 Hydrolysis of PNVF into polyvinylamine

PNVF is a major precursor of polyvinylamine (PVAm), and its controlled incorporation into complex macromolecular structures can pave the way to new PVAm-based materials. To illustrate this possibility, I undertook the basic hydrolysis according to a previously published procedure[24] of PVCL-*b*-PNVF to yield the dual

thermo- and pH-responsive PVCL-*b*-PVAm, with LCST properties of the PVCL block[32] and the cationic polyelectrolyte character of PVAm.[33,34] The reaction was followed by ^{1}H NMR and the total disappearance of the formamide characteristic signals of the NVF units at 7.5-8 ppm in the final PVCL-*b*-PVAm copolymer was observed, indicating the successful transformation of the formamide groups into primary amines. (Figure 2-13b and 2-13c). However, I didn't investigate the physicochemical properties of this relatively complex stimuli-responsive copolymer.

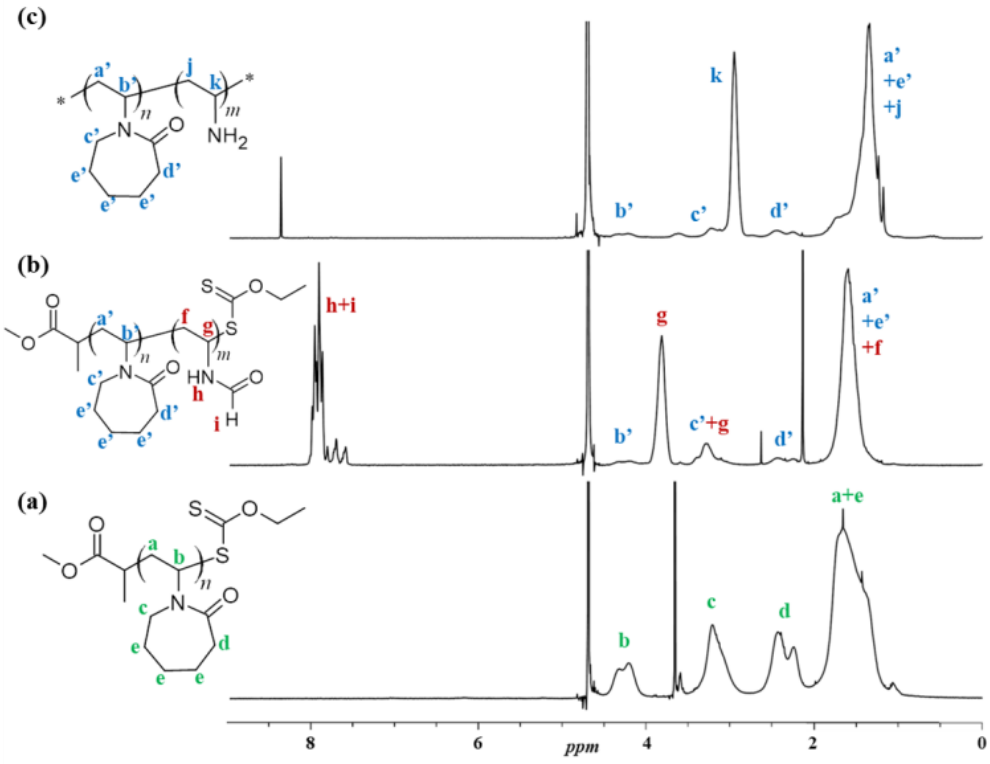

Figure 2-13. ^{1}H NMR spectra of **(a)** PVCL-CTA1, **(b)** PVCL-*b*-PNVF and **(c)** PVCL-*b*-PVAm. Measured on a 300MHz apparatus.

2.3 CONCLUSION

The polymerization of *N*-vinylformamide was successfully controlled on a wide range of molar masses with low dispersities via RAFT polymerization at 35°C in DMSO, using a xanthate. The quality of the control was confirmed by ESI-TOF-MS spectrometry. Well-defined PNVF-based double hydrophilic block copolymers were also synthesized and characterized by AF4 and ^{1}H DOSY-NMR. Finally, the selective hydrolysis of PNVF block in PVCL-*b*-PNVF block copolymer was performed, thereby giving access to a new PVCL-*b*-PVAm copolymer, marking the starting line for future developments in the synthesis, properties and applications of complex copolymers comprising tailor-made PVAm segments.

Thanks to the results of this chapter, in addition to the previous Chapter 1, I was able to establish a way to control the RAFT polymerization of an acyclic *N*-alkyl-*N*-vinylalkylamide (NMVA, Chapter 1) and a *N*-vinylamide (NVF, Chapter 2), and I observed that the latter is significantly more reactive than the former. In the next chapter, the RAFT polymerization of a *N*-vinylalkylamide, *N*-vinylisobutyramide (NVIBA) will be investigated. Moreover, as NVIBA leads to polymers showing thermoresponsive properties, the synthesis and characterization of new NVIBA-based block copolymers will also be studied.

2.4 EXPERIMENTAL SECTION

2.4.1 Characterization

NMR analysis.

^{1}H NMR spectra were recorded at 25°C on a Bruker Avance 300 instrument at an operating frequency of 300 MHz. All samples except for the hydrolysis experiment were dissolved in dimethylsulfoxide (DMSO-d_6). The hydrolysis experiment samples were dissolved in deuterium oxide (D_2O). Coupling constants (J) are reported to ± 0.5 Hz. The resonance multiplicities are described as s (singlet), d (doublet), t (triplet), q (quartet) or m (multiplet). Chemical shifts δ are reported in parts per million (ppm) and are referenced to the residual solvent peak (DMSO: H = 2.5 ppm; D_2O: H = 4.7 ppm).

^{1}H and 2D DOSY NMR analysis.

All NMR experiments were acquired on a Bruker Avance 500 spectrometer operating at a frequency of 500 MHz, equipped with a 5 mm dual ^{1}H-^{13}C TCI cryoprobe at 5°C. Samples were dissolved in dimethyl sulfoxide (DMSO-d_6.) 1D ^{1}H NMR profiles were obtained by using a classical NMR pulse sequence with a relaxation delay of 2 s, a flip angle of 90°, an acquisition time of 5.45 s and a spectral width of 12 ppm. The self-diffusion coefficients (D) were measured with specific pulsed field gradient NMR sequences, by incrementing the gradient strength for a series of 1D spectra and by fitting the decay behavior of the NMR signal attenuation with the Stejskal-Tanner equation.[35]

$$I = I_0 e^{[-(\gamma g \delta)^2 \left(\Delta - \frac{\delta}{3}\right) D]}$$

Where I is the signal intensity and I_0 the signal intensity without gradient, γ the gyromagnetic ratio, g and δ the strength and the length of the pulsed field gradient, Δ the diffusion time and D the self-diffusion coefficient.

Diffusion ^{1}H NMR spectra were recorded with a bipolar pulse pairs-stimulated echo pulse sequence with longitudinal eddy current delay and convection compensation (dstebpgp3s in Bruker library).[36] The acquisition parameters were as follows: 64K data points, acquisition time 5.45 s, spectral width 12 ppm, number of scans 16, relaxation delay 3 s and a recovery delay after each gradient 3 ms. The field gradient length and diffusion time were respectively 5.8 ms and 550 ms for PDMA-CTA1 and PNIPAAm-CTA1, 4.8 ms and 300 ms for PVCL-CTA1, and 10 ms and 1000 ms for the block copolymers (PDMA-*b*-PNVF, PNIPAAm-*b*-PNVF, PVCL-*b*-PNVF). The spoiler gradients were 0.6 ms long with a field strength of -9.26, -8.32 and -7.12 G cm^{-1}. Twenty experiments were recorded with a linear gradient sampling from 5 to 95%. The gradient system was calibrated to 54.1 G cm^{-1} at maximum intensity. DOSY NMR data were processed with the DOSY workup module including in the Topspin 3.2 software. The data sets of diffusion NMR experiments were generated and extracted with the Topspin 3.2 software and transferred to the Origin 9.1 software. The exponential fit tool was then used to determine D values using the equation $y = a*\exp(-D*x)$ where $y = I$, $a = I_0$ and $x = [(\gamma g \delta)^2(\Delta - \delta/3)]$. Standard deviations (SD) for diffusion NMR were obtained from the exponential fit tool included in the Origin 9.1 software.

Size-exclusion chromatography.

Size-exclusion chromatography (SEC) analysis in water + 0.2 M NaCl + 0.025 M $NaHPO_4$ + 0.025 M Na_2HPO_4 were performed on a system composed of a SB-G precolumn followed by a set of two SB-806M HQ and SB-802.5 HQ (Shodex) columns. Detections were conducted using an Agilent 1260 Infinity II refractive index detector, a Varian ProStar UV detector (dual wavelength analysis at 290 and 254 nm) and a Wyatt Dawn HELEOS multi-angle light scattering detector. Aqueous SEC was used to characterize PNVFs, PDMA-*b*-PNVF, PVCL-*b*-PNVF and PNIPAAm-*b*-PNVF polymers and copolymers. $(dn/dc)_{PNVF}$ = 0.162 mL g^{-1} was measured with a PSS DnDc-2010 differential refractometer.

SEC analysis in DMF/LiBr (10 mM) was performed on a system composed of an Agilent technologies guard column (PLGel20 µm, 50 × 7.5 mm) and a set of two KD-

804 and KD-805L (Shodex) columns. Detections were conducted using a Wyatt Optilab® rEX refractive index detector, a Varian ProStar UV detector (dual wavelength analysis at 290 and 254 nm) and a Wyatt MiniDawn TREOS multi-angle light scattering detector. Analyses were performed at 55°C and a flow rate of 1.0 mL min^{-1}. Organic SEC was used to characterize PDMA, PVCL and PNIPAAm polymers.

$(dn/dc)_{PNIPAAm}$ = 0.087 mL g^{-1},[37] $(dn/dc)_{PDMA}$ = 0.087 mL g^{-1},[38] $(dn/dc)_{PVCL}$ = 0.092 mL g^{-1}.[32]

Asymmetrical flow field flow fractionation (AF4) coupled with multiangle light scattering and differential refractometer.

AF4 analyses were done using a Thermo Scientific Dionex UltiMate3000 HPLC System with pump, thermostated autosampler (set at 25°C) and UV detector (set at 290 nm). The pump was coupled with the Eclipse AF4 (Wyatt Technology) to regulate flows in the separation channel (long channel, Wyatt Technology). An ultrafiltration membrane of regenerated cellulose material with a cut-off at 2 kDa (Wyatt Technology) was used. A 350 µm thick Mylar spacer of trapezoidal geometry (length of 23.6 cm, initial breadth of 2.1 cm and final breadth of 0.6 cm) was inserted between the membrane and the upper glass plate. A multi-detection system including an 8-angle Dawn8+ MALS detector and an Optilab T-rEX dRI (Wyatt Technology) was coupled with the AF4 system. Chromeleon 7.2.10 software was used to control the autosampler, pump and Eclipse flows. Acquisition of UV, MALS-Qels and dRI data was performed by the Astra 7.1.2.5 software. Zimm model was used to obtain the average molecular weight M_w via MALS.[39]

dn/dc of the polymers and copolymers were measured on the same Optilab T-rEX dRI detector (Wyatt Technology) and acquisitions performed using Astra 7.1.2.5. $(dn/dc)_{PDMA}$ = 0.161 mL g^{-1}; $(dn/dc)_{PDMA\text{-}b\text{-}PNVF}$ = 0.165 mL g^{-1}; $(dn/dc)_{PVCL}$ = 0.174 mL g^{-1}; $(dn/dc)_{PVCL\text{-}b\text{-}PNVF}$ = 0.170 mL g^{-1}; $(dn/dc)_{PNIPAAm}$ = 0.150 mL g^{-1}; $(dn/dc)_{PNIPAAm\text{-}b\text{-}PNVF}$ = 0.168 mL g^{-1}.

The system was calibrated using a standard bovine serum albumin (BSA, Sigma-Aldrich) solution. The eluent used was composed of Milli-Q Water with 0,1 mol L^{-1}

sodium nitrate and 0,02 wt% sodium azide, filtered through 0,1 μm with PTFE filter (Merck). For separation, the detector flow rate was maintained at 1 mL min^{-1}. During the focus/injection step, the focus-flow rate was set at 3 mL min^{-1}. After 1 min, samples were injected at 0.2 mL min^{-1} over a period of 4 min. The focus-flow was then maintained for 2 min. During the elution step, the cross-flow was first set at 5 mL min^{-1} then decreased exponentially to reach 0.1 mL min^{-1} after 16 min. It was then maintained at 0.1 mL min^{-1} for 5 min. The system was rinsed with eluent for 28 min after each sample.

Electrospray ionization- time of flight mass spectrometry (ESI-TOF-MS).

ESI-TOF mass spectra were acquired with a QTOF Premier mass spectrometer (Waters), in electrospray ionization, in positive mode. Samples of PNVF were dissolved in water, diluted at 1/20 in methanol and then NaI was added. The resulting samples were directly infused in the source. The source temperature and desolvation temperature were 110 °C and 200 °C, respectively, and the cone voltage was optimized at 30 V. The acquisition software was Masslynx (Waters) and the spectra were processed by using Masslynx and Polymerix 3.0 (Sierra Analytics).

Dynamic light scattering.

Dynamic Light Scattering (DLS) measurements were carried out using a Malvern ZetaSizer Nano ZS with a He-Ne laser at 633 nm at 25°C and 35°C. Sample was prepared at a concentration 0.5 mg mL^{-1} in ultrapure water. The size distribution was taken by the number as the mean of the 5 measurements.

2.4.2 Materials

Potassium ethylxanthogenate (Sigma-Aldrich, 96%), bromoacetonitrile (Sigma-Aldrich,97%), methyl-2-bromopropionate (Sigma-Aldrich, 98%), ethanol (Sigma-Aldrich, 96%), diethyl ether (Sigma-Aldrich, 99.9%), ethyl acetate (Sigma-Aldrich, 99.7%), petroleum ether (Sigma-Aldrich), silica gel pore size 60 Å 220-440 mesh particle size, 35-75 mm particle size (Sigma-Aldrich), 2,2'-azobis(4-methoxy-2,4-

dimethylvaleronitrile) (V-70, Wako), 1,4-dioxane (Sigma-Aldrich, 99.8%), *N*-vinylcaprolactam (VCL, Sigma-Aldrich, 98%), dimethyl sulfoxide (DMSO, Sigma-Aldrich, 99.9%) were used as received. *N*-vinylformamide (NVF, Sigma-Aldrich, 98%) was distilled under reduced pressure before use. *N*-isopropylacrylamide (NIPAAm, Sigma-Aldrich, 97%) was recrystallized twice from hexane before use. 2,2′-Azobis(2-methylpropionitrile) (AIBN, Sigma-Aldrich, 98%) was recrystallized from methanol before use. *N*,*N*-dimethylacrylamide (DMA, Sigma-Aldrich,99%) was passed through basic alumina before use. DMSO-d6 (99.8% D) and deuterium oxide (99.9% D) (Eurisotop) were used as received.

2.4.3 Synthesis of chain transfer agents CTA1 and CTA2.

methyl 2-((ethoxycarbonothioyl)thio)propanoate (CTA1)[40] and *S*-(cyanomethyl) *O*-ethyl carbonodithioate (CTA2)[41] were synthesized according to previously published procedures.

2.4.4 Synthesis of PNVF-CTA2.

A typical procedure is described as follows: NVF (2.10 g, 29.5 mmol), CTA2 (17 mg, 0.11 mmol), DMSO (4.90 g) and V-70 (11 mg, 0.04 mmol), were added to a 50 ml round-bottomed flask. 1 ml of the stock solution was added to several glass tubes which were flame sealed under vacuum after degassing by three freeze-pump-thaw cycles. The tubes were immersed into an oil bath at 35°C and withdrawn at given intervals. For kinetic studies, samples were rapidly cooled down in liquid nitrogen and directly analyzed by ^{1}H NMR and SEC without purification. Dry polymers were obtained after purification by three cycles of solubilization in water, precipitation in cold acetone and filtration, and drying under vacuum. NVF conversion was determined via ^{1}H NMR spectroscopy (Fig. 14).

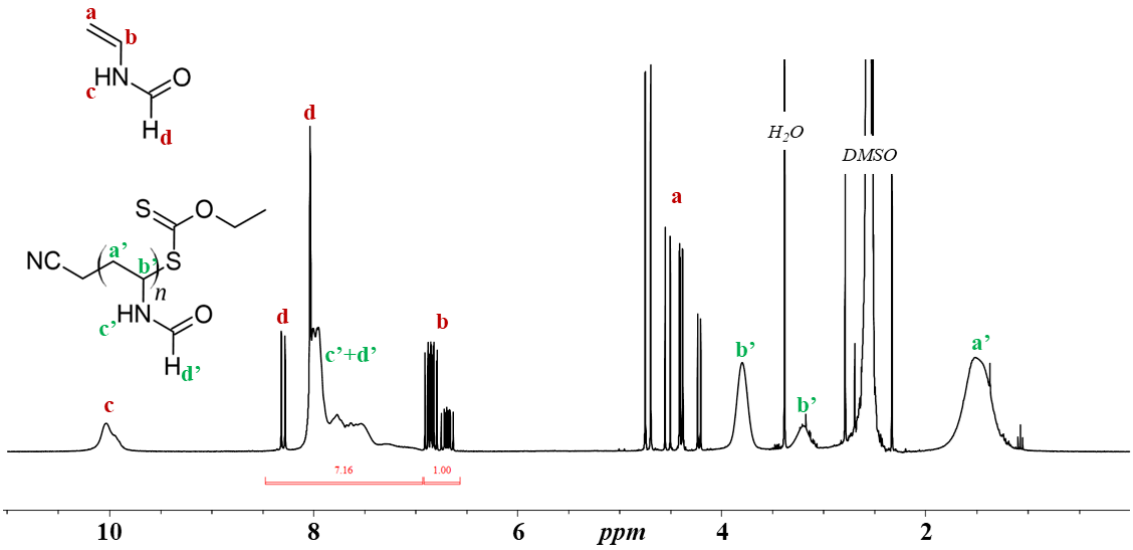

Figure 2-14. ^{1}H NMR spectrum of a crude mixture of NVF polymerization with CTA2 (Table 2-S1 entry 13). Conversion (%) $= \frac{(d+c'+d')-b}{(d+c'+d')+b} \times 100$. Measured on a 300MHz apparatus.

2.4.5 Synthesis of PNIPAAm-CTA1.

NIPAAm (5 g, 44.2 mmol), CTA1 (0.218 g, 1.04 mmol), AIBN (26 mg, 0.16 mmol), and dioxane (5.81 g) were added to a Schlenk tube and degassed by bubbling argon for 30 min and immersed into an oil bath at 70°C for 16 h. The polymerization was stopped by cooling down the reaction mixture with liquid nitrogen, and a sample withdrawn to determine a conversion of 99% by ^{1}H NMR. The polymer was purified by precipitation in cold diethyl ether, filtrated, dried under vacuum, and analyzed by SEC ($M_{n,SEC}$ = 6300 g mol^{-1}, $Đ$ = 1.31).

2.4.6 Synthesis of PNIPAAm-*b*-PNVF.

NVF (3 g, 42.2 mmol), PNIPAAm-CTA1 (0.526 g, 0.09 mmol), DMSO (7 g) and V-70 (9 mg, 0.03 mmol) were added to a Schlenk tube and degassed by three freeze- pump-thaw cycles. The Schlenk tube was immersed into an oil bath at

35°C for 16h. The polymerization was stopped by rapidly cooling down the reaction mixture with liquid nitrogen and a sample directly analyzed by ^{1}H NMR to determine a conversion of 81%. The block copolymer was purified by 2 cycles of solubilization in water, precipitation in cold acetone, filtration and dried under vacuum.

2.4.7 Synthesis of PDMA-CTA1.

DMA (5 g, 50.4 mmol), CTA1 (0.217 g, 1.04 mmol), AIBN (13 mg, 0.08 mmol), and ethyl acetate (6.05 g) were added to a Schlenk tube, degassed by four freeze-pump-thaw cycles, put under argon and immersed into an oil bath at 60°C for 16h. The polymerization was stopped by rapidly cooling down the reaction mixture with liquid nitrogen, and a sample withdrawn to determine a conversion of 99% by ^{1}H NMR. The polymer was purified and dried under vacuum, and analyzed by SEC ($M_{n,SEC}$ = 6200 g mol^{-1}, $Đ$ = 1.30).

2.4.8 Synthesis of PDMA-*b*-PNVF.

NVF (3 g, 42.2 mmol), PDMA-CTA1 (0.675 g, 0.11 mmol), DMSO (7 g) and V-70 (12 mg, 0.04 mmol) were added to a Schlenk tube and degassed by three freeze- pump-thaw cycles. The Schlenk was immersed into an oil bath at 35°C for 16h. The polymerization was stopped by rapidly cooling down the reaction mixture with liquid nitrogen and a sample directly analyzed by ^{1}H NMR to determine a conversion of 83%. The block copolymer was purified by 2 cycles of solubilization in water, precipitation in cold acetone, filtration and dried under vacuum.

2.4.9 Synthesis of PVCL-CTA1.

VCL (5 g, 35.9 mmol), CTA1 (0.217 g, 1.04 mmol), AIBN (0.177g, 1.08 mmol), and dioxane (7.5 g) were added to a Schlenk tube, degassed by four freeze- pump-thaw cycles, put under Argon and immersed into an oil bath at 65°C for 16 h. The polymerization was stopped by rapidly cooling down the reaction mixture with liquid nitrogen, and a sample withdrawn to determine a conversion of 99% by ^{1}H NMR. The polymer was purified by precipitation in cold pentane, filtration, dried under vacuum and analyzed by SEC ($M_{n,SEC}$ = 6400 g mol^{-1}, $Đ$ = 1.11).

2.4.10 Synthesis of PVCL-*b*-PNVF.

NVF (3 g, 42.2 mmol), PVCL-CTA1 (0.602 g, 0.10 mmol), DMSO (7g) and V-70 (10 mg, 0.03 mmol) were added to a Schlenk tube and degassed by three freeze-pump-thaw cycles. The Schlenk tube was immersed into an oil bath at 35°C for 16h. The polymerization was stopped by rapidly cooling down the reaction mixture with liquid nitrogen and a sample directly analyzed by ^{1}H NMR to determine a conversion of 82%. The block copolymer was purified by 2 cycles of solubilization in water, precipitation in cold acetone, filtration and dried under vacuum.

2.4.11 Hydrolysis of PVCL-*b*- PNVF.

PVCL-*b*-PNVF (0.5 g, $M_{n,AF4}$ = 37200 g mol^{-1}, $Đ$ = 1.27) was dissolved in 10 mL of 2 M NaOH in a round-bottomed flask. The resulting solution was heated at 80°C for 3h. After complete hydrolysis was confirmed by ^{1}H NMR in D_2O, the reaction mixture was dialyzed against 1L for 60h, changing the water several times. The final product was isolated by lyophilization.

2.5 REFERENCES

(1) Pelton, R. Polyvinylamine: A Tool for Engineering Interfaces. *Langmuir* **2014**, *30*, 15373–15382.

(2) Qiu, Y.; Holland, N. B.; Ruegsegger, M.; Marchant, R. E. Biomimetic Surface Engineering: Synthesis and Surface-Induced Assembly of Novel Oligosaccharide Surfactant Polymers. *ACS Symp. Ser.* **1999**, *736*, 180–193.

(3) Bailey, M. M.; Kline, S. R.; Anderson, M. D.; Staymates, J. L.; Berkland, C. Chemically Modifiable Fluorinated Copolymer Nanoparticles for 19F-MRI Contrast Enhancement. *J. Appl. Polym. Sci.* **2012**, *126*, 1218–1227.

(4) Tachaboonyakiat, W.; Ajiro, H.; Akashi, M. Controlled DNA Interpolyelectrolyte Complex Formation or Dissociation via Stimuli-Responsive Poly(Vinylamine-Co-N-Vinylisobutylamide). *J. Appl. Polym. Sci.* **2016**, *133*.

(5) Karagoz, B.; Bayramoglu, G.; Altintas, B.; Bicak, N.; Arica, M. Y. Amine Functional Monodisperse Microbeads via Precipitation Polymerization of N-Vinyl Formamide: Immobilized Laccase for Benzidine Based Dyes Degradation. *Bioresour. Technol.* **2011**, *102*, 6783–6790.

(6) Takemoto, Y.; Ajiro, H.; Asoh, T.; Akashi, M. Fabrication of Surface-Modified Hydrogels with Polyion Complex for Controlled Release. *Chem. Mater.* **2010**, *22*, 2923–2929.

(7) Sheikholeslami, P.; Muirhead, B.; Baek, D. S. H.; Wang, H.; Zhao, X.; Sivakumaran, D.; Boyd, S.; Sheardown, H.; Hoare, T. Hydrophobically-Modified Poly(Vinyl Pyrrolidone) as a Physically-Associative, Shear-Responsive Ophthalmic Hydrogel. *Exp. Eye Res.* **2015**, *137*, 18–31.

(8) Chen, Q.; Xu, R.; Yao, D. Preparation and Properties of Poly(Vinylamine/Acrylonitrile) Fiber. *Appl. Mech. Mater.* **2012**, *155–156*, 1005–1008.

(9) Shan, B.; Tang, B.; Zhang, S.; Tan, W. Synthesis and Dyeing Properties of Polyvinylamine Dyes for Cotton. *Color. Technol.* **2020**, Ahead of Print.

(10) Gustafsson, E.; Pelton, R.; Waagberg, L. Rapid Development of Wet Adhesion between Carboxymethylcellulose Modified Cellulose Surfaces Laminated with Polyvinylamine Adhesive. *ACS Appl. Mater. Interfaces* **2016**, *8*, 24161–24167.

(11) Jr, R. K. P.; Lai, T.-W. Enhanced Oil Recovery with High Molecular Weight Polyvinylamine Formed In-Situ. US4931194A, June 5, 1990.

(12) Awual, Md. R.; Urata, S.; Jyo, A.; Tamada, M.; Katakai, A. Arsenate Removal from Water by a Weak-Base Anion Exchange Fibrous Adsorbent. *Water Res.* **2008**, *42*, 689–696.

(13) Li, P.; Wang, Z.; Liu, Y.; Zhao, S.; Wang, J.; Wang, S. A Synergistic Strategy via the Combination of Multiple Functional Groups into Membranes towards Superior CO2 Separation Performances. *J. Membr. Sci.* **2015**, *476*, 243–255.

(14) Yue, M.; Imai, K.; Miura, Y.; Hoshino, Y. Design and Preparation of Thermo-Responsive Vinylamine-Containing Micro-Gel Particles for Reversible Absorption of Carbon Dioxide. *Polym. J. Tokyo Jpn.* **2017**, *49*, 601–606.

(15) Gao, Y.; Qiao, Z.; Zhao, S.; Wang, Z.; Wang, J. In Situ Synthesis of Polymer Grafted ZIFs and Application in Mixed Matrix Membrane for CO2 Separation. *J. Mater. Chem. Mater. Energy Sustain.* **2018**, *6*, 3151–3161.

(16) Zubair, N. A.; Nasef, M. M.; Mohamad, N. A.; Abouzari-Lotf, E.; Ting, T. M.; Abdullah, E. C. Kinetic Studies of Radiation Induced Grafting of N-Vinylformamide onto Polyethylene/Polypropylene Fibrous Sheets and Testing Its Hydrolysed Copolymer for CO2 Adsorption. *Radiat. Phys. Chem.* **2020**, *171*, 108727.
(17) Achari, A. E.; Coqueret, X.; Lablache-Combier, A.; Loucheux, C. Preparation of Polyvinylamine from Polyacrylamide: A Reinvestigation of the Hofmann Reaction. *Makromol. Chem.* **1993**, *194* (7), 1879–1891.
(18) Nadal, C.; Gineste, S.; Coutelier, O.; Tourrette, A.; Marty, J.-D.; Destarac, M. A Deeper Insight into the Dual Temperature- and PH-Responsiveness of Poly(Vinylamine)-b-Poly(N-Isopropylacrylamide) Double Hydrophilic Block Copolymers. *Colloids Surf. Physicochem. Eng. Asp.* **2022**, *641*, 128502.
(19) Maki, Y.; Mori, H.; Endo, T. Controlled RAFT Polymerization of N-Vinylphthalimide and Its Hydrazinolysis to Poly(Vinyl Amine). *Macromol. Chem. Phys.* **2007**, *208* (24), 2589–2599.
(20) Reynolds, D. D.; Kenyon, W. O. The Preparation of Polyvinylamine, Polyvinylamine Salts, and Related Nitrogenous Resins. *J. Am. Chem. Soc.* **1947**, *69* (4), 911–915.
(21) Pinschmidt, R. K., Jr. Polyvinylamine at Last. *J. Polym. Sci. Part Polym. Chem.* **2010**, *48*, 2257–2283.
(22) Gu, L.; Zhu, S.; Hrymak, A. N. Acidic and Basic Hydrolysis of Poly(N-Vinylformamide). *J. Appl. Polym. Sci.* **2002**, *86*, 3412–3419.
(23) Yamamoto, K.; Imamura, Y.; Nagatomo, E.; Serizawa, T.; Muraoka, Y.; Akashi, M. Synthesis and Functionalities of Poly(N-Vinylalkylamide). XIV. Polyvinylamine Produced by Hydrolysis of Poly(N-Vinylformamide) and Its Functionalization. *J. Appl. Polym. Sci.* **2003**, *89*, 1277–1283.
(24) Fan, W.; Yamago, S. Synthesis of Poly(N-Vinylamide)s and Poly(Vinylamine)s and Their Block Copolymers by Organotellurium-Mediated Radical Polymerization. *Angew. Chem. Int. Ed.* **2019**, *58*, 7113–7116.
(25) Shi, L.; Chapman, T. M.; Beckman, E. J. Poly(Ethylene Glycol)-Block-Poly(N-Vinylformamide) Copolymers Synthesized by the RAFT Methodology. *Macromolecules* **2003**, *36*, 2563–2567.
(26) Peng, H.; Xu, W.; Pich, A. Temperature and PH Dual-Responsive Poly(Vinyl Lactam) Copolymers Functionalized with Amine Side Groups via RAFT Polymerization. *Polym. Chem.* **2016**, *7*, 5011–5022.
(27) Kawatani, R.; Kelland, M. A.; Ajiro, H. Design of a Rigid Side Chain for Poly(N-Vinylamide) Derivatives Bearing an Alkenyl Group and Evaluation of Their Ability to Inhibit Tetrahydrofuran Hydrate Crystal Growth. *J. Appl. Polym. Sci.* **2020**, *137* (38), 49154.
(28) Dupre--Demorsy, A.; Coutelier, O.; Destarac, M.; Nadal, C.; Bourdon, V.; Ando, T.; Ajiro, H. RAFT Polymerization of N-Methyl-N-Vinylacetamide and Related Double Hydrophilic Block Copolymers. *Macromolecules* **2022**, *55* (4), 1127–1138.

(29) Nakamura, Y.; Kitada, Y.; Kobayashi, Y.; Ray, B.; Yamago, S. Quantitative Analysis of the Effect of Azo Initiators on the Structure of α-Polymer Chain Ends in Degenerative Chain-Transfer-Mediated Living Radical Polymerization Reactions. *Macromolecules* **2011**, *44* (21), 8388–8397.
(30) Liu, X.; Wang, M.; Harrisson, S.; Debuigne, A.; Marty, J.-D.; Destarac, M. Enhanced Stabilization of Water/ScCO2 Interface by Block-Like Spontaneous Gradient Copolymers. *ACS Sustain. Chem. Eng.* **2017**, *5* (11), 9645–9650.
(31) Beija, M.; Marty, J.-D.; Destarac, M. Thermoresponsive Poly(N-Vinyl Caprolactam)-Coated Gold Nanoparticles: Sharp Reversible Response and Easy Tunability. *Chem. Commun.* **2011**, *47* (10), 2826–2828.
(32) Zhao, X.; Coutelier, O.; Nguyen, H. H.; Delmas, C.; Destarac, M.; Marty, J.-D. Effect of Copolymer Composition of RAFT/MADIX-Derived N-Vinylcaprolactam/N-Vinylpyrrolidone Statistical Copolymers on Their Thermoresponsive Behavior and Hydrogel Properties. *Polym. Chem.* **2015**, *6* (29), 5233–5243.
(33) Feng, X.; Pelton, R.; Leduc, M. Mechanical Properties of Polyelectrolyte Complex Films Based on Polyvinylamine and Carboxymethyl Cellulose. *Ind. Eng. Chem. Res.* **2006**, *45*, 6665–6671.
(34) Serizawa, T.; Kawanishi, N.; Akashi, M. Polyelectrolyte Multilayers of Poly(Vinylamine Hydrochloride-Co-N-Vinylformamide) with Variable Primary Amine Content and a Weak Polyacid Poly(Acrylic Acid). *J. Appl. Polym. Sci.* **2006**, *102*, 3927–3933.
(35) Stejskal, E. O.; Tanner, J. E. Spin Diffusion Measurements: Spin Echoes in the Presence of a Time‐Dependent Field Gradient. *J. Chem. Phys.* **1965**, *42* (1), 288–292.
(36) Jerschow, A.; Müller, N. Suppression of Convection Artifacts in Stimulated-Echo Diffusion Experiments. Double-Stimulated-Echo Experiments. *J. Magn. Reson.* **1997**, *125* (2), 372–375.
(37) Read, E.; Guinaudeau, A.; Wilson, D. J.; Cadix, A.; Violleau, F.; Destarac, M. Low Temperature RAFT/MADIX Gel Polymerisation: Access to Controlled Ultra-High Molar Mass Polyacrylamides. *Polym. Chem.* **2014**, *5* (7), 2202–2207.
(38) Despax, L.; Fitremann, J.; Destarac, M.; Harrisson, S. Low Concentration Thermoresponsive Hydrogels from Readily Accessible Triblock Copolymers. *Polym. Chem.* **2016**, *7* (20), 3375–3377.
(39) Zimm, B. H. The Scattering of Light and the Radial Distribution Function of High Polymer Solutions. *J. Chem. Phys.* **1948**, *16* (12), 1093–1099.
(40) Liu, X.; Coutelier, O.; Harrisson, S.; Tassaing, T.; Marty, J.-D.; Destarac, M. Enhanced Solubility of Polyvinyl Esters in ScCO2 by Means of Vinyl Trifluorobutyrate Monomer. *ACS Macro Lett.* **2015**, *4* (1), 89–93.
(41) Chiefari, J.; Mayadunne, R. T.; Moad, G.; Rizzardo, E.; Thang, S. H. Polymerization Process with Living Characteristics and Polymers Made Therefrom. US6747111B2, June 8, 2004.

CHAPTER 3.

RAFT POLYMERIZATION OF *N*-VINYLISOBUTYRAMIDE AND NEW THERMORESPONSIVE DOUBLE-HYDROPHILIC BLOCK COPOLYMERS WITH *N*-VINYLFORMAMIDE.

3.1 INTRODUCTION

Smart materials are capable of reversibly altering their physico-chemical properties upon a stimulus from their environment. As such, factors like light, temperature, mechanical stress, electricity or pH can be played with to induce a response from the material.[1] Polymer hydrogels,[2,3] which can absorb important amounts of water in their network's interstitial spaces, are particularly interesting from a biological or biomedical point of view, as they can be used for tissue engineering, drug-release systems or antibiotics among other applications.[4–7]

Of the thermoresponsive polymers that show a lower critical solution temperature (LCST) in water, such as poly(methyl vinyl ether),[8] poly(2-isopropyl-2-oxazoline),[9] poly(*N*,*N*'-(dimethylamino)ethyl methacrylate)[10] or poly(*N*-acryloyl-*N*'-propylpiperazine)[11] among others,[12] poly(isopropylacrylamide) (PNIPAAm) is one of the most studied materials.[13] At temperatures above 32°C, PNIPAAm undergo a coil-to-globule transition, effectively changing its physico-chemical characteristics. Although this property makes it very interesting for applications in biomedicine, such as drug delivery agent,[14] one major drawback remains. Due to the nature of its acrylamide backbone, the hydrolysis of PNIPAAm results in the formation of small amino products, which are toxic for the human body.[15] To avoid this, other ways were explored and new materials designed. One such way is through *N*-vinylamide

polymers. By having their amide nitrogen directly attached to the polymer backbone, *N*-vinylamide polymers don't produce toxic amino compounds though hydrolysis. They are also water-soluble, and their biocompatibility was investigated and shown.[15,16] Among those, some show thermoresponsive behavior, such as poly(*N*-vinylcaprolactam) (PVCL) and poly(*N*-vinylisobutyramide) (PNVIBA), which show LCST in water at around 32°C and 39°C respectively.[17,18] Due to the above-mentioned interesting properties, PVCL has been the focus of extensive studies on its synthesis and on the preparation of PVCL-based materials, membranes, gels, for biomedical applications.[16,19,20] Its polymerization was successfully controlled using different techniques such as tellurium-mediated radical polymerization (TERP),[21] cobalt-mediated radical polymerization (CMRP),[22,23] atom-transfer radical polymerization (ATRP)[24–27] and reversible addition-fragmentation chain-transfer (RAFT).[28–30] Tunability of the LCST property of the obtained material has also been successfully achieved by changing the polymer's molecular weight, concentration, as well as the copolymers' composition or architecture.[19,23,28,31]

On the other hand, PNVIBA is also a thermoresponsive poly(*N*-vinylamide) which shows a LCST in water. NVIBA, an isomer of NIPAAm which has its amide nitrogen directly attached to the vinyl group, is mostly used in the preparation of thermoresponsive hydrogels,[32–34] as is or copolymerized with other monomers such as *N*-vinylformamide (NVF) in order to get polyvinylamine-based thermo- and pH-responsive smart materials.[35,36] Its LCST properties in water have also been investigated.[18,37,38] However, the polymer synthesis is exclusively done through free-radical polymerization, and there is a lack of studies on its controlled radical polymerization.

After a first chapter on the N-alkyl-N-vinylalkylamide NMVA and a second chapter on the N-vinylamide NVF, this third chapter will first focus on the controlled RAFT polymerization of NVIBA, a *N*-vinylalkylamide with isopropyl substituent. Homopolymerization will be demonstrated through two sets of experimental conditions of different initiation methods, and characterization via analytical techniques (^{1}H NMR, SEC, mass spectrometry) are used to highlight the controlled

nature of the polymerization. Then in a second part, random and block RAFT copolymerizations of NVIBA with hydrophilic NVF will be demonstrated. The influence of parameters such as copolymer composition and microstructure on their thermoresponsive character will be investigated.

3.2 RESULTS AND DISCUSSION

3.2.1 Homopolymerization of NVIBA

3.2.1.1 Reaction conditions

In the previous chapters,[39,40] it was observed that a relatively high amount of thermal initiator is required for the RAFT polymerization of acyclic *N*-vinylamides, with a $[Initiator]_0/[CTA]_0$ ratio of up to 1.49 in the case of NMVA (chapter 1).[39] To avoid the use of initiator, I turned to purple LEDs (λ = 400 nm) photo-initiation of xanthate. This was motivated by the fact that xanthates show photo-iniferter behavior, and the successful photo-RAFT polymerization of NVF recently revealed by our group.[41] In this chapter, polymerizations were carried out by thermal initiation using monomer (NVIBA), CTA2 (*S*-cyanomethyl-*O*-ethyl xanthate), solvent (DMSO) and an azo-initiator (V-70) to serve as a basis of comparison with the previous chapters, in addition to polymerizations carried out by photo-initiation using only monomer, CTA and solvent (scheme 3-1).

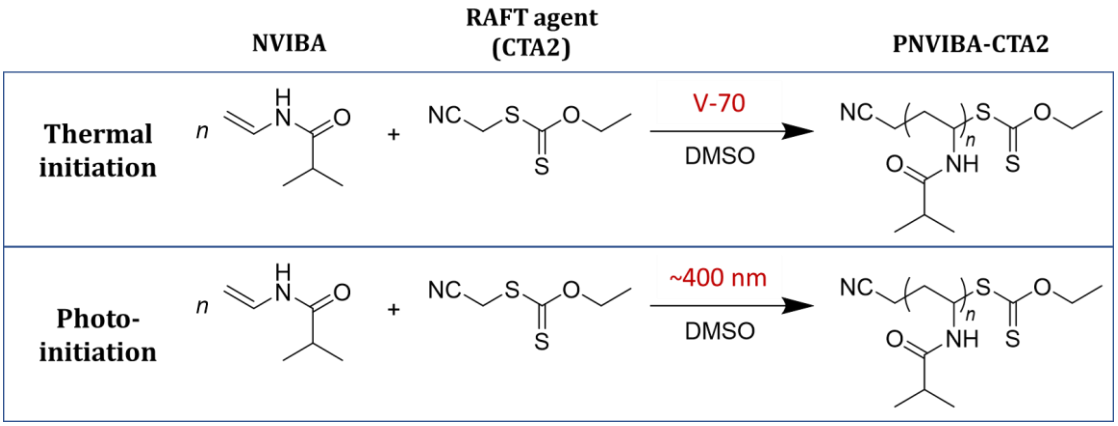

Scheme 3-1. General scheme for the polymerization of NVIBA using CTA2 in DMSO, at 35°C (V-70 initiation) for thermal initiation and using purple LEDs for photo-initiation.

At first, I studied the effect of CTA2 on monomer conversion, molar masses and dispersities of obtained PNVIBA. Without using CTA2, a conversion of 96% was attained after 16h at 35°C by thermal initiation. When adding CTA2, with increasing initial concentrations of $[CTA2]_0$ = 33.6, 50, 152 mmol L^{-1} corresponding to

[initiator]$_0$/[CTA2]$_0$ of 1.50, 1 and 0.33 respectively, the monomer conversion sharply decreased to respectively 75%, 53% and less than 5% (Table 3-1). This retardation phenomenon falls in line with what was previously observed in the cases of NMVA and NVF (chapters 1 and 2) albeit with a more pronounced effect, and we chose to keep a [initiator]$_0$/[CTA2]$_0$ ratio of 1.5 throughout polymerizations done by thermal initiation similarly to our NMVA study to have a satisfying compromise between monomer conversion and used amount of initiator.[39]

Table 3-1. RAFT polymerization of NVIBA in DMSO with CTA2 at different initial concentrations at 35°C. [NVIBA]$_0$ = 5.9 mol L^{-1}, [V-70]$_0$ = 50 mmol L^{-1}.

Entry	[CTA2]$_0$ (mmol L^{-1})	Time (h)	Conversion [a] (%)
1	0	16	96
2	33.6	16	75
3	50.1	16	53
4	152	16	<5

[a]Calculated by ^{1}H NMR (Figure 3-1).

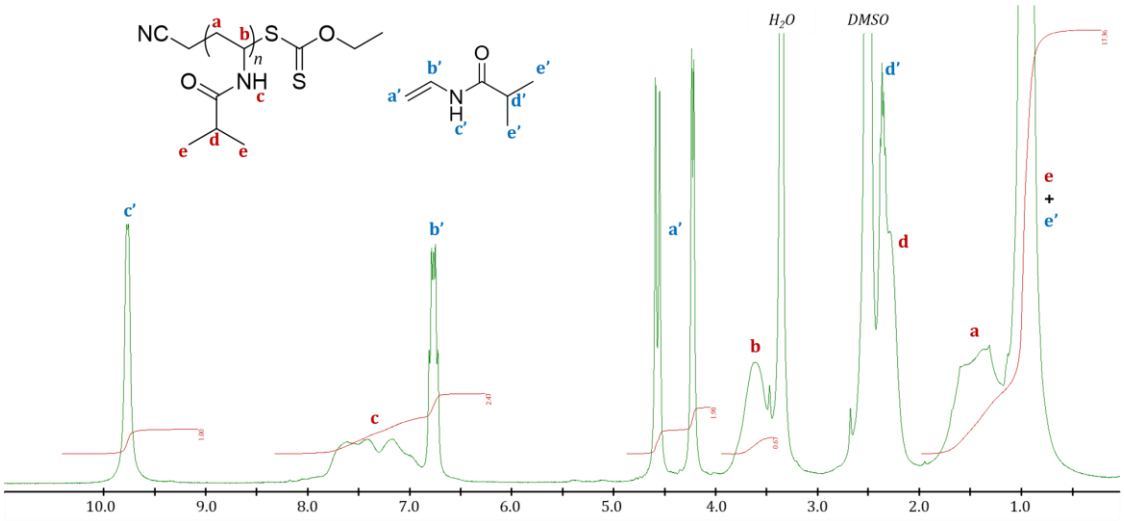

Figure 3-1. ^{1}H NMR spectra in DMSO-*d*6 of a crude mixture after NVIBA polymerization to determine conversion. $Conversion\% = 100 \times \frac{(c+b')-c\prime}{c+b\prime}$. Measured on a 400MHz apparatus.

Looking at SEC analysis, monomodal SEC-RI traces were obtained with molar mass values decreasing with the increasing initial CTA2 concentration. While $M_{n,SEC}$ = 138 kg mol^{-1} and $Đ$ = 1.82 was obtained without using CTA, adding $[CTA2]_0$ = 33.6 mmol L^{-1} gave a $M_{n,SEC}$ = 19.3 kg mol^{-1} for a theoretical $M_{n,th}$ = 15.0 kg mol^{-1} and a dispersity of $Đ$ = 1.17 (Figure 3-2).

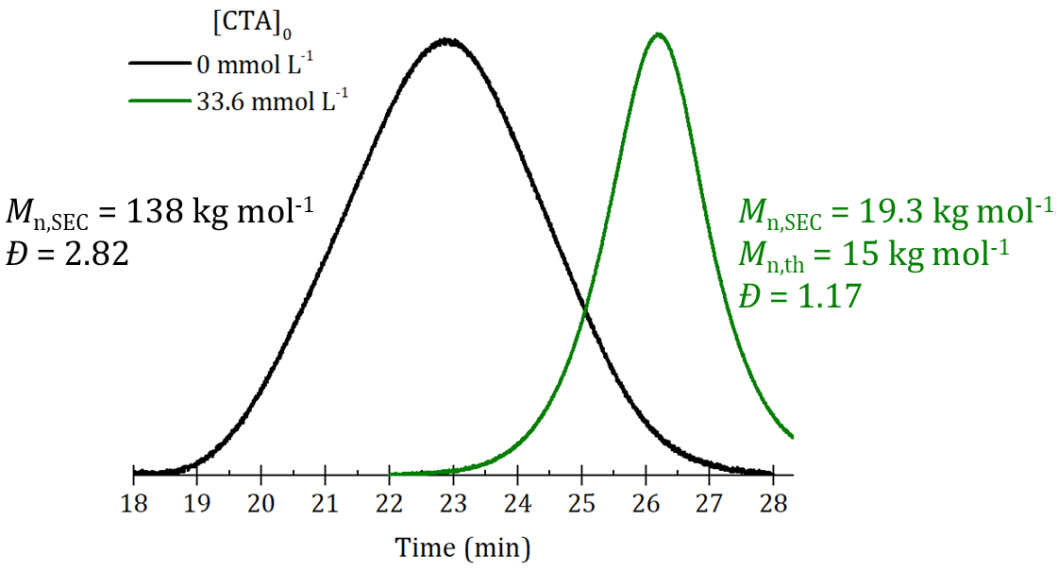

Figure 3-2. SEC-RI traces of NVIBA polymerization in DMSO at 35°C with $[CTA2]_0$ = 0 and 33.6 mmol L^{-1}. $[NVIBA]_0$ = 5.9 mol L^{-1}, $[V\text{-}70]_0$ = 50 mmol L^{-1}.

On the other hand, going through photo-initiated polymerization, no external initiator was used and the source of radicals lies in the CTA. Thus, as could be expected, no polymerization was observed in the absence of CTA. Adding CTA2 with initial concentrations of $[CTA2]_0$ = 33.6 and 235 mmol L^{-1} gave a steady increase of monomer conversion to 50% and 66% respectively after 16h of reaction in a photo-reactor containing 60 purple LEDs and of light intensity around 4.0 mW cm^{-2}. As CTA2 is the source of radicals here, a concentration increase is indeed accompanied by an increase of radical concentration, and of the reaction rate. SEC analysis gave monomodal SEC-RI traces, with molar mass values in agreement with theoretical values ($M_{n,SEC}$ = 16.5 kg mol^{-1} for a theoretical $M_{n,th}$ = 13.2 kg mol^{-1}, and $M_{n,SEC}$ = 2.1

kg mol^{-1} for $M_{n,th}$ =1.6 kg mol^{-1}) and with dispersities below 1.4 (Table 3-2 and Figure 3-3).

Table 3-2. RAFT polymerization of NVIBA in DMSO with CTA2 at different initial concentrations under purple light irradiation (4.0 mW cm^{-2}). $[NVIBA]_0$ = 5.9 mol L^{-1}, λ = 400 nm.

Entry	$[CTA2]_0$ (mmol L^{-1})	Time (h)	Conversion [a] (%)
1	0	16	0
2	33.6	16	50
3	235	16	66

[a]Calculated by ^{1}H NMR (Figure 3-1).

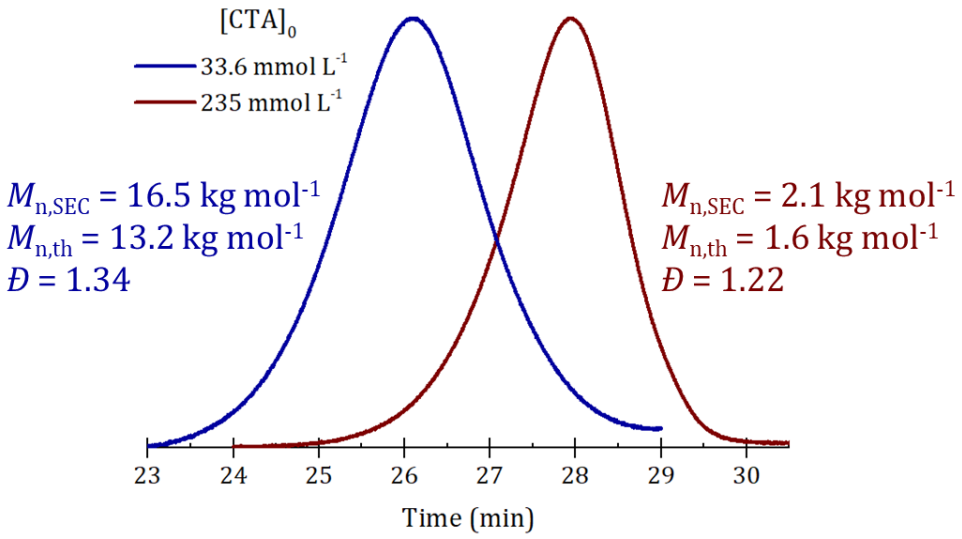

Figure 3-3. SEC-RI traces of NVIBA polymerization in DMSO in purple LED photo-reactor (4.0 mW cm^{-2}). $[NVIBA]_0$ = 5.9 mol L^{-1}, λ = 400 nm.

Following those encouraging preliminary results, I kept the experimental conditions of $[CTA2]_0$ = 33.6 mmol L^{-1}, corresponding to a targeted M_n of 20kg mol^{-1}. In the case of thermal initiation, a $[initiator]_0/[CTA2]_0$ ratio of 1.5 was also kept. Then, I studied the evolution of molar masses and dispersities with monomer conversion in both cases.

For the thermal initiation polymerization, a linear increase of the molar masses with NVIBA conversion was observed with values close to what was expected and dispersity values were maintained under 1.4 (Table 3-3 and Figure 3-4a). Monomodal SEC-RI traces were obtained, with a gradual peak shift towards lower elution times with increasing NVIBA conversion (Figure 3-4b), comforting us on the controlled character of the polymerization.

Table 3-3. RAFT polymerization of NVIBA in DMSO with CTA2 at 35°C. $[NVIBA]_0$ = 5.9 mol L^{-1}, $[V\text{-}70]_0$ = 50 mmol L^{-1}, $[CTA2]_0$ = 33.6 mmol L^{-1}.

Entry	Targeted M_n (kg mol^{-1})	Time (h)	Conversion [a] (%)	$M_{n,th}$ [b] (kg mol^{-1})	$M_{n,SEC}$ [c] (kg mol^{-1})	$Đ$
1	20	0.5	5	1.2	2.8	1.19
2		1	20	4.1	5.4	1.38
3		1.5	33	6.7	8.3	1.28
4		2	44	8.9	9.8	1.35
5		3	50	10.1	11.0	1.33
6		4	60	12.0	13.9	1.35
7		6	69	13.8	16.7	1.34
8		16	75	15.0	19.3	1.17

[a]Calculated by ^1H NMR, [b]$M_{n,th}=[NVIBA]_0/[CTA2]_0\times M_{NVIBA}\times Conv.+M_{CTA2}$, [c]$M_{n,SEC}$ measured with LALS/RALS detection. M_{NVIBA} =113 g mol^{-1}; M_{CTA2} =161 g mol^{-1}.

Table 3-4. RAFT polymerization of NVIBA in DMSO with CTA2 under purple light irradiation (4.0 mW cm^{-2}). $[NVIBA]_0$ = 5.9 mol L^{-1}, $[CTA2]_0$ = 33.6 mmol L^{-1}, λ = 400 nm.

Entry	Targeted M_n (kg mol^{-1})	Time (h)	Conversion [a] (%)	$M_{n,th}$ [b] (kg mol^{-1})	$M_{n,SEC}$ [c] (kg mol^{-1})	$Đ$
1	20	1	7	1.5	4.3	1.11
2		1.5	15	3.1	6.3	1.19
3		2	22	4.5	8.8	1.14
4		4	43	8.7	13.3	1.27
5		6	48	9.7	14.0	1.21
6		10	62	12.4	16.0	1.37
7		16	66	13.2	16.5	1.34

[a]Calculated by ^1H NMR, [b]$M_{n,th}=[NVIBA]_0/[CTA2]_0\times M_{NVIBA}\times Conv.+M_{CTA2}$, [c]$M_{n,SEC}$ measured with LALS/RALS detection. M_{NVIBA} =113 g mol^{-1}; M_{CTA2} =161 g mol^{-1}.

Through the photo-initiation, SEC analysis showed a relatively linear increase of molar masses, higher than what was obtained in the thermo-way but still in agreement with theoretical values, and with dispersities also maintained under 1.4 (Table 3-4 and Figure 3-4a).A deviation in molar masses was systematically observed, maybe due to a loss of CTA from the beginning of polymerization. Monomodal SEC-RI traces were obtained, with a gradual peak shift towards lower elution times with increasing NVIBA conversion (Figure 3-4c), once again comforting us on the controlled character of the polymerization.

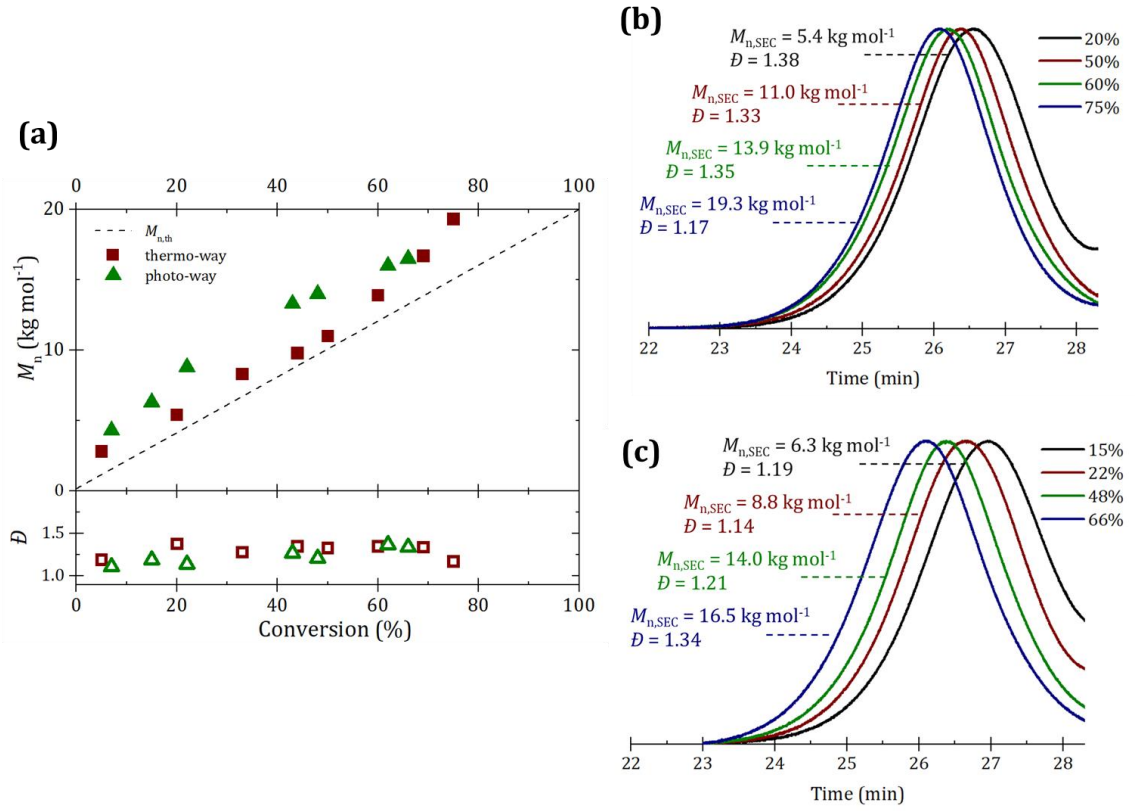

Figure 3-4. Evolution of **(a)** $M_{n,SEC}$, $Đ$ and SEC-RI traces with monomer conversion for the polymerization of NVIBA **(b)** at 35°C or **(c)** using purple LED light photo-reactor (4.0 mW cm^{-2}). $[NVIBA]_0$ = 5.9 mol L^{-1}, $[V\text{-}70]_0$ = 50 mmol L^{-1}, $[CTA2]_0$ = 33.6 mmol L^{-1}, λ = 400 nm.

Thus, the control of NVIBA polymerizations seem to be successfully achieved by using two different ways of initiation, one through heat by using an external azo-initiator, and the other through light at 400 nm.

For the next step in confirming the controlled character of NVIBA polymerization via RAFT, and with the future prospect of obtaining copolymers of controlled sequences, the presence of CTA-capped polymer chains should be confirmed.

3.2.1.2 Chain-end fidelity

Two low molar mass polymers, PNVIBA$_{3k,thermo}$-CTA2 and PNVIBA$_{3k,photo}$-CTA2, were targeted by both thermal and photo initiation, respectively. After precipitation, a PNVIBA$_{3k,thermo}$-CTA2 of $M_{n,SEC}$ = 3.4 kg mol^{-1} ($M_{n,th}$ = 2.4 kg mol^{-1}) and $Đ$ = 1.1 and PNVIBA$_{3k,photo}$-CTA2 of $M_{n,SEC}$ = 3.1 kg mol^{-1} ($M_{n,th}$ = 1.6 kg mol^{-1}) and $Đ$ = 1.1 were obtained. Those polymers were then first analyzed by matrix-assisted laser desorption/ionization–time of flight mass spectrometry (MALDI-TOF-MS) and Electron spray ionization-time of flight mass spectrometry (ESI-TOF-MS), and also used as macro-CTAs for a chain extension experiment with NVIBA targeting a final molar mass of 30 kg mol^{-1} in each case (Table 3-5).

In the case of PNVIBA$_{3k,thermo}$-CTA2, synthesized by thermal initiation, the MALDI-TOF spectrum showed two major populations A and B (Figure 3-5a). The major population A of general formula C_2H_2N-($C_6H_{11}NO)_n$-$C_6H_{10}NO$,Na^+ corresponds to PNVIBA chains capped with the R-group of CTA2 on one end and terminated by a double bond on the other end, most likely resulting from the degradation of the xanthate chain-end during the analysis, as often observed with poly(*N*-vinylpyrrolidone)[19] as well as in the previous chapters on NMVA[39] and NVF.[40] The other major population, B, of general formula $C_8H_{14}NO$-($C_6H_{11}NO)_n$-$C_6H_{10}NO$,Na^+ corresponds to PNVIBA chains initiated by the V-70 initiator and also terminated by a double bond on the other end. Two minor populations were also observed but not identified. As an analytical technique under milder conditions, ESI-TOF should allow us to observe polymer chains without xanthate degradation at the chain-ends. The ESI-TOF spectrum of PNVIBA$_{3k,thermo}$-CTA2 in figure 3-5b shows several overlapping populations. Through simulation, populations A, C and D were identified, with population C of general formula C_2H_2N-($C_6H_{11}NO)_n$-$C_3H_5OS_2$,Na^+ corresponding to PNVIBA chains capped with the R- and Z-groups of CTA2, and population D of general formula $C_8H_{14}NO$-($C_6H_{11}NO)_n$-$C_3H_5OS_2$,Na^+ corresponding to PNVIBA chains initiated by the V-70 initiator and capped with the Z-group of CTA2 (Figure 3-5b). Other populations were observed but not identified as they don't seem to

correspond to PNVIBA chains initiated by the initiator or R-group of CTA2 and terminated by a double bond, the Z-group of CTA2, SH or H group.

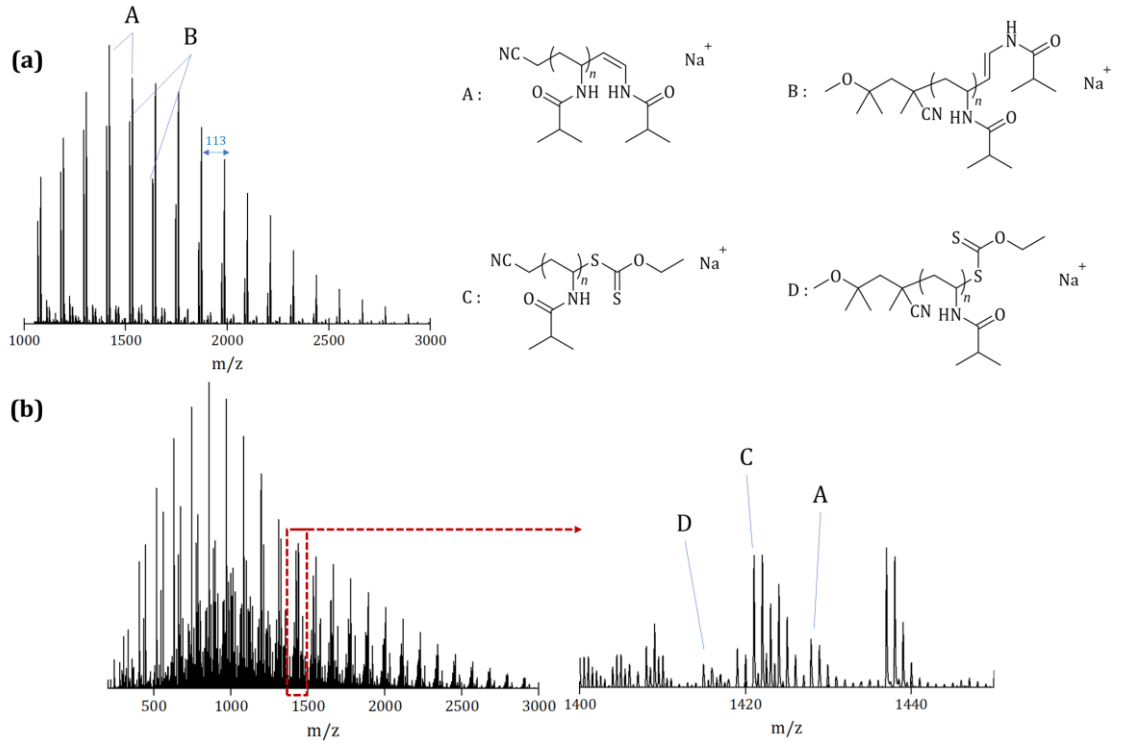

Figure 3-5. (a) MALDI-TOF and **(b)** ESI-TOF spectra of $PNVIBA_{3k,thermo}$-CTA2.

In the case of $PNVIBA_{3k,photo}$-CTA2 synthesized by photo-initiation, the MALDI-TOF spectrum showed one major population A' of general formula C_2H_2N-$(C_6H_{11}NO)_n$-$C_6H_{10}NO,Na^+$ corresponding to PNVIBA chains capped with the R-group of CTA2 on one end and terminated by a double bond on the other end (Figure 3-6a). One minor population was also observed but not identified. On the ESI-TOF spectrum on figure 3-6b, overlapping populations were observed in a similar fashion than on Figure 3-5b. Population A', as well as two populations C' and C'' of general formulas C_2H_2N-$(C_6H_{11}NO)_n$-$C_3H_5OS_2,Na^+$ and C_2H_2N-$(C_6H_{11}NO)_n$-$C_3H_5OS_2,2Na^+$ respectively, corresponding to PNVIBA chains capped with the R- and Z-groups of CTA2 were identified.

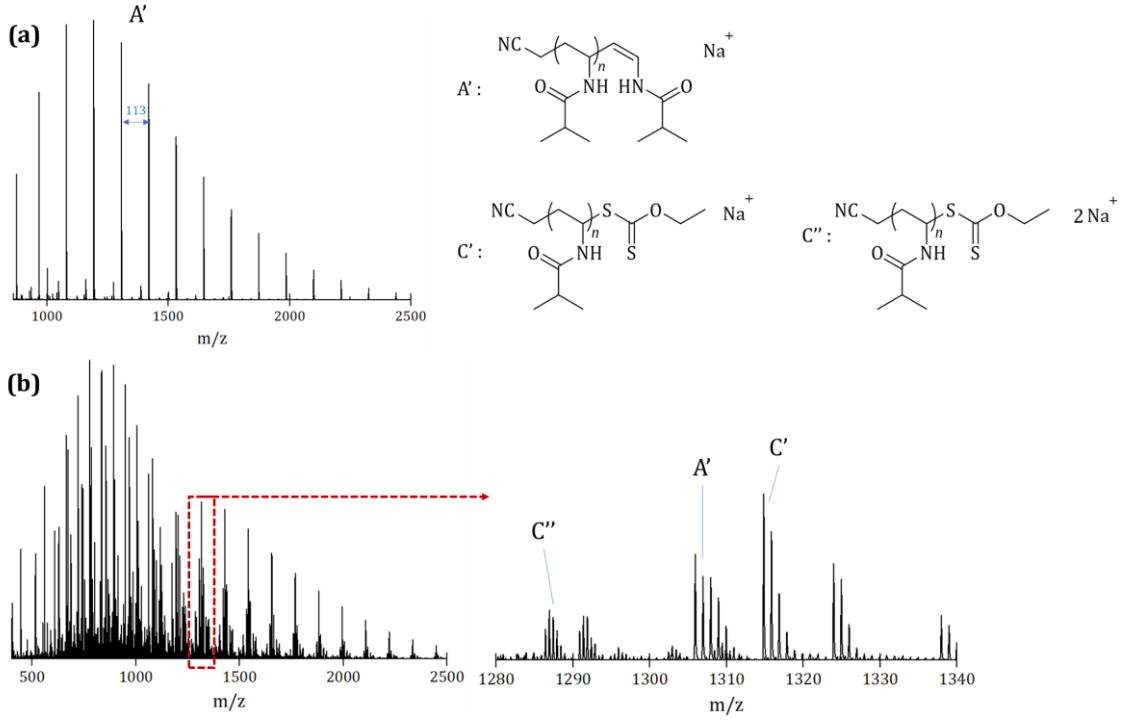

Figure 3-6. (a) MALDI-TOF and **(b)** ESI-TOF spectra of PNVIBA$_{3k,photo}$-CTA2.

From the mass spectrometry analysis of the two polymers, PNVIBA$_{3k,thermo}$-CTA2 and PNVIBA$_{3k,photo}$-CTA2, it appeared that photo-initiation is more suited for the controlled polymerization of NVIBA, as polymer chains derived from an external initiator can be avoided this way. Although the presence of PNVIBA chains capped with CTA2 was confirmed, the ESI-TOF spectra show many populations, likely due to multi-charged polymer chains as we previously observed in Chapters 1 and 2.[39,40]

Another strategy to further attest of the presence of CTA at the polymer chain-ends, and their "living" character, is to carry out chain extension experiments using those low molar mass polymers as macro-CTA for the polymerization of NVIBA (Table 3-5).

In the thermal initiation case, a relatively linear increase of $M_{n,SEC}$ with NVIBA conversion was obtained, however with values below theoretical ones and high dispersity values ($M_{n,SEC}$ = 19.0 kg mol^{-1} for $M_{n,th}$ = 22.0 kg mol^{-1} and $Đ$ = 2.33 after 6h, Table 3-5 entry 6, Figure 3-7a). Bimodal SEC-RI traces were obtained, and

although the extended polymer population peaks shift towards lower elution times with increasing monomer conversion, another population can be observed and seem to correspond to the unreacted macro-RAFT agent (Figure 3-7b) or to generated dead chains from the polymerization. Due to the high $[initiator]_0/[CTA]_0$ ratio of 1.5 that way first used in the polymerization of NVIBA to obtain the low molecular weight polymer, and secondly used in its further chain extension, a non-negligible amount of dead chain could be expected to be generated during the whole experiment.

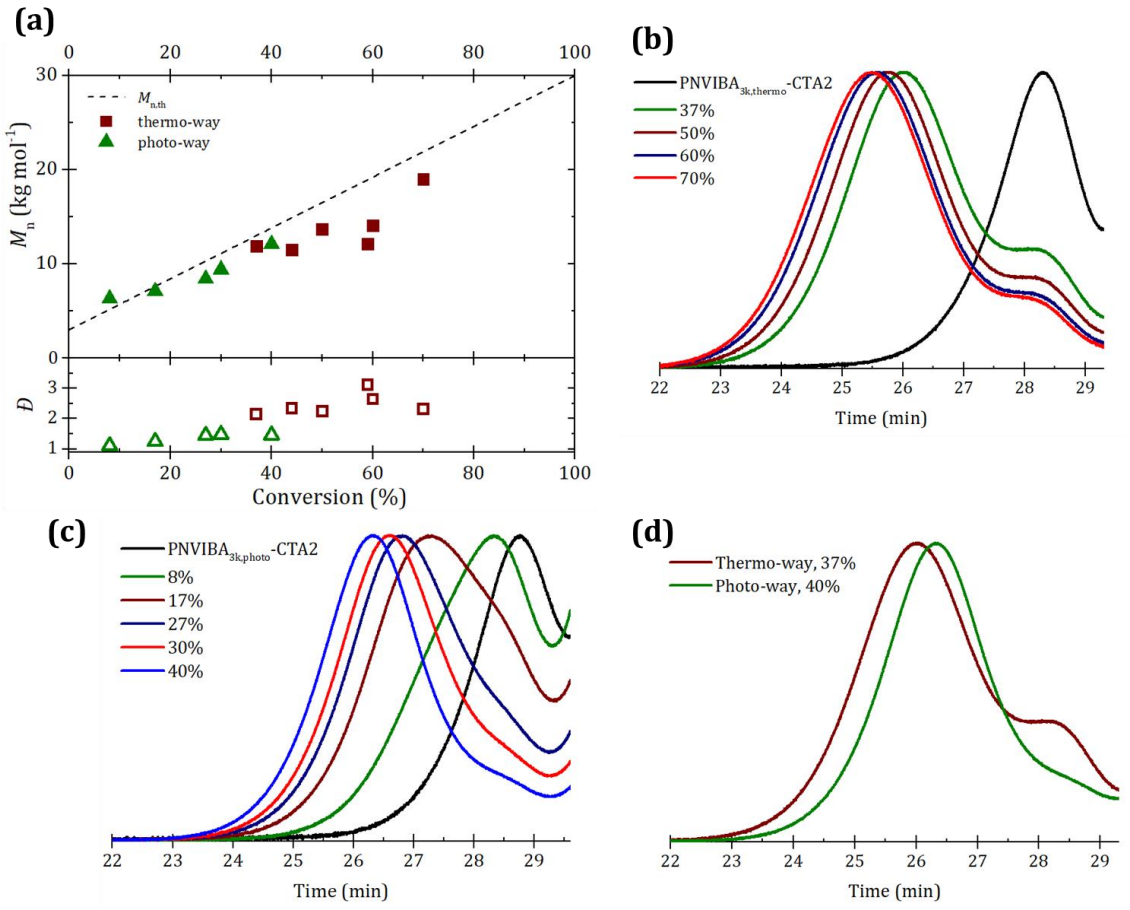

Figure 3-7. Evolution of **(a)** $M_{n,SEC}$, $Đ$ and SEC-RI traces with monomer conversion for the chain extension of **(b)** PNVIBA$_{3k,thermo}$-CTA2 at 35°C or **(c)** PNVIBA$_{3k,photo}$-CTA2 using purple LED light photo-reactor (4.0 mW cm^{-2}). **(d)** Comparison of SEC-RI traces of similar monomer conversion.

Table 3-5. RAFT polymerization of NVIBA in DMSO using a $PNVIBA_{3k,thermo}$-CTA2 at 35°C (thermal initiation with V-70) or a $PNVIBA_{3k,photo}$-CTA2 (photo-initiation under purple LED light, 4.0 mW cm^{-2}) macro-CTA. $[NVIBA]_0$ = 5.9 mol L^{-1}, $[V\text{-}70]_0$ = 38 mmol L^{-1}, $[PNVIBA\text{-}CTA2]_0$ = 25 mmol L^{-1}.

Entry	Macro-CTA	Targeted M_n (kg mol^{-1})	Time (h)	Conversion[a] (%)	$M_{n,th}$[b] (kg mol^{-1})	$M_{n,SEC}$[c] (kg mol^{-1})	$Đ$
1	$PNVIBA_{3k,thermo}$-CTA2	30	1	37	13.2	11.9	2.16
2			1.5	44	15.1	11.5	2.35
3			2	50	16.7	13.7	2.24
4			3	59	19.1	12.1	3.11
5			4	60	19.4	14.1	2.65
6			6	70	22.0	19.0	2.33
7	$PNVIBA_{3k,photo}$-CTA2	30	1	8	5.3	6.3	1.11
8			2	17	7.7	7.1	1.25
9			3	27	10.4	8.4	1.45
10			4	30	11.2	9.4	1.48
11			6	40	13.9	12.1	1.46

[a]Calculated by ^1H NMR, [b]$M_{n,th}=[NVIBA]_0/[PNVIBA\text{-}CTA2]_0 \times M_{NVIBA} \times Conv. + M_{PNVIBA\text{-}CTA2}$, [c]$M_{n,SEC}$ measured with LALS/RALS detection. M_{NVIBA} =113 g mol^{-1}, $M_{PNVIBA3k,thermo\text{-}CTA2}$=3.4 kg mol^{-1} and $M_{PNVIBA3k,photo\text{-}CTA2}$=3.1 kg mol^{-1}.

Through photo-initiation, a first observation was made on the slower reaction rate with only 40% NVIBA conversion reached after 6h compared with 70% conversion obtained through thermal initiation (Table 3-5 entries 6 and 11). Despite this, a linear increase of the obtained $M_{n,SEC}$ with NVIBA conversion was still observed, with this time significantly lower dispersities than the ones obtained by thermal initiation and maintained below 1.5 (Figure 3-7a and Table 3-5). On the SEC analysis, a shift of the SEC-RI traces is observed towards lower elution times with increasing NVIBA conversion. Although a shoulder can be noticed in the lower molar masses region, with similar elution time as the initial macro-CTA (Figure 3-7c), is it

of much lower intensity compared to the shoulder observed on the SEC-RI traces obtained from thermal initiation. A comparison of overlapped SEC-RI traces of similar NVIBA conversion is shown in Figure 3-7d to highlight this fact, with a relative intensity between the extended population and remaining macro-CTA significantly higher in the photo-initiated polymerization than the thermally initiated one. Indeed, as the thermal initiation requires an external azo-initiator, more dead chains are generated during the polymerization. As the photo-initiation doesn't, the shoulder observed in SEC-RI in the low molar masses region is thus of lower intensity.

In light of all those results, it can be inferred that the RAFT polymerization of NVIBA is feasible, and that photo-initiation is more suitable than thermal initiation for further copolymerization, which I will use for the next part of this study.

3.2.2 Copolymerization of NVIBA with NVF

In order to investigate the thermoresponsive character of PNVIBA-based materials, I turned to the copolymerization of NVIBA with NVF targeting M_n of around 20kg mol^{-1}. Block and random copolymers were synthesized via photo-RAFT polymerization (scheme 3-2), containing different proportions of NVIBA, to study the effect of polymer composition and microstructure on the LCST in water. Those copolymers will be referred as PNVIBA$_{X\%}$-*b*-PNVF$_{Y\%}$ for the block copolymers and P(NVIBA$_{X\%}$-*r*-NVF$_{Y\%}$) for the random copolymers containing X wt% of NVIBA and Y wt% of NVF.

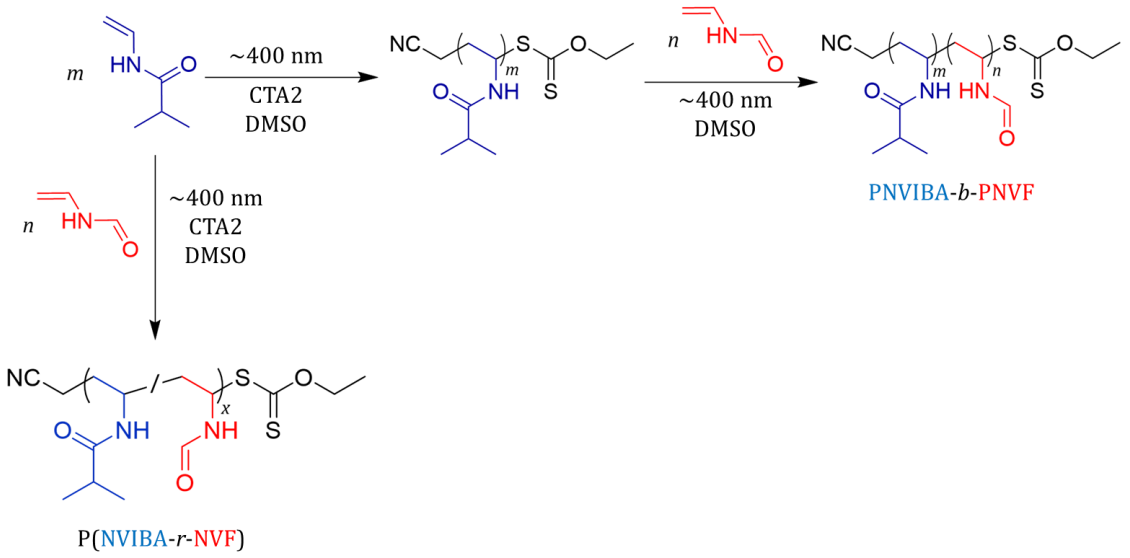

Scheme 3-2. General scheme of the copolymerization of NVIBA with NVF.

A series of two block copolymers was synthesized. I first tried to do the block copolymerization starting from a PNVF-CTA2 first block, as better control was achieved on the RAFT polymerization of NVF (see Chapter 2), however extremely low values of monomer conversion were obtained when trying to synthesize the second block PNVIBA. When polymerizing NVIBA using PNVF-CTA2 as the macro-CTA, more solvent was actually required in order to fully solubilize everything. The resulting decrease in initial monomer concentration $[NVIBA]_0$ which was reduced to 2.6 mol L^{-1}, less than half of the previously used 5.9 mol L^{-1} in the NVIBA homopolymerization part, had a significant negative impact on the polymerization.

Starting from a PNVIBA-CTA2 first block of $M_{n,SEC}$ = 11.4 kg mol^{-1} ($M_{n,th}$ = 7.0 kg mol^{-1}) and $Đ$ = 1.1, synthesized in similar conditions as described previously in the homopolymerization part, it was then used as macro-CTA for the polymerization of NVF. The original targeted molar composition of those block copolymers were of NVIBA:NVF = 53:47 mol% and 60:40 mol%. Although those are quite similar, the obtained weight composition values of NVIBA:NVF = 23:77 wt% and 43:57 wt% respectively (Table 3-6) guided me in keeping them for the further study which will be discussed later. Those unexpected, significant differences in final copolymers

compositions were observed after purification via precipitation, and two $PNVIBA_{23wt\%}$-*b*-$NVF_{77wt\%}$ and $PNVIBA_{43wt\%}$-*b*-$NVF_{57wt\%}$ were obtained.

Table 3-6. Block copolymerization of NVIBA and NVF under purple light irradiation (4.0 mW cm^{-2}) to obtain block copolymers of different compositions. PNVIBA-CTA2 first block of $M_{n,SEC}$ = 11.4 kg mol^{-1} and $Đ$ = 1.1, $[NVF]_0$ = 4.35 mol L^{-1}, $[PNVIBA\text{-}CTA2]_0$ = 23 mmol L^{-1}.

Entry	Polymer	NVF conversion (%)	$M_{n,th}$[a] (kg mol^{-1})	$M_{n,SEC}$[b] (kg mol^{-1})	$Đ$[b]	Targeted composition[c] (mol%)	Composition[d] (mol%)
1	$PNVIBA_{23wt\%}$-*b*-$NVF_{77wt\%}$	74	21.5	38.5	3.18	53% NVIBA 47% NVF	16% NVIBA 84% NVF
2	$PNVIBA_{43wt\%}$-*b*-$NVF_{57wt\%}$	57	19.2	27.7	2.07	60% NVIBA 40% NVF	32% NVIBA 68% NVF

[a]$M_{n,th}=[NVF]_0/[PNVIBA\text{-}CTA2]_0\times M_{NVF}\times Conv.+M_{PNVIBA\text{-}CTA2}$, [b]$M_{n,SEC}$ measured with PMMA standard calibration curve by SEC in in DMSO, [c]$Comp._{NVIBA}$ (mol%) = $100\times(M_{PNVIBA\text{-}CTA2}/M_{n,th})$, [d]Determined by ^1H NMR (Figure 3-8). M_{NVF}=71 g mol^{-1}.

The purification process was indeed found quite difficult to carry, as simultaneous precipitation of PNVIBA and PNVF blocks, and removal of the DMSO solvent have to be done. I first tried to dissolve the crude mixture in water, then precipitate the copolymers in an acetone:diethyl ether (1:1) mix solvent. This prove to successfully precipitate the random copolymers with satisfying compositions, as it will be shown later. However in the case of block copolymers, low amounts of materials where obtained and very poor in NVIBA. Among other organic solvents miscible with water, only acetonitrile was found to only partially solubilize a PNVIBA homopolymer. I then proceeded to use acetonitrile to precipitate the block copolymers, leading to the results shown in table 3-6 and figure 3-8. The observed difference of composition in the block copolymers could come from the non-precipitation of chains rich in PNVIBA. However, the absence of polymer signals in

the ^{1}H NMR spectrum of the filtered part after precipitation (Figure 3-8 insert) doesn't indicate a significant fractionation occurring however.

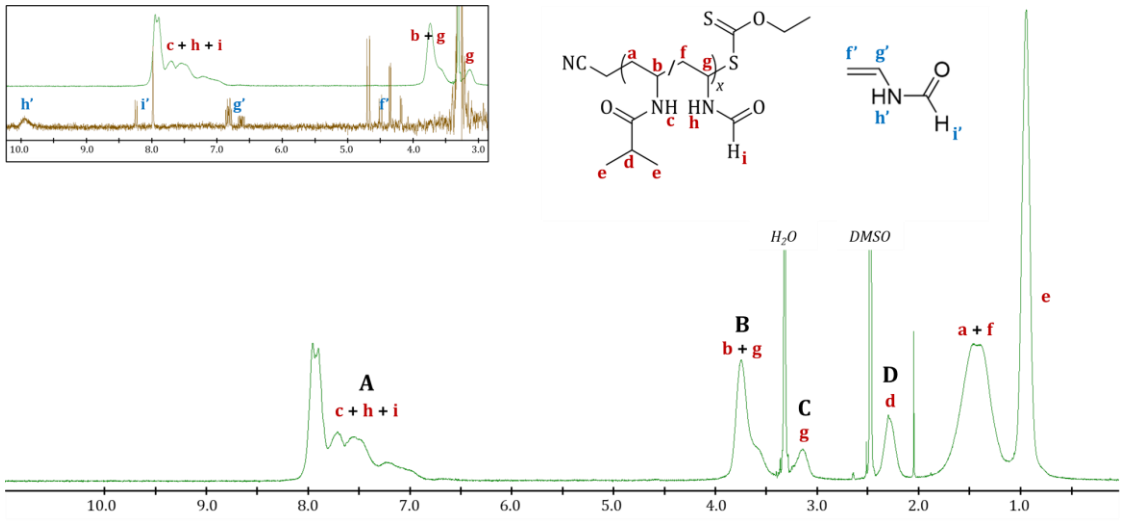

Figure 3-8. ^{1}H NMR spectra in DMSO-*d*6 of a purified PNVIBA-*b*-PNVF (Table 3-7 entry 2). $\%_{PNVIBA} = \frac{D}{B+C}$ *and* $\%_{PNVF} = \frac{B+C-D}{B+C}$ and in insert the filtered supernatant after precipitation. Measured on a 400MHz apparatus.

Another possibility could be that all PNVIBA-CTA2 first block didn't start the polymerization of NVF, as it was observed earlier in the chain extension experiment (Figure 3-7c). However, the SEC-RI traces of the block copolymers (Figure 3-10a) don't show an obvious shoulder in the lower molar masses region. Additionally, the UV-vis transmittance spectra should show two phase transition temperatures if residual PNVIBA-CTA2 was left in the mixture with the corresponding block copolymer, which they don't (Figure 3-11). The observed deviation might be due to an effect of the copolymer microstructure (random/block), further studies are needed to answer this point.

A series of three random copolymers was first synthesized by mixing different amounts of NVIBA and NVF depending on the desired final copolymer composition, CTA2 and DMSO as solvent, and copolymerization were carried under purple light irradiation (4.0 mW cm^{-2}) (Table 3-7 and figure 3-10b). Three random copolymers, P(NVIBA$_{22wt\%}$-*r*-NVF$_{78wt\%}$), P(NVIBA$_{51wt\%}$-*r*-NVF$_{49wt\%}$), P(NVIBA$_{86wt\%}$-*r*-NVF$_{14wt\%}$) were obtained (Table 3-7). From the reactivity ratios of r1 = 1.08 and r2 = 0.92 (with M1 being NVF and M2 being NVIBA), as reported by Yamamoto and coworkers,[35] it can be inferred that the copolymers of the series have random sequence distributions. As stated before, no difficulties were encountered in the purification process of the random copolymers.

Table 3-7. Copolymerization of NVIBA and NVF using CTA2 under purple light irradiation (4.0 mW cm^{-2}) to obtain random copolymers of different compositions.

Entry	Polymer	Conversion[a] (%)		$M_{n,th}$[b] (kg mol^{-1})	$M_{n,SEC}$[c] (kg mol^{-1})	$Đ$[c]	Theoretical composition[d] (mol%)	Composition[e] (mol%)
		NVIBA	NVF					
1	P(NVIBA$_{22wt\%}$-*r*-NVF$_{78wt\%}$)	84	94	22.9	33.4	2.14	20% NVIBA 80% NVF	15% NVIBA 85% NVF
2	P(NVIBA$_{51wt\%}$-*r*-NVF$_{49wt\%}$)	65	80	21.5	25.6	3.13	49% NVIBA 51% NVF	40% NVIBA 60% NVF
3	P(NVIBA$_{86wt\%}$-*r*-NVF$_{14wt\%}$)	76	88	19.7	25.8	1.70	80% NVIBA 20% NVF	79% NVIBA 21% NVF

[a]Determined by ^{1}H NMR, [b]$M_{n,th}=(([NVIBA]_0\times M_{NVIBA}\times Conv._{NVIBA}+[NVF]_0\times M_{NVF}\times Conv._{NVF})/M_{CTA2})+M_{CTA2}$. [c]$M_{n,SEC}$ measured with PMMA standard calibration curve by SEC in DMSO, [d]$Comp._{NVIBA}$ (mol%) = $100\times(([NVIBA]_0\times M_{NVIBA}\times Conv._{NVIBA}/M_{CTA2})+M_{CTA2})/M_{n,th}$. [e]Determined by ^{1}H NMR (Figure 3-9). M_{NVIBA}=113 g mol^{-1}, M_{NVF}=71 g mol^{-1}.

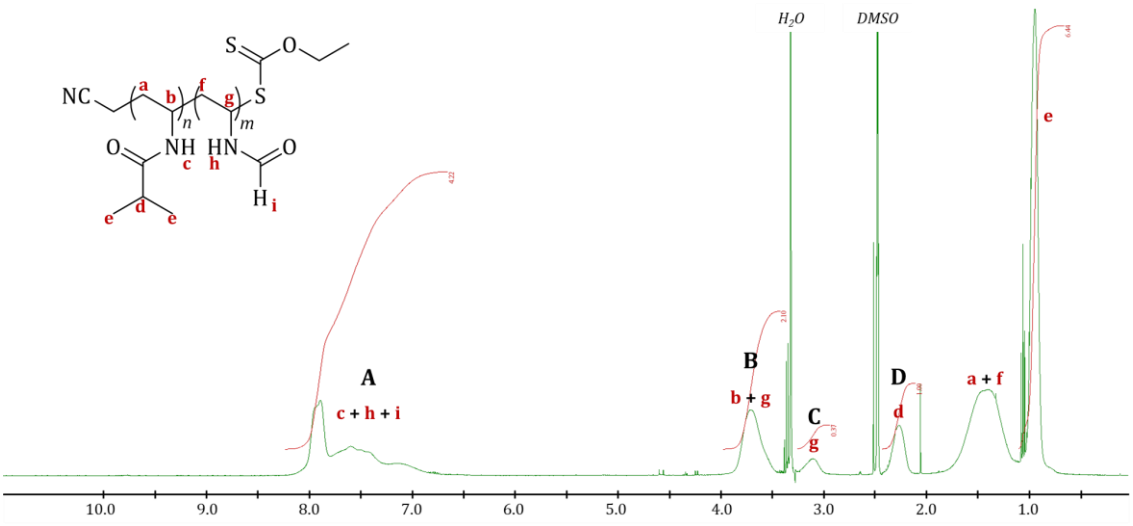

Figure 3-9. ^{1}H NMR spectrum in DMSO-*d*6 of a precipitated P(NVIBA-r-NVF) (Table 3-6 entry 2). $\%_{PNVIBA} = \frac{D}{B+C}$ *and* $\%_{PNVF} = \frac{B+C-D}{B+C}$. Measured on a 400MHz apparatus

From the nature of the two comonomers, PNVF is characterized by aqueous SEC whereas PNVIBA is characterized by organic SEC. Thus, the precise characterization of the resulting copolymers was quite challenging. I proceeded to using conventional SEC in DMSO, one of the few common solvents of the two polymers, and successfully obtain SEC-RI traces. Determination of molar masses and dispersities was done using a calibration curve with PMMA standard, and although the SEC-RI traces showed monomodal distribution in all cases (Figure 3-10), the obtained values of $M_{n,SEC}$ and $Đ$ in particular were unexpectedly high with dispersities going up to 3.18 (for a $M_{n,SEC}$ = 38.5 kg mol^{-1}, $M_{n,th}$ = 21.5 kg mol^{-1}) in the case of block copolymers, and up to 3.13 (for a $M_{n,SEC}$ = 25.6 kg mol^{-1}, $M_{n,th}$ = 21.5 kg mol^{-1}) in the case of random copolymers (Tables 3-6 and 3-7).

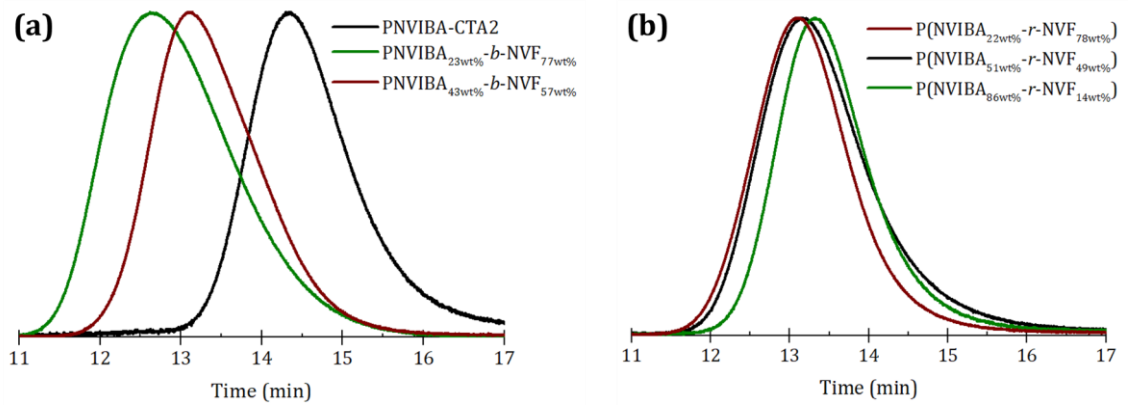

Figure 3-6. SEC-RI traces of **(a)** the first block PNVIBA-CTA2 and block copolymers and **(b)** the random copolymers.

Additionally, a series of PNVIBA-CTA2 homopolymers of $M_{n,SEC}$ = 4.8 and 15.0 kg mol^{-1} ($M_{n,th}$ = 3.3 and 10.3 kg mol^{-1}) and $Đ$ = 1.1 and 1.23 respectively were synthesized in order to investigate the influence of molar mass on the LCST property of the polymer.

3.2.3 LCST determination via UV-Vis measurement

PNVIBA is known to show LCST in water at around 39°C,[18] a bit higher than poly(*N*-isopropylacrylamide). By adding hydrophilic units such as NVF, it is expected for the resulting copolymers to show higher LCST as it is a commonly observed phenomenon.[42]

UV-Vis absorbance measurements were carried over a range of temperature from 25°C to 70°C in ultrapure water for the previously described polymers and copolymers, with a weight concentration of PNVIBA of 2 mg mL^{-1} in each case. The evolutions of calculated percentage of transmittance from heating and cooling processes are shown in figure 3-11 and phase transition temperature values are reported in table 3-8.

First, it was observed that PNVIBA-CTA2 homopolymers show a decrease in phase transition temperature with the increase of molar mass (Figure 3-11a and

table 3-8 entries 1-3) towards the reported value of 39°C. This phenomenon has been observed in the case of PVCL, which is categorized as a "type I" exhibiting classical Flory-Huggins thermoresponsive behavior in water.[28,43] Thus, it can be hypothesized that PNVIBA might follow the same behavior, meaning that its LCST can be tuned by controlling the polymer molecular weight alone. Hysteresis was observed in all cases between the heating and cooling curves (Figure 3-11). Compared to PVCL, for which it has been shown that almost no hysteresis is observed,[28] and PNIPAAm for which some hysteresis has been observed,[44] the behavior of PNVIBA in water seems to follow the latter. At temperatures above its LCST, additional intra- and inter-chain hydrogen bonds might form, thus introducing a difference in the effective temperature to do the phase transitioning during the cooling process, at a lower temperature than during the heating process.

Table 3-8. LCST of the different polymers and copolymers of NVIBA and NVF, determined as the temperature at 50% UV-Vis transmittance.

Entry	Polymer (NVIBA:NVF wt%)	LCST (°C)
1	PNVIBA-CTA2 4.8k	50.5
2	PNVIBA-CTA2 11.4k	43.5
3	PNVIBA-CTA2 15.0k	41.8
4	P(NVIBA$_{22wt\%}$-*r*-NVF$_{78wt\%}$)	-
5	P(NVIBA$_{51wt\%}$-*r*-NVF$_{49wt\%}$)	-
6	P(NVIBA$_{86wt\%}$-*r*-NVF$_{14wt\%}$)	61.5
7	PNVIBA$_{23wt\%}$-*b*-NVF$_{77wt\%}$	48.8
8	PNVIBA$_{43wt\%}$-*b*-NVF$_{57wt\%}$	45.3

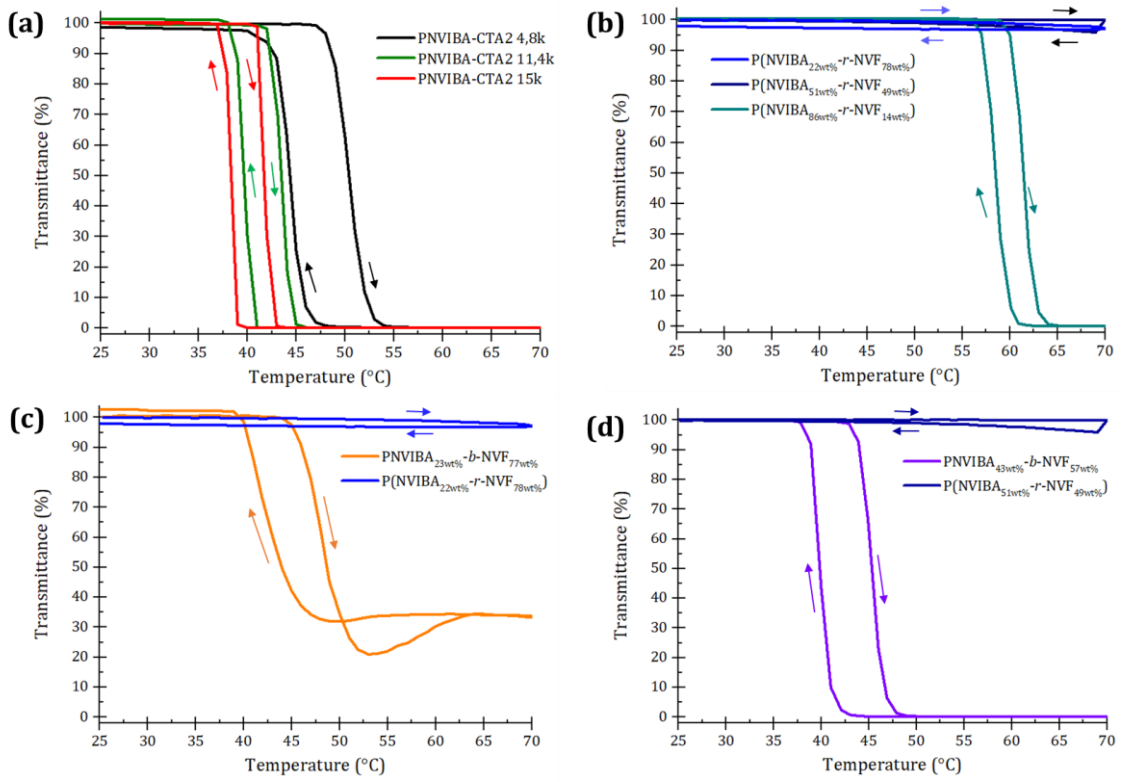

Figure 3-7. Evolution of UV-Vis transmittance of aqueous solutions of copolymers of NVIBA and NVF with the temperature, prepared at a NVIBA concentration of 2 mg mL^{-1}. Heating and cooling curves are indicated by arrows, at a rate of 1°C min^{-1}. **(a)** PNVIBA-CTA2 homopolymers, **(b)** P(NVIBA-*r*-NVF) random copolymers, **(c)** comparison of random and block copolymers with ~20wt% NVIBA and **(d)** ~45wt% NVIBA.

Secondly, in the case of random copolymers, a phase transition was only observed for the high composition in NVIBA of 86 wt%, and at an elevated temperature of 61.5°C compared to PNVIBA homopolymers (Figure 3-11b and table 3-8 entries 4-6). At high NVIBA compositions, there is a higher chance of having successive NVIBA units, thus a higher chance of having PNVIBA "blocks" in the polymer chain, resulting in an apparent thermoresponsive character. For NVIBA compositions of 51 wt% and lower however, no phase transition was observed. Using conventional radical polymerization, Yamamoto and coworkers also studied the phase transition temperature of random copolymers of NVIBA and NVF with molar masses around 30 kg mol^{-1}, containing from 61 wt% up to 95 wt% of NVIBA.[35] In their studies, LCST values were obtained for all compositions with temperatures

ranging from 45°C up to 70°C for copolymers containing respectively 95 wt% and 61 wt% of NVIBA. As the observed phase transition temperature increased with the decrease of NVIBA content, it should be expected to observe the absence of LCST for copolymers containing lower proportions of NVIBA, which is in accordance to the observation made just above.

Thirdly, the influence of monomer sequence distribution is highlighted in figure 3-11c and 3-11d with the comparison of two sets of block and random copolymers of similar NVIBA compositions. For copolymers containing 22~23 wt% (Figure 3-11c and table 3-8 entries 4 and 7) and 40~50 wt% of NVIBA (Figure 3-11d and table 3-8 entries 5 and 8), it is observed that only the block copolymers show a reversible phase transition. Interestingly, the LCST increasing effect due to a higher hydrophilicity (resulting from the PNVF block) is indeed also shown as the PNVIBA block is the same for the two PNVIBA-*b*-PNVFs, with phase transition temperatures of 48.8°C for the one containing 23 wt% and of 45.3°C for the one containing 40 wt% of NVIBA. From those comparisons, it can be inferred that the monomer sequence distribution is essential for keeping the material's thermoresponsive character.

3.3 CONCLUSION

The reversible-deactivation radical polymerization of NVIBA was successfully conducted for the first time by the RAFT process. Despite a slightly slower polymerization rate compared to using thermal initiation, using photo-RAFT is more suited for the polymerization of NVIBA. Thanks to the photo-iniferter character of xanthates, the high amount of 1.5 equivalents of azo-initiator compared to CTA required when conducting thermal RAFT polymerization can be avoided. Thus, the polymerization of NVIBA using purple LEDs (λ = 400 nm, 4.0 mW cm^{-2}) was conducted. Through analytical methods such as mass spectrometry (MALDI-TOF and ESI-TOF) and chain extension experiment, the effective presence of polymers chains capped with the CTA was shown. For the first time, block copolymers of NVIBA and NVF were synthesized using photo-RAFT block copolymerization starting from a PNVIBA-CTA2 macro-CTA, albeit with a deviation in their compositions compared to what was expected. Further studies need to be conducted to answer this problem, and in order to obtain block copolymers containing higher proportions of NVIBA. The thermoresponsive behavior of block copolymers and random copolymers were investigated, and the essential impact of monomer sequence distribution on LCST was shown, as phase transition temperatures were measured for block copolymers (of respectively 48.8°C and 45.3°C for block copolymers containing 23wt% and 43wt% NVIBA) whereas none was observed for the corresponding random copolymers containing the same proportion of NVIBA. This in turn further shines light on the advantage of using controlled radical polymerization techniques such as RAFT in order to obtain copolymers of controlled architectures in order to fine-tune temperature-induced polymer assemblies with predetermined LCST properties. Furthermore, the perspective of obtaining polyvinylamine moieties from the hydrolysis of the PNVF part of those copolymers might open the way to new kinds of multiresponsive materials in the near future. The influence of vinylamine units on the thermoresponsive behavior of the block and random copolymers can also be investigated and compared with the influence of NVF units. On another hand, further studies on the materials, such as dynamic

light scattering (DLS) or Fourier-transform infrared (FTIR) spectroscopy can be conducted at different temperatures around the materials' LCST, in order to show the behavior and interactions of surrounding water molecules with the polymeric chains.

3.4 EXPERIMENTAL SECTION

3.4.1 Characterization

NMR analysis

^{1}H NMR spectra were measured using a JEOL JNM-ECX400 apparatus operating at a frequency of 400MHz. All samples were dissolved in DMSO-d_6. Coupling constants (J) are reported to ± 0.5 Hz. The resonance multiplicities are described as s (singlet), d (doublet), t (triplet), q (quartet) or m (multiplet). Chemical shifts δ are reported in parts per million (ppm) and are referenced to the residual solvent peak (DMSO: H = 2.5 ppm).

Size-exclusion chromatography

Size-exclusion chromatography (SEC) analysis in DMF + 0.1M LiBr were performed on a system composed of an OHpak SB-G guard column and a set of 3 OHpak SB-806M HQ columns (Shodex).

SEC analysis in DMSO were performed on a system composed of a TSKgel α guard column, a TSKgel α-3000 column and a TSKgel α-M column (Tosoh).

Analysis were conducted using a Malvern 270 dual detector for LALS/RALS measurements, a Jasco RI-2031Plus refractive index detector, a Jasco PU-4580 pump, a Jasco DG-2080-53 degasser, a Jasco AS-4550 HPLC autosampler, a Jasco CO-2065Plus column oven, and OmniSEC 5.0 software was used to treat data. PMMA standards were used to calibrate the LALS/RALS detectors. PMMA standards were also used to calculate a calibration curve for SEC in DMSO. Analysis were performed at 40°C and a flow rate of 1 mL min^{-1}.

Matrix-assisted laser desorption/ionization-time of flight mass spectrometry (MALDI-TOF-MS) and electron spray ionization-time of flight mass spectrometry (ESI-TOF-MS)

MALDI-TOF-MS analysis were performed on a JEOL spiralTOF JMS-S3000 apparatus. Analysis were carried out with DCBT in chloroform as matrix and TFANa in THF as cationizing agent. Data was acquired using ms Tornado Analysis software.

ESI-TOF-MS analysis were performed on a LC-TOFMS (JEOL AccuTOF LC-plus 4G, DART/ESI/CSI/APCI) apparatus in ESI positive mode. Samples of PNVIBA were dissolved in chloroform, diluted to 1/10 and NaI was added. The resulting samples were directly infused in the source. The source temperature and desolvation temperature were 80°C and 200°C respectively, and the cone voltage was optimized at 100V. Data was acquired with ms Axel data Processing LP software.

LCST measurement

UV-Vis transmittance measurement were performed on a Shimadzu UV-2600 apparatus at 500 nm with heating and cooling from 25°C to 70°C at a rate of 1°C min^{-1}. Samples were prepared by solubilizing polymers in ultrapure water at a NVIBA concentration of 2 mg mL^{-1}. LCST was defined as the temperature at 50% transmittance in the heating process.

3.4.2 Materials

N-vinylformamide (NVF, TCI, 96%) and isobutyryl chloride (TCI, 98%) were distilled before use. Potassium ethylxanthogenate (TCI, 95%), bromoacetonitrile (TCI, 97%), triethylamine (Et_3N, TCI, 99%), 2,2'-azobis(4-methoxy-2,4-dimethylvaleronitrile) (V-70, Wako), NaOH 5M solution (Nacalai tesque), tetrahydrofuran (THF, Kanto chemical), ethyl acetate (Wako), dimethyl sulfoxide (DMSO, solvent for synthesis Wako, SEC solvent Nicalai tesque), acetone (Wako), ethanol (Wako), hexane (Wako), diethyl ether (Wako), dimethyl formamide (DMF, Nicalai tesque), acetonitrile (Wako), DMSO-d_6 (CIL, 99.9%) were used as received.

Non-waterproof, flexible purple LED strip (5V, 2M, 5050 SMD, λ=400 nm) were purchased on amazon.co.jp.

3.4.3 Purple LED photo-reactor

A strip of 60 purple LEDs was sticked to the interior of a cylindrical aluminum can of diameter 8.5 cm and height 10 cm. A cooling fan was placed under the photo-reactor to ensure some thermoregulation through a constant flow of air. Schlenk tubes used for experiments were placed at the center of the photo-reactor and covered with aluminum foil during the reactions.

3.4.4 Synthesis of NVIBA monomer

The synthesis of NVIBA was done according to a published protocol.[45] NVF (14.22g, 0.20mol), Et_3N (24.29g, 0.24mol) THF (150mL) were added to a round-bottom tricol flask with a magnetic stirrer, and cooled to 0°C in an ice bath under N_2 flow. Isobutyryl chloride (25.58g, 0.24mol) was slowly added dropwise at a temperature maintained under 5°C, and the reaction stirred under N_2 atmosphere for 3h. NaOH 5M solution (120mL) was slowly added while maintaining the temperature under 5°C and the reaction mixture was stirred further for 3h. The reaction mixture was then extracted with ethyl acetate (3x 100mL). The obtained organic phases were washed with distilled water (3x 200mL) and saturated NaCl solution (100 mL), dried with $MgSO_4$, filtered and solvent was partially evaporated. The resulting yellow/orange liquid was then purified by column chromatography with a hexane:ethyl acetate 60:40 v/v eluent. Solvent was then evaporated to give a white/pale yellow solid (14.1g, 62% yield).

^{1}H NMR (400MHz, DMSO-d_6): δ (ppm) = 1.1 (d, J=6.0Hz, 6H, -CH-(C<u>H</u>$_3$)$_2$), 2.4 (sept, J=6.8Hz, 1H, -C<u>H</u>-(CH$_3$)$_2$), 4.3 (d, J=8.9Hz, 1H, -CH=C<u>H</u>$_2$), 4.6 (d, J=16.0Hz, 1H, -CH=C<u>H</u>$_2$), 6.9 (ddd, J=3.2; 10.3; 16.1Hz, -NH-C<u>H</u>=CH$_2$), 8.4 (broad, 1H, N<u>H</u>)

3.4.5 Synthesis of CTA2

S-(cyanomethyl) *O*-ethyl carbonodithioate (CTA2) was synthesized according to previously published procedure.[46]

3.4.6 Synthesis of PNVIBA-CTA2

Thermal initiation

Typically, NVIBA (2g, 17.7mmol), CTA2 (16.3mg, 0.1mmol), V-70 (46.6mg, 0.2mmol), DMSO (0.86g) were added to a Schlenck tube, degassed by four freeze-pump-thaw cycles, and immersed into an oil bath at 35°C for a certain time. The polymerization was stopped by rapidly cooling down the mixture with liquid nitrogen and samples were directly withdrawn and analyzed via ^{1}H NMR to determine the conversion, and via SEC in DMF+0.1M LiBr to determine molar mass and dispersity. Purification of the polymers were conducted by solubilization in distilled water, then precipitation in a cold diethyl ether, filtered and dried under vacuum.

Photo-initiation

Typically, NVIBA (2g, 17.7mmol), CTA2 (16.3mg, 0.1mmol), DMSO (0.86g) were added to a Schlenck tube, degassed by four freeze-pump-thaw cycles, and immersed into a 60 LEDs photo-reactor (λ = 400 nm, 4.0 mW cm^{-2}) equipped with a fan ($T_{reactor}$=30°C) and covered in aluminum foil for a certain time. The polymerization was stopped by turning off the reactor lights and samples were directly withdrawn and analyzed via ^{1}H NMR to determine the conversion, and via SEC in DMF+0.1M LiBr to determine molar mass and dispersity. Purification of the polymers were conducted by solubilization in distilled water, then precipitation in a cold diethyl ether, filtered and dried under vacuum.

3.4.7 Chain extension experiment with PNVIBA-CTA2

Thermal initiation

NVIBA (2g, 17.7mmol), PNVIBA$_{3k,thermo}$-CTA2 (0.256g, 0.08mmol), V-70 (34.8mg, 0.11mmol), DMSO (0.86g) were added to a Schlenck tube, degassed by four freeze-pump-thaw cycles, and immersed into an oil bath at 35°C for a certain time. The

polymerization was stopped by rapidly cooling down the mixture with liquid nitrogen and samples were directly withdrawn and analyzed via ^{1}H NMR to determine the conversion, and via SEC in DMF+0.1M LiBr to determine molar mass and dispersity.

Photo-initiation

NVIBA (2g, 17.7mmol), PNVIBA$_{3k,photo}$-CTA2 (0.231g, 0.07mmol), DMSO (0.86g) were added to a Schlenck tube, degassed by four freeze-pump-thaw cycles, and immersed into a 60 LEDs photo-reactor (λ = 400 nm, 4.0 mW cm^{-2}) equipped with a fan ($T_{reactor}$=30°C) and covered in aluminum foil for a certain time. The polymerization was stopped by turning off the reactor lights and samples were directly withdrawn and analyzed via ^{1}H NMR to determine the conversion, and via SEC in DMF+0.1M LiBr to determine molar mass and dispersity.

3.4.8 Synthesis of P(NVIBA-*r*-NVF) random copolymer

Typically, NVIBA (1.26g, 11.1mmol), NVF (1.08g, 15.2mmol), CTA2 (12.7mg, 0.08mmol), DMSO (0.86g) were added to a Schlenck tube, degassed by four freeze-pump-thaw cycles, and immersed into a 60 LEDs photo-reactor (λ = 400 nm, 4.0 mW cm^{-2}) equipped with a fan ($T_{reactor}$=30°C) and covered in aluminum foil for 16h. The polymerization was stopped by turning off the reactor lights and samples were directly withdrawn and analyzed via ^{1}H NMR to determine the monomers conversion. Purification of the polymers were conducted by solubilization in distilled water, then precipitation in a cold mixture of acetone:diethyl ether (50/50 v/v), filtered and dried under vacuum.

3.4.9 Synthesis of PNVIBA-*b*-PNVF block copolymer

Starting from a PNVIBA-CTA2 of $M_{n,SEC}$=11.4kg mol-1 and $Đ$=1.1 synthesized and purified according to the procedure in 3.4.5 Photo-way.

Typically, NVF (0.50g, 4.42mmol), PNVIBA-CTA2 (0.419g, 0.04mmol), DMSO (1.17g) were added to a Schlenk tube, degassed by four freeze-pump-thaw cycles, and immersed into a 60 LEDs photo-reactor (λ = 400 nm, 4.0 mW cm^{-2}) equipped with a fan ($T_{reactor}$=30°C) and covered in aluminum foil for 16h. The polymerization was stopped by turning off the reactor lights and samples were directly withdrawn and analyzed via ^{1}H NMR to determine the monomers conversion. Purification of the polymers were conducted by solubilization in distilled water, then precipitation in cold acetonitrile, filtered and dried under vacuum.

3.5 REFERENCES

(1) Aktas Eken, G.; Hayri Acar, M. Chapter 9 - PVDF-Based Shape Memory Materials. Elsevier, **2020**; 247–274.
(2) Osada, Y.; Matsuda, A. Shape Memory in Hydrogels. *Nature* **1995**, *376* (6537), 219–219.
(3) Sun, J.-Y.; Zhao, X.; Illeperuma, W. R. K.; Chaudhuri, O.; Oh, K. H.; Mooney, D. J.; Vlassak, J. J.; Suo, Z. Highly Stretchable and Tough Hydrogels. *Nature* **2012**, *489* (7414), 133–136.
(4) Yoshida, R. Design of Functional Polymer Gels and Their Application to Biomimetic Materials. *Curr. Org. Chem.* **2005**, *9* (16), 1617–1641.
(5) Peppas, N. A.; Hilt, J. Z.; Khademhosseini, A.; Langer, R. Hydrogels in Biology and Medicine: From Molecular Principles to Bionanotechnology. *Adv. Mater.* **2006**, *18* (11), 1345–1360.
(6) Mano, J. F. Stimuli-Responsive Polymeric Systems for Biomedical Applications. *Adv. Eng. Mater.* **2008**, *10* (6), 515–527.
(7) Nandi, N.; Gayen, K.; Ghosh, S.; Bhunia, D.; Kirkham, S.; Sen, S. K.; Ghosh, S.; Hamley, I. W.; Banerjee, A. Amphiphilic Peptide-Based Supramolecular, Noncytotoxic, Stimuli-Responsive Hydrogels with Antibacterial Activity. *Biomacromolecules* **2017**, *18* (11), 3621–3629.
(8) Verdonck, B.; Goethals, E. J.; Du Prez, F. E. Block Copolymers of Methyl Vinyl Ether and Isobutyl Vinyl Ether With Thermo-Adjustable Amphiphilic Properties. *Macromol. Chem. Phys.* **2003**, *204* (17), 2090–2098.
(9) Park, J.-S.; Akiyama, Y.; Yamasaki, Y.; Kataoka, K. Preparation and Characterization of Polyion Complex Micelles with a Novel Thermosensitive Poly(2-Isopropyl-2-Oxazoline) Shell via the Complexation of Oppositely Charged Block Ionomers. *Langmuir* **2007**, *23* (1), 138–146.
(10) Fournier, D.; Hoogenboom, R.; Thijs, H. M. L.; Paulus, R. M.; Schubert, U. S. Tunable PH- and Temperature-Sensitive Copolymer Libraries by Reversible Addition−Fragmentation Chain Transfer Copolymerizations of Methacrylates. *Macromolecules* **2007**, *40* (4), 915–920.
(11) Gan, L. H.; Gan, Y. Y.; Deen, G. R. Poly(N-Acryloyl-N'-Propylpiperazine): A New Stimuli-Responsive Polymer. *Macromolecules* **2000**, *33* (21), 7893–7897.
(12) Aseyev, V.; Tenhu, H.; Winnik, F. M. Non-Ionic Thermoresponsive Polymers in Water. Springer: Berlin, Heidelberg, **2011**; 29–89.
(13) Fujishige, S.; Kubota, K.; Ando, I. Phase Transition of Aqueous Solutions of Poly(N-Isopropylacrylamide) and Poly(N-Isopropylmethacrylamide). *J. Phys. Chem.* **1989**, *93* (8), 3311–3313.
(14) Schmaljohann, D. Thermo- and PH-Responsive Polymers in Drug Delivery. *Adv. Drug Deliv. Rev.* **2006**, *58* (15), 1655–1670.
(15) Vihola, H.; Laukkanen, A.; Valtola, L.; Tenhu, H.; Hirvonen, J. Cytotoxicity of Thermosensitive Polymers Poly(N-Isopropylacrylamide), Poly(N-Vinylcaprolactam) and Amphiphilically Modified Poly(N-Vinylcaprolactam). *Biomaterials* **2005**, *26* (16), 3055–3064.

(16) Kostanski, L. K.; Huang, R.; Ghosh, R.; Filipe, C. D. M. Biocompatible Poly(N-Vinyllactam)-Based Materials with Environmentally-Responsive Permeability. *J. Biomater. Sci. Polym. Ed.* **2008**, *19* (3), 275–290.
(17) Sun, S.; Wu, P. Infrared Spectroscopic Insight into Hydration Behavior of Poly(N-Vinylcaprolactam) in Water. *J. Phys. Chem. B* **2011**, *115* (40), 11609–11618.
(18) Suwa, K.; Wada, Y.; Kikunaga, Y.; Morishita, K.; Kishida, A.; Akashi, M. Synthesis and Functionalities of Poly(n-Vinylalkylamide). IV. Synthesis and Free Radical Polymerization of N-Vinylisobutyramide and Thermosensitive Properties of the Polymer. *J. Polym. Sci. Part Polym. Chem.* **1997**, *35*, 1763–1768.
(19) Liu, J.; Debuigne, A.; Detrembleur, C.; Jérôme, C. Poly(N-Vinylcaprolactam): A Thermoresponsive Macromolecule with Promising Future in Biomedical Field. *Adv. Healthc. Mater.* **2014**, *3* (12), 1941–1968.
(20) Srivastava, A.; Kumar, A. Synthesis and Characterization of a Temperature-Responsive Biocompatible Poly(N-Vinylcaprolactam) Cryogel: A Step towards Designing a Novel Cell Scaffold. *J. Biomater. Sci. Polym. Ed.* **2009**, *20* (10), 1393–1415.
(21) Fan, W.; Nakamura, Y.; Yamago, S. Synthesis of Multivalent Organotellurium Chain-Transfer Agents by Post-Modification and Their Applications in Living Radical Polymerization. *Chem. - Eur. J.* **2016**, *22* (47), 17006–17010.
(22) He, F.; Tang, G.; Min, X.; Hu, M.; Shao, L.; Bi, Y. Living/Controlled Free Radical Polymerization of N-Vinyl Caprolactam. *Huaxue Jinzhan* **2016**, *28* (2–3), 328–336.
(23) Kermagoret, A.; Mathieu, K.; Thomassin, J.-M.; Fustin, C.-A.; Duchêne, R.; Jérôme, C.; Detrembleur, C.; Debuigne, A. Double Thermoresponsive Di- and Triblock Copolymers Based on N-Vinylcaprolactam and N-Vinylpyrrolidone: Synthesis and Comparative Study of Solution Behaviour. *Polym. Chem.* **2014**, *5* (22), 6534–6544.
(24) Simula, A.; Nurumbetov, G.; Anastasaki, A.; Wilson, P.; Haddleton, D. M. Synthesis and Reactivity of α,ω-Homotelechelic Polymers by Cu(0)-Mediated Living Radical Polymerization. *Eur. Polym. J.* **2015**, *62*, 294–303.
(25) Yang, Y.; Tang, G.; Hu, M.; Shao, L.; Li, J.; Bi, Y. High-Efficiency Synthesis of Well-Defined Cyclic Poly(N-Vinylcaprolactam) and Its Solution Properties. *Polymer* **2015**, *68*, 213–220.
(26) Long, Z.; Ding, Q.; Zhou, X.; Liang, D.; Zhang, G. Synthesis and Application of Vinyl Lactam Block Copolymer as Kinetic Hydrate Inhibitors. *Fuel* **2019**, *254*, 115706.
(27) Yang, Z.; Wang, F.; Liu, H. Dual Responsive Spiropyran-Ended Poly(N-Vinyl Caprolactam) for Reversible Complexation with Metal Ions. *J. Polym. Res.* **2019**, *26* (4), 1–11.
(28) Beija, M.; Marty, J.-D.; Destarac, M. Thermoresponsive Poly(N-Vinyl Caprolactam)-Coated Gold Nanoparticles: Sharp Reversible Response and Easy Tunability. *Chem. Commun.* **2011**, *47* (10), 2826–2828.

(29) Ponce-Vargas, S. M.; Cortez-Lemus, N. A.; Licea-Claveríe, A. Preparation of Poly(N-Vinylcaprolactam) (NVCL) and Statistical Copolymers of NVCL with Variable Cloud Point Temperature by Using A Trithiocarbonate RAFT Agent. *Macromol. Symp.* **2013**, *325–326* (1), 56–70.
(30) Cortez-Lemus, N. A.; Castro-Hernández, A. Intrinsic Viscosity of Poly(N-Vinylcaprolactam) with Varying the Architecture. *J. Polym. Res.* **2020**, *27* (8), 225.
(31) Zhao, X.; Coutelier, O.; Nguyen, H. H.; Delmas, C.; Destarac, M.; Marty, J.-D. Effect of Copolymer Composition of RAFT/MADIX-Derived N-Vinylcaprolactam/N-Vinylpyrrolidone Statistical Copolymers on Their Thermoresponsive Behavior and Hydrogel Properties. *Polym. Chem.* **2015**, *6* (29), 5233–5243.
(32) Suwa, K.; Wada, Y.; Kishida, A.; Akashi, M. Synthesis and Functionalities of Poly(N-Vinylalkanamide). VI. A Novel Thermosensitive Hydrogel Crosslinked Poly(N-Vinylisobutyramide). *J. Polym. Sci. Part Polym. Chem.* **1997**, *35*, 3377–3384.
(33) Yoshida, H.; Furumai, H.; Ajiro, H. Preparation and Characterization of Thermoresponsive Poly(N-Vinylisobutyramide) Microgels. *Langmuir* **2022**, *38* (17), 5269–5274.
(34) Kan, K.; Ajiro, H. Switchable Thermal Responsive Interpenetrated Polymer Network Gels of Poly(N-Vinylacetamide) and Poly(N-Vinylisobutyramide). *Chem. Lett.* **2018**, *47*, 591–593.
(35) Yamamoto, K.; Serizawa, T.; Muraoka, Y.; Akashi, M. Synthesis and Functionalities of Poly(N-Vinylalkylamide). XII. Synthesis and Thermosensitive Property of Poly(Vinylamine) Copolymer Prepared from Poly(N-Vinylformamide-Co-N-Vinylisobutyramide). *J. Polym. Sci. Part Polym. Chem.* **2000**, *38*, 3674–3681.
(36) Tachaboonyakiat, W.; Ajiro, H.; Akashi, M. Controlled DNA Interpolyelectrolyte Complex Formation or Dissociation via Stimuli-Responsive Poly(Vinylamine-Co-N-Vinylisobutylamide). *J. Appl. Polym. Sci.* **2016**, *133*
(37) Akashi, M.; Nakano, S.; Kishida, A. Synthesis of Poly(N-Vinylisobutyramide) from Poly(N-Vinylacetamide) and Its Thermosensitive Property. *J. Polym. Sci. Part Polym. Chem.* **1996**, *34*, 301–303.
(38) Kunugi, S.; Takano, K.; Tanaka, N.; Suwa, K.; Akashi, M. Effects of Pressure on the Behavior of the Thermoresponsive Polymer Poly(N-Vinylisobutyramide) (PNVIBA). *Macromolecules* **1997**, *30*, 4499–4501.
(39) Dupre--Demorsy, A.; Coutelier, O.; Destarac, M.; Nadal, C.; Bourdon, V.; Ando, T.; Ajiro, H. RAFT Polymerization of N-Methyl-N-Vinylacetamide and Related Double Hydrophilic Block Copolymers. *Macromolecules* **2022**, *55* (4), 1127–1138.
(40) Dupre--Demorsy, A.; Kurowska, I.; Balayssac, S.; Hennetier, M.; Ric, A.; Bourdon, V.; Ando, T.; Ajiro, H.; Coutelier, O.; Destarac, M. RAFT Polymerisation of N-Vinylformamide and the Corresponding Double Hydrophilic Block Copolymers. *Polym. Chem.* **2022**, *13* (44), 6229–6237.

(41) Kurowska, I.; Dupre–Demorsy, A.; Balayssac, S.; Hennetier, M.; Ric, A.; Bourdon, V.; Ando, T.; Ajiro, H.; Coutelier, O.; Destarac, M. Tailor-Made Poly(Vinylamine) via Purple LED-Activated RAFT Polymerization of N-Vinylformamide. *Macromol. Rapid Commun. n/a* (n/a), 2200729.
(42) Chee, C. K.; Rimmer, S.; Shaw, D. A.; Soutar, I.; Swanson, L. Manipulating the Thermoresponsive Behavior of Poly(N-Isopropylacrylamide). 1. On the Conformational Behavior of a Series of N-Isopropylacrylamide−Styrene Statistical Copolymers. *Macromolecules* **2001**, *34* (21), 7544–7549.
(43) Meeussen, F.; Nies, E.; Berghmans, H.; Verbrugghe, S.; Goethals, E.; Du Prez, F. Phase Behaviour of Poly(N-Vinyl Caprolactam) in Water. *Polymer* **2000**, *41* (24), 8597–8602.
(44) Cheng, H.; Shen, L.; Wu, C. LLS and FTIR Studies on the Hysteresis in Association and Dissociation of Poly(N-Isopropylacrylamide) Chains in Water. *Macromolecules* **2006**, *39* (6), 2325–2329.
(45) Tu, S.; Zhang, C. Facile Preparation of N-Vinylisobutyramide and N-Vinyl-2-Pyrrolidinone. *Org. Process Res. Dev.* **2015**, *19*, 2045–2049.
(46) Chiefari, J.; Mayadunne, R. T.; Moad, G.; Rizzardo, E.; Thang, S. H. Polymerization Process with Living Characteristics and Polymers Made Therefrom. US6747111B2, June 8, 2004.

GENERAL CONCLUSION AND PERSPECTIVES

This thesis on the reversible addition-fragmentation chain-transfer (RAFT) polymerization of acyclic *N*-vinylamides was motivated after the observation of a lack of studies on the controlled radical polymerization of acyclic *N*-vinylamides, contrasting with the extensive amount of literature on the cyclic *N*-vinylamides derivatives and especially concerning their RAFT polymerization. Even though, (co)-polymers containing acyclic *N*-vinylamide monomers are used in a wide array of applications in fields such as biomedicine, water treatment, energy and batteries, textile, petroleum industry, for their interesting properties as they are water-soluble, biocompatible, and in some cases thermoresponsive or kinetic hydrate inhibitors. This further reinforced our interest on providing an efficient and easy way to obtain polymers and copolymers of controlled molar masses, dispersities and architectures.

In the Chapter 1, a first example was demonstrated with *N*-methyl-*N*-vinylacetamide (NMVA). As the starting point of this study, polymerization conditions were established through the study on several parameters. As less activated monomers (LAMs), xanthates and dithiocarbamates are indicated to be used as chain transfer agents (CTAs), and the RAFT polymerization of NMVA was successfully conducted using those with a xanthate, *S*-cyanomethyl-*O*-ethylxanthate, showing the most promising results. Some important factors were also highlighted through the homopolymerization study. On one hand, the combined effects of low azo-initiator efficiency, moderate reactivity of NMVA and RAFT retardation led to poor monomer conversions when using typical [initiator]/[CTA] concentration ratios. To counterbalance this effect and obtain satisfactory conversions, an unusually high [initiator]/[CTA] ratio of 1.49/1 was applied. Unexpectedly, the contribution of initiator-derived chains was relatively low considering the amounts used, as it was revealed through analytical techniques (^{1}H NMR, MALDI-TOF and ESI MS, SEC). On the other hand, working at an elevated temperature of 65°C (AIBN initiation) resulted in the appearance of bimodality in molar mass distributions of

PNMVA-CTA1. This was attributed to thermal degradation of the RAFT end-group, which prompted us to carry on the study at 35°C (V-70 initiation). Thus, experimental conditions were established and allowed a satisfying control of the RAFT polymerization of NMVA. Additionally, original block copolymers, poly(ethylene oxide)-*b*-PNMVA (PEO-*b*-PNMVA) and poly(*N*-isopropylacrylamide)-*b*-PNMVA (PNIPAAm-*b*-PNMVA), were successfully synthesized, demonstrating the ability of the *N*-vinylamide monomer to be copolymerized in a controlled fashion. Moreover, PNIPAAm-*b*-PNMVA showed thermoresponsive behavior in water with formation of block copolymer aggregates above 36.5°C, with a fully reversible LCST phase transition.

In the Chapter 2, a second example was demonstrated with *N*-vinylformamide (NVF). Using the newfound knowledge of Chapter 1, similar conditions were applied for its RAFT homopolymerization. *S*-cyanomethyl-*O*-ethylxanthate was used as the CTA and 35°C as the working temperature (V-70 initiation), with the addition of DMSO as the solvent. Interestingly, the lower $[initiator]_0/[CTA]_0$ ratio of 0.33 was sufficient for achieving a satisfying control of the polymerization, attesting of the higher reactivity of NVF compared to NMVA. Well-defined PNVF-based double hydrophilic block copolymers were also synthesized, poly(*N*,*N*-dimethylacrylamide)-*b*-poly(*N*-vinylformamide) (PDMA-*b*-PNVF), poly(*N*-vinylcaprolactam)-*b*-poly(*N*-vinylformamide) (PVCL-*b*-PNVF) and poly(*N*-isopropylacrylamide)-*b*-poly(*N*-vinylformamide) (PNIPAAm-*b*-PNVF). To find a way through their challenging characterization by conventional SEC, I turned to other analytical methods, asymmetrical flow field flow fractionation (AF4) and diffusion-ordered spectroscopy NMR (DOSY-NMR) to successfully obtain data on the molar masses and dispersities of the block copolymers. Finally, the selective hydrolysis of PNVF block in PVCL-*b*-PNVF block copolymer was performed, giving access to a new PVCL-*b*-PVAm copolymer.

In the Chapter 3, the third example was demonstrated with *N*-vinylisobutyramide (NVIBA). Similarly to the Chapters 1 and 2, thermally initiated RAFT polymerization was conducted using *S*-cyanomethyl-*O*-ethylxanthate was

used as the CTA, 35°C as the working temperature (V-70 initiation), and DMSO as the solvent. In the NVIBA case, the high $[initiator]_0/[CTA]_0$ ratio of 1.5 was required for a satisfying polymerization, exhibiting a reactivity more similar to NMVA than to NVF. To avoid using such a high amount of initiator, another initiation way was investigated, photo-initiation using purple LEDs (λ = 400 nm, 4.0 mW cm^{-2}). As xanthates show iniferter behavior, no external photo-initiator is thus needed for the photo-RAFT polymerization of NVIBA which was successfully conducted. Using complementary chain extension experiment, and analytical techniques (MALDI-TOF and ESI-TOF mass spectrometry, SEC in DMSO), photo-initiation was shown to give a better control than thermal-initiation as the proportion of generated dead chains was significantly lower in the former case. Lastly, the synthesis of original block copolymers PNVIBA-*b*-PNVF was successfully conducted. As PNVIBA is a thermoresponsive polymer showing LCST behavior in water, its properties were measured via UV-vis spectroscopy. Block copolymers as well as random copolymers were analyzed, and their phase transition temperature measured. The influence of the copolymers microstructure on their properties was highlighted, as LCST was mainly observed for block copolymers. In the case of random copolymers, a LCST behavior was only observed when the proportion of NVIBA was sufficiently high (of more than 50 wt%).

Finally, through this project I was able to demonstrate that the RAFT polymerization of acyclic *N*-vinylamides can be successfully achieved, albeit with peculiar conditions especially on the required amount of thermal initiator which differs from more conventional conditions. This can be attributed to several factors, such as a low efficiency of the azo-initiator or the relatively low reactivity of the monomers. The latter might be attributed to the substitution of the amide group of the monomer, as it was observed that NVF, a *N*-vinylamide, was significantly more reactive than NMVA, a *N*-alkyl-*N*-vinylalkyamide, and NVIBA, a *N*-vinylalkyamide.

For future studies, I hope that this work can serve as a basis for further investigations on the controlled polymerization of acyclic *N*-vinylamides and on *N*-vinylamide-based materials.

On the synthesis part, more investigations can be conducted on the reactivity of those monomers. As non-conjugated monomers, further understanding the reactivity nature of acyclic *N*-vinylamides may be of help to generally understand more about less activated monomers (LAMs) for which the controlled radical polymerization is a challenge due to the unstable character of the growing radicals and relatively poor reactivity of vinyl double bonds.[1] The reactivity of acyclic *N*-vinylamides is also different from their cyclic counterparts. Studies on the monomers amide group structure can be conducted, and on the effect of its substituents' nature. In this project, only some alkyls substituents were used (NMVA and NVIBA) with a focus on the carbonyl side of the amide group. Previous studies using conventional radical polymerizaiton showed that having bulky substituents on the nitrogen side don't have a very significant impact on the polymerizability of the monomers, but seem to have an effect on the obtained polymers structure. However, having an additional substituent, here a methyl group, on the carbonyl side of the monomers amide group was revealed to negatively impact the polymerization.[2,3] I also observed a significantly higher reactivity for NVF in Chapter 2. Thus, investigating the effect of substituents of different natures might lead to fine-tuning the reactivity of acyclic *N*-vinylamides.

On the materials part, a whole new range of copolymers can result from this work. In the different chapters, only a few examples of new block copolymers containing acyclic *N*-vinylamide and *N*-vinylamine units were shown. With the very broad variety of copolymers that are used today, numerous possibilities can be imagined. Taking a further step, the controlled polymerization of acyclic *N*-vinylamides allows the synthesis of new well-defined building blocks and precursors of nanomaterials and larger objects that can be used for the already existing applications. New water-soluble, biocompatible hydrogels for drug-delivery agents, or tissue engineering, of tunable thermoresponsivity, pH-responsivity or viscosity can be envisioned for biomedical applications. The kinetic hydrate inhibition character may be enhanced and fine-tuned with materials of varying molar masses, microstructures or architectures may be obtained for petroleum industrials. Other *N*-vinylamide-based materials in fields such as energy,

textile industry or water treatment, may also see the emergence of efficient materials with enhanced properties.

As a concluding remark, I hope that this work can help making the interest of scientists grow for this family of monomers and make Science take another step forward.

REFERENCES

(1) Harrisson, S.; Liu, X.; Ollagnier, J.-N.; Coutelier, O.; Marty, J.-D.; Destarac, M. RAFT Polymerization of Vinyl Esters: Synthesis and Applications. *Polymers* **2014**, *6* (5), 1437–1488.
(2) Ajiro, H.; Akashi, M. Radical Polymerization of Novel N-Substituted-N-Vinylacetamides and Regulated Polymer Structures by Bulky Substituents and Menthol Coordination. *Macromolecules* **2009**, *42* (2), 489–493.
(3) Ajiro, H.; Akashi, M. Radical Polymerization of Novel N-Substituted-N-Vinylformamide Derivatives with Bulky Chiral Substitutents. *J. Polym. Sci. Part Polym. Chem.* **2012**, *50* (1), 134–141.